DESIGN AND RESISTANCE FACTOR CALIBRATION OF PIPE PILES FOR CALIFORNIA

By

YUJIE HU

Presented to the Faculty of the Graduate School of

The University of Texas at Arlington in Partial Fulfillment

of the Requirements

for the Degree of

MASTER OF SCIENCE IN CIVIL ENGINEERING

THE UNIVERSITY OF TEXAS AT ARLINGTON

May 2016

Acknowledgements

First of all, I would like to express my deep and sincere gratitude to Dr. Xinbao Yu. His timely advice, constant inspiration, support and care have greatly helped me to accomplish this task. Dr. Yu served as my advisor from my first year of college, providing me with excellent guidance and scholarly advice throughout my studies both in my course work and my thesis. I deeply appreciate the help that Dr. Yu has provided me and the trust that he has had in me.

It is a genuine pleasure to also express my deep thanks to Dr. Anand J. Puppala and Dr. Laureno R. Hoyos for their willingness to serve as my thesis committee members, and Dr. Sahadat Hossain, Dr. Stefan Romanoschi, Dr. Doyle L Hawkins and Dr. Aravind Pedarla for sharing with me their professional knowledge and suggestions during class and lab.

I would also like to thank Dr. Nan Zhang in our research group, for his generous help and inspirations during my entire course study and thesis work.

In addition, I would like to express my special thanks to my fiancé Xinlong Wang, I could not have finished my work without his understanding and magnanimity.

I owe a deep sense of gratitude to my parents, who provided me tremendous support and encouragement in my academic career and daily life. Thanks to my family for their unconditional understanding and love.

April 04, 2016

Abstract

Design and Resistance Factor Calibration of Pipe Piles for California

Yujie Hu, MS

The University of Texas at Arlington, 2016

Supervising Professor: Xinbao Yu

Steel pipe piles, either open-ended or close-ended, are widely used in the state of California as bridge foundations due to high load-bearing capacity, light weight, and outstanding workability. The design methods currently used by Caltrans were developed based on limited field data and are lack of field validations of more recent steel pipe piles. In this thesis study, 45 high-quality steel pipe pile load tests performed in various soil conditions were collected from Caltrans' load test data to evaluate available design methods and calibrate the resistance factors of selected design methods. A total of 26 static capacity prediction methods for pile skin and tip resistance were selected to predict total static pile capacity. The performance of the 26 design methods were systematically evaluated by comparing the estimated (Q_c) and measured ultimate pile capacities (Q_m). The evaluation was based on best fit line for predicted capacity Q_c versus measured capacity Q_m, mean and standard deviation for Q_c/Q_m values, cumulative probability of Q_c/Q_m values, and the histogram and log-normal distribution for Q_c/Q_m values. All the prediction methods were first ranked according to each single criterion and then ranked according to an overall rank index (RI) which considered the combination of all four single criterion.

Load and Resistance Factor Design (LRFD) calibration was performed on each calibration method using Monte Carlo Simulation (MCS) method. Bias statistics were obtained by using mean and standard deviation of all measured bias and best fit lower

tail of the measured bias. Monte Carlo simulation of 10,000 iterations was performed to calibrate resistance factors ϕ at target reliability index β of 2.33 for investigated methods. In addition, the relationship of resistance factors ϕ with various reliability index β has also been determined for best prediction method resulting from above mentioned assessment system.

Table of Contents

List of Illustrations

List of Tables

Chapter 1

INTRODUCTION

Pile foundations have been used increasingly to support bridges and other structures to ensure safely transferring loads into deep ground. Steel pipe pile is a very common type of pile foundation. They are commonly used where variable pile lengths are required since splicing is relatively easy. Common offshore or near shore applications of pipe piles include use as bridge foundation piles, fender systems, and large diameter mooring dolphins. With the increased ductility requirements for earthquake resistant design, pipe piles are being used extensively in seismic areas. According to the pile database from California Department of Transportation (CALTRANS), steel pipe pile is the majority pile type within investigated piles.

Determining of pile resistance and accounting for uncertainties in the process of construction are always challenges to engineers. Several methods have been applied in the geotechnical field for predicting ultimate axial bearing capacity, including traditional static method sand dynamic analysis methods. In this thesis, several static analysis methods, based on soil properties (i.e. SPT, S_u) obtained from where the pile was driven, have been selected to estimate pile resistance. Measured bearing capacity was determined from the pile load test according to 1 inch settlement. Predictions of capacity were based on static methods recommended by CALTRANS, including API (25 and 33), Dennis, α-Tomlinson, Kraft and β methods for skin friction, API for tip resistance in clayey soil, Nordlund, API, Decour and Olson for skin friction, and API and Nordlund methods for tip resistance in sandy soil.

In order to account for uncertainties associated with estimated loads and resistances in those specifications for structural and geotechnical design, the Bridge Design Specifications published by the American Association of Highway and

Transportation Officials (AASHTO) has introduced the LRFD method. The goal in the development of load and resistance factors is to provide a consistent margin of safety for the design of all structural components. The process of using data, from which statistical parameters characteristic of the design method can be derived, and the determination of the magnitude of load and resistance factors needed to obtain acceptable margins of safety, is termed calibration (Allen et al. 2005). The use of Load and Resistance Factor Design (LRFD) for highway bridges has been mandated by AASHTO and the Federal Highway Administration (FHWA). All bridge design should be based on this approach by October 2007 (Hannigan et al. 2006), including foundations and driven piles.

Since the resistance factors of AASHTO design specifications based on the soil sites may not necessarily reflect local soil conditions in California, it becomes more practicable to use reliability theory analysis based on local driven pile data to produce a resistance factor which is consistent with local soil.

In this thesis, analysis and estimations were derived from 45 pipe pile cases driven into California soil provided by CALTRANS. An assessment system was established, aiming to describe the performance of different static methods for predicting axial ultimate capacity. Thereafter, resistance factors were calibrated according to various static design methods at a certain reliability index β (related to safety margin).

Chapter 2

LITERATURE REVIEW

Steel pipe piles have been used generally and increasingly as deep foundations for offshore and onshore structures, such as bridge foundation piles, fender systems, and large diameter mooring dolphins. They can be used in friction, toe bearing, a combination of both, or as rock socketed piles. They are also commonly used in place where variable pile lengths are required since splicing is relatively easy. With the increased ductility requirements for earthquake resistant design, pipe piles are being used extensively in seismic areas (FHWA). Pipe piles diameters typically range from 8 to 48 in, larger sizes are available, but not commonly used in land or near shore applications. Typical wall thickness range 0.188 to 1 in, but it can increase up to 2.5 in. Typical lengths are ranging from 15 to 130 ft.

Pipe piles may be driven either open-ended or close-ended. If the capacity from the full pile toe area is required, the pile toe should be closed with a flat plate or a conical tip. Pipe pile driven with open end can cause low soil displacement, leading pile installation to further and deeper soil.

2.1 Prediction of Bearing Capacity for Pipe Piles

There are a variety of static methods for predicting bearing capacity of pile foundation, not only for steel pipe piles. Except several methods recommended by CALTRANS (shown in Chapter 3), other methods such as Meyerhof (based on SPT for cohesionless soil) and Schmertmann method (based on CPT) are also used in predicting pile capacity.

The Meyerhof (1976) method is quick and is easy to use. Meyerhof (1976) reported that the average unit shaft resistance, f_s, of driven displacement piles, such as closed-end pipe piles and precast concrete piles, in kPa is:

$$f_s = 2N' \leq 100\ \text{kPa} \quad (2\text{-}1)$$

The average unit shaft resistance of driven non-displacement piles, such as H-piles, in kPa is

$$f_s = N' \leq 100\ \text{kPa} \quad (2\text{-}2)$$

Where N' is the average corrected SPT resistance value, in blows per 300 mm (1 ft), along the embedded length of pile. Typically, the soil profile is delineated into 3 to 6 m (10 to 20 ft) thick layers, and the average unit shaft resistance is calculated for each soil layer.

Meyerhof (1976) recommended that the unit toe resistance, q_t, in kPa for piles driven into sands and gravels may be approximated by:

$$q_t = 400\overline{N_o'} + \frac{(40\overline{N_B'} - 40\overline{N_o'})D_B}{b} \leq 400\overline{N_B'} \quad (2\text{-}3)$$

Where:

$\overline{N_o'}$ = Average corrected SPT N' value for the stratum overlying the bearing stratum.

$\overline{N_B'}$ = Average corrected SPT N' value of the bearing stratum.

D_B = Pile embedment depth into the bearing stratum in meters.

b = Pile diameter in meters.

It is recommended that the average corrected SPT N' value, $\overline{N_B'}$, are calculated by averaging N' values within the zone extending 3 diameters below the pile toe.

However, because the method is based on SPT test data which can be influenced by numerous factors, this method should only be used for preliminary estimates and not for final design (FHWA, 2006).

Schmertmann Method predicts pile bearing capacity by using CPT data. The ultimate shaft resistance, R_S, in cohesionless soils may be derived from unit sleeve friction using the following expression:

$$R_s = K\left[\frac{1}{2}(\overline{fs}A_s)_{0\ to\ 8b} + (\overline{fs}A_s)_{8b\ to\ D}\right] \quad (2\text{-}4)$$

Where:

K = Ratio of unit pile shaft resistance to unit cone sleeve friction

fs = Average unit sleeve friction over the depth interval indicated by subscript.

A_S = Pile-soil surface area over fs depth interval.

b = Pile width or diameter.

D = Embedded pile length.

O to 8b = Range of depths for segment from ground surface to a depth of 8b.

8b to D = Range of depths for segment from a depth equal to 8b to the pile toe.

For shaft resistance in cohesive soils, the ultimate shaft resistance, R_S, is obtained from the sleeve friction values using the following expression:

$$R_s = \alpha'\overline{fs}A_s \quad (2\text{-}5)$$

α' = Ratio of pile shaft resistance to cone sleeve friction, varies as a function of sleeve friction, f_s.

Open-ended pile may behave as low displacement piles through the soil, or act as displacement piles if a soil plug forms near the pile toe. Determination of the axial capacity of open-ended pipe piles has been a difficult problem, and this can be largely attributed to the complicated behavior of soil plugging.

When open-ended pipe piles are driven into ground, some soil will enter inside of pile, if the pile moves downwards relatively to the internal soil column, and pile penetration depth (D_1) is equal to the length of soil column (L_1) inside of pile, this

behavior is referred as “unplug”. As the driven depth (D_2) increase, soil plug is formed at the bottom of pile (L_2) to prevent or partially restrict additional soil from entering inside, this behavior is defined as “plugged”, in which length of soil plug is less than pile penetration depth. If the penetration depth keeps increasing (D_3), while soil column length (L_3) inside of pile stops increasing, it means reaching a status of “fully plugged”. In order to quantify the effect of soil plugging on pile capacity, PLR (plug length ratio) which is most widely used, has been introduced to define degree of soil plugging.

$$PLR = L/D \qquad (2\text{-}6)$$

Where D=pile penetration depth; L= length of soil plug.

Another indicator of soil plugging is incremental filling ratio (IFR), which is a first derivative of PLR, meaning that IFR is a slop of curve of plug length versus pile penetration depth plot, can be defined as:

$$IFR = dL/dD \qquad (2\text{-}7)$$

Where dL= increment of soil plug length; dD = increment of pile penetration depth.

The process of soil plug describes in Figure 2-1, in the case of a fully coring mode (unplugged), PLR and IFR both equal to 1.

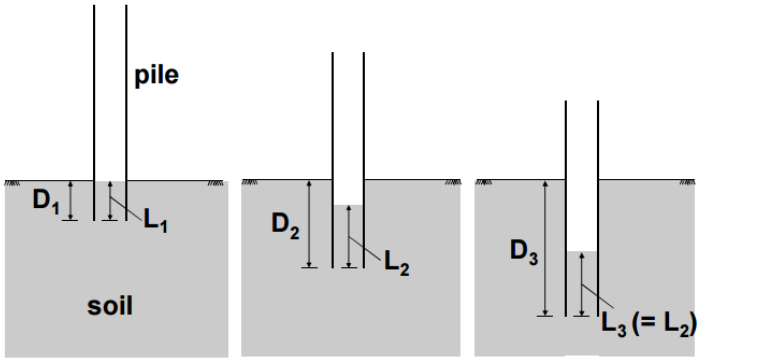

Figure 2-1 Soil plugging mode

Once plugged, an open-ended pipe behaves like a displacement pile and driving becomes more difficult. Pipe piles in clay are expected to plug at a depth ratio of D/B ≈10-20 and for sand at D/B≈ 25-35. (Paikowsky and Whitman, 1990). Unlike Plugging of open pipe piles in sand, plugging of open pipe piles in clay does not contribute significantly to the capacity of the pile. Side friction of soil plug inside can be considered as half of the outside side friction.

Paikowsky and Whitman (1990) recommend that the static capacity of an open end pipe pile be calculated from the lesser of the following equations:

Plugged Condition: $Q_u = f_{so}A_s + q_t A_t$

Unplugged Condition: $Q_u = f_{so}A_s + f_{si}A_{si} + q_t A_p - w_p$ (2-8)

Where:

Q_u = Ultimate pile capacity in kN (kips).

F_{so} = Exterior unit shaft resistance in kPa (ksf).

A_s = Pile exterior surface area in m^2 (ft^2).

F_{si} = Interior unit shaft resistance in kPa (ksf).

A_{si} = Pile interior surface area in m^2 (ft^2).

Q_t = Unit toe resistance in kPa (ksf).

A_t = Toe area of a plugged pile in m^2(ft^2).

A_p = Pile cross sectional area of an unplugged pile in m^2 (ft^2).

W_p = Weight of the plug kN (kips)

For open end pipe piles in cohesionless soils, Tomlinson (1994) recommends that the static pile capacity be calculated using a limiting value of 5000 kPa (105 ksf) for the unit toe resistance, regardless of the pile size or soil density. For open end pipe piles driven in stiff clay, static pile capacity can be calculated as follows when field measurements confirm a plug is formed and carried down with the pile:

$$Q_u = 0.8\, c_a A_s + 4.5\, C_u A_t \quad (2\text{-}9)$$

Where:

Q_u = Ultimate pile capacity in kN (kips).

C_a = Pile adhesion from Figure 3-4 in kPa (ksf).

A_s = Pile-soil surface area in m^2 (ft^2).

c_u = Average undrained shear strength at the pile toe in kPa (ksf).

A_t = Toe area of a plugged pile in m^2 (ft^2).

Hannigan et al. (2006) suggests static pile capacity calculations for open end pipe piles in cohesionless soils should be performed using the Paikowsky and Whitman equations. For open end pipe piles in predominantly cohesive soils, the Tomlinson equation should be used.

California Amendments To AASHTO LRFD Bridge Design Specifications suggests Tomlinson method and API (in Chapter 3) for cohesive and cohesionless soil, also for open-ended pipe piles, the nominal axial resistances should be calculated for both plugged and unplugged conditions. The lower of the two nominal resistances should be used for design.

Gudavalli and Safaqah (2013) did the research on effect of soil plugging on axial capacity of open-ended pipe piles in sand, also suggested new equations for estimating skin friction and unit end bearing value for piles driven in dense to very dense sands based on PLR ratio.

Gudavalli and Safaqah (2013) measured plug lengths for 1355 piles, the outer diameter ranged from 406 mm to 914 mm (corresponding to 16 in to 36 in), inner diameter ranged from 387 mm to 876 mm (corresponding to 15 in to 35 in). The pile penetration depths ranged between 10 m to 30 m. They found the mean value of PLR increases with increase of pile diameter. This trend showed agreement with the

relationship suggested by Yu and Yang (2011), while PLR ratio appeared lower than what Yu and Yang (2011) obtained. Also, piles having large embedment depth are more likely to have higher PLR values than those short embedment piles.

In order to estimate pile capacity, dynamic load tests were performed on 99 piles using PDA, pile capacity were estimated by CAPWAP Method. In their study, axial capacity equation recommended by American Petroleum Institute (API) (2005) had been used, and the skin factor and end-bearing factor had been back-calculated from CAPWAP, then compared with those values in API method. Accordingly, Gudavalli and Safaqah (2013) established new equation for estimating pile capacity, taking into account both PLR ratio and penetration depth.

Unit skin friction recommended by American Petroleum Institute (API) (2005) is defined as

$$q_s = K\sigma_v' tan\delta = \beta\sigma_v' \qquad (2\text{-}10)$$

Incorporated K and δ together, shaft factor β can be obtained. According to API (2005), β value ranges from 0.37 to 0.56 for open-ended pipe piles in unplugged mode driven to medium dense to dense sand, 0.46 to 0.7 was recommended for fully plugged or closed-ended pipe piles.

Based on back-calculated data, Gudavalli and Safaqah (2013) established the new equation to estimate β:

$$\beta = (3.5 - 3.2PLR)e^{-0.023D} \qquad (2\text{-}11)$$

Where PLR= plug length ratio (0.76 to 0.91) and penetration depth ranged from 10 m to 30m.

The mean β value they obtained decreased from 0.83 to 0.42 with PLR ratio increasing from 0.76 to 0.89. It showed skin factor β is a function of PLR, which in turn is a function of pile diameter, while β is independent of the pile diameter in API method. The

new established equation resulted higher β value than value recommended in API for pile diameter less than 504mm (20 in).

Since soil plug happens at the end of pile, considerable effort has been made to investigate end-bearing of pipe piles in sand. Unit end bearing for piles installed in sandy soil recommended by American Petroleum Institute (API) (2005) is defined as:

$$q_b = N_q \sigma_v' \qquad (2\text{-}12)$$

Where σ_v'= vertical effective stress at the base of pile, N_q= end bearing factors ranging from 40 to 50 for dense to very dense sand.

Based on the pile data they measured, Gudavalli and Safaqah (2013) obtained new equation for N_q by fitting the mean values:

$$N_q = 12.3PLR^{-8.4} \qquad (2\text{-}13)$$

Where PLR= plug length ratio is between 0.76 and 0.91.

From this new equation, it can be seen N_q decreases with increasing of PLR value. API recommendations for end bearing factor seem to be more appropriate for large diameter piles from 762mm to 914 mm (30 to 36 inch), but significantly underestimated that for small piles with a diameter of 406mm (16 inch), since the N_q value obtained for small diameter piles is134, which is close to the value suggested by Paik and Salgado (2004) for fully plugged open-ended pipe piles in dense sand is 130 when K_0 =0.4 (earth pressure coefficient).

It should be noted that the equations suggested by Gudavalli and Safaqah (2013) for skin and end-bearing factor are based on pipe pile from dense to very dense sand with PLR value ranging between 0.76 and 0.91. Therefore, these equations might not be appropriate for loose and medium dense sands. In addition, it only considers outer area of pile-soil interface for skin friction, and gross section area of pile tip, that may under estimate bearing capacity.

CPT based design model also is included for estimating effect of soil plugging on bearing capacity of pipe piles. Reviews in Lethane and Xu (2005), showing that University of Western Australia (UWA) method (Lethane and Xu 2005) and Imperial Coleege pile (ICP) method (Jardine and Chow 1996)have more advantages.

The ICP method was developed from a database of pile load test and CPT data, targeted for both open-end and close-end piles. To estimate base capacity, this method first required determination of the plugging mode, a pipe pile was determined as unplugged when either of the two following conditions fulfilled:

$$d \geq 2.0\ (D_r - 0.3) or\ d \geq 0.03 q_{c,a} \qquad (2\text{-}14)$$

Where d=inner diameter of pile (m); D_r = relative density of the soil near the pile tip; and $q_{c,a}$= averaged CPT tip resistance over a specified range in the vicinity of the pile base (MPa). If none of the conditions above fulfilled, the pile was classified as fully plugged. Then the ultimate unit base resistance q_b was determined for both unplugged and plugged conditions, respectively:

Unplugged: $q_b/q_{c,a} = 1 - (d/D)^2$

Plugged: $q_b/q_{c,a} = max\left[0.14 - 0.25 log D, 0.15, 1 - (d/D)^2\right]$ (2-15)

Where D= pile outer diameter (m)

The equation indicates that unit bearing from the ICP method is a function of diameter and relative density of the sand at the tip. However, this method does not incorporate the relationship between the degree of soil plugging and embedded length. Moreover, this method assumes that there were only two cases of plugging—fully plugged and fully coring. This method does not account for a partially plugged mode. Additionally, for the unplugged mode, the ICP method underestimates the predictions because it excludes the contribution of plug resistance.

UWA method was developed based on ICP method by incorporating more factors. The base capacity (Xu et al. 2008) for an open-ended pipe pile, corresponding to a base displacement of 0.1D, is calculated as below:

$$q_b/q_{c,a} = 0.6 - 0.45(d/D^2)IFR \quad (2\text{-}16)$$

Compared with ICP method, UWA method does not require determination of the plugging mode. It accounts for degree of soil plugging effect by incorporating IFR parameter. However, IFR value over the final 3D penetration cannot be easily determined during pile driven, moreover, this method gives an overall estimate of base capacity instead of offering explicit estimates of individual contributions from annulus and plug to the base capacity.

An improved approach, referred to as Hong Kong University (HKU), which is also based on cone penetration test (CPT), takes into consideration the mechanism of annulus and plug resistance mobilization. In this method the annulus resistance is properly linked to the ratio of pile length to the diameter—a key factor reflecting the influence of pile embedment, whereas the plug resistance is related to the plug length ratio, which reflects the degree of soil plugging in a practical yet rational way (Yu and Yang 2011).

The overall base capacity consists of annulus and plug resistance for an open-ended pile can be determined by:

$$Q_b = \frac{\pi}{4}\left[d^2 q_{plug} + (D^2 - d^2)q_{ann}\right] \quad (2\text{-}17)$$

Where q_{ann}= unit annulus resistance (MPa) and q_{plug}= unit base resistance of soil plug

The expression below proposed to relate the annulus resistance, normalized by the corresponding CPT tip resistance, has a good correlation with L/D values, showing the normalized annulus resistance decreases linearly with an increase in L/D.

$$q_{ann} = [1.063 - 0.045(L/D)]q_{c,a} \geq 0.46q_{c,a} \quad (2\text{-}18)$$

Where L= pile length (m).

This equation proposed shows a useful explicit relationship between the normalized annulus resistance and the combination of pile embedment and diameter. The lower bound appears to be reasonable for closed-ended pile.

The plug capacity is mainly mobilized from the friction along the inner pile wall, particularly along the lower part of the soil plug. The relationship between plug resistance and PLR values are obtained based on 48 sets of data:

$$q_{plug} = 1.063\exp(-1.933PLR)q_{c,a} \quad (2\text{-}19)$$

The plug resistance takes a maximum value 1.063 for PLR =0, representing an extreme case of the fully plugged mode without soil entering inside of pile throughout the pile driven process. Furthermore, for a fully plugged pile with nonzero PLR (which is common in real applications), PLR=0.202 when IFR =0, which yields a plug capacity equal to 68% of the base capacity of close-ended pile.

HKU method also recommended a set of influence zones for various conditions to obtain average $q_{c,a}$ value based on considerations of the effects of pile embedment.

Although FHWA and CALIFORNIA AMENDMENTS TO AASHTO LRFD BRIDGE DESIGN SPECIFICATIONS recommends check both of plug and unplug conditions, to take the lower one as design capacity, while in some common design methods (such as Tomlinson, API, Nordlund), it suggests using pile diameter multiplied by penetration depth as shaft area, only steel cross section area at pile toe unless there is reasonable assurance and previous experience that a soil plug would form, that may lead to conservative design capacities.

2.2 Resistance Factor for Prediction of Pipe Pile Capacity

Most of resistance calibration work was based on the database which include a variety types of piles (i.e. pipe pile, concrete pile, H pile), hence the calibrated resistance

factor remains as a general term rather than a specific term for pipe pile. Rare cases calibrated resistance factor based on certain pile types.

Minnesota DOT completed its first phase LRFD calibration of resistance factors based on dynamic driving formula (Paikowsky et al. 2009). MnDOT uses its MnDOT driving formula to verify driven pile capacity during construction. The MnDOT driving formula used weight of the hammer, height of fall of the hammer, final set of pile and different factors for timber, concrete, shell, steel and H piles. The MnDOT driving formula was analyzed along with four additional dynamic formulae using two databases of driven piles. The two databases were MNDOT LT 2008 H-Piles database and MNDOT LT 2008 Pipe piles database. The research also proposed a new MnDOT formula that was tailored for the pile driving practices of MnDOT.

Regarding to pipe piles, 104case histories were assembled in Mn/DOT LT 2008 database.The static capacity of the piles was determined by Davisson's failure criterion, established as the measured resistance. The calculated capacities were obtained using dynamic equations Mn/DOT.

Target reliability and distribution of resistance and load was used in calibration as shown by Paikowsky (2004) in Phase I. Resistance factors resistance factors were evaluated in three ways – First Order Second Moment (FOSM), Monte Carlo Simulation (MCS), and recommendation based on results from FOSM and MCS rounded to the closest 0.05. The measured static capacity was determined using Davisson failure criterion and bias was calculated as ratio of measured static capacity to predicted capacity. Similar calibration approach was taken in Phase II study.

The database analysis found that current MnDOT driving formula over-predicted pile capacity with a mean bias of 0.8 where the bias was calculated as the ratio of measured capacity to dynamically predicted capacity. Additionally, the current MnDOT

produced large scatter with coefficient of variation of 0.5 to 0.8 for H and pipe piles at EOD condition. This leaded to the resistance factor of 0.25 when using original MnDOT equation for both H and pipe piles. For new proposed Mn/DOT equation, addressing EOD conditions of all hammers with all energies and driving resistances, the associated resistance factors, ϕ=0.45. (Resistance Factors were calculated for a target reliability β=2.33, and probability of failure p_f=1%)

Due to the resistance factors established in Phase I study being conservative with then current practice in MnDOT, Phase II study was performed. Also, the resistance factors needed to be re-evaluated. The database was compiled and provided by Messrs. Ben Borree and Derrick Dasenbrock of the MnDOT Foundations unit. The database consist of accumulated PDA data from various projects with supplemented DOT data (stroke, blow count, etc.) The compiled database contained 126 pipe pile cases including hammer type and rated energies that matched for the most part the MnDOT practice. The Phase II study extended the analysis by incorporating pipe pile cases from the study into timber and pre-stressed precast concrete piles, and also proposed a new formula MPF12 which is appropriate for MnDOT driven pile construction practice by performing WEAP analysis. The MPF12 incorporated weight of hammer, stroke height, and pile set with different modification factor for different piles. The resistance factors came out to be 0.5 for pipe piles for blow counts of more than 2 and less than or equal to 15 (for target reliability β=2.33, probability of failure p_f=1%).

The vast majority of the database case histories were related to SPT and CPT field testing. The case histories were divided on the basis of soil conditions (clay, sand, and mixed) and pile types (H pile, concrete piles, pipe piles). In summary, given field conditions were used via various soil parameter identifications and pile capacity

evaluation procedures to determine capacity. The obtained capacity was then compared to measured static capacity.

The pipe pile database incorporated in NCHRP report 507 (Paikowsky 2004) containing 78 cases based on static analysis was developed at the University of Florida, mostly through the integration of databases gathered by the University of Florida, the FHWA (DiMillio 1999), the University of Massachusetts Lowell (Paikowsky and LaBelle 1994), and the Louisiana Transportation Research Center.

Based on the review of the state of the art, the survey of common practice, and the evaluation of the above values, the following reliability indices and probability of failure were developed and were recommended in conjunction with methods for capacity evaluation of single piles:

1. For redundant piles, defined as 5 or more piles per pile cap, the recommended probability of failure is $p_f = 1\%$, corresponding to a target reliability index of $\beta = 2.33$.
2. For non-redundant piles, defined as 4 or fewer piles per pile cap, the recommended probability of failure is $p_f = 0.1\%$, corresponding to a reliability index of $\beta = 3.00$.

The factors were evaluated using FORM (First Order Reliability Method) with dead load (DL) to live load (LL) ratios ranging from 1 to 4. The results for a bias of 1, a coefficient of variation of 0.4 and target reliability values of 2.0, 2.5, and 3.0 are presented in Figure 2-2, suggesting very little sensitivity of the resistance factors to the DL to LL ratio. A similar trend is observed using DL to LL ratio of 10. The large dead-to-live-load ratios represents conditions of bridge construction, typically associated with very long bridge spans. The relative small influence of the dead-to-live-load ratio on the calculated resistance factors suggests that (1) the use of a DL to LL ratio of 2 or 2.5 as a

typical value is reasonable, and (2) the obtained factors are, by and large, applicable for long span bridges (Paikowsky 2004).

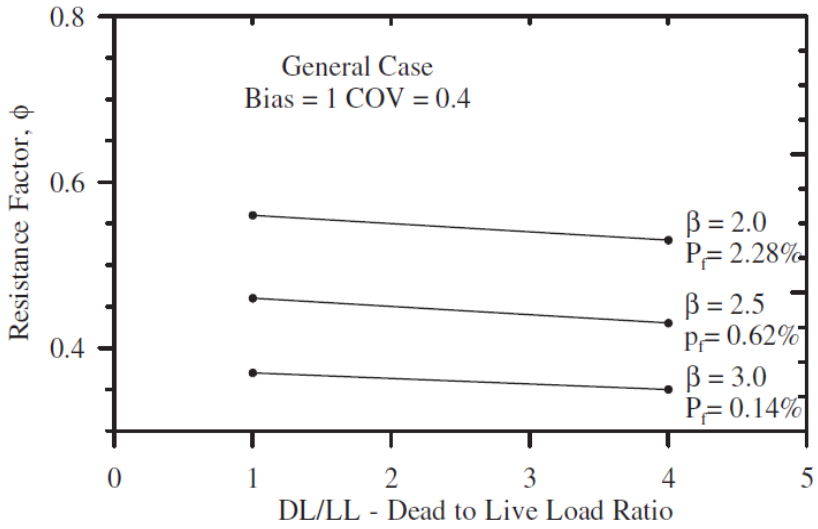

Figure 2-2 Calculated resistance factors for a general case showing the influence of the dead-to-live-load ratio (NCHRP Report 507)

With the chosen load distribution parameters (from AASHTO), DL to LL ratio of 2.5 and a target reliability $\beta = 2.33$, the influence of resistance factor and bias, also COV had been investigated. The obtained relationship shows that a perfect prediction ($\lambda = 1, COV = 0$) would result in a resistance factor of $\phi = 0.80$. With a prediction method for which the bias is 1 but the distribution is greater ($COV > 0$), the resistance factor would sharply decrease. Therefor when COV value changes from 0 to 0.4, the resistance factor would reduce from 0.8 to 0.44. The influence of the bias of the method (λ, or mean ratio of measured over predicted) on the resistance factor is equally important. As seen in the Figure 2-3, an under predictive method ($\lambda > 1$) has a “built in” safety and hence a higher resistance factor is used in order to achieve the same target reliability.

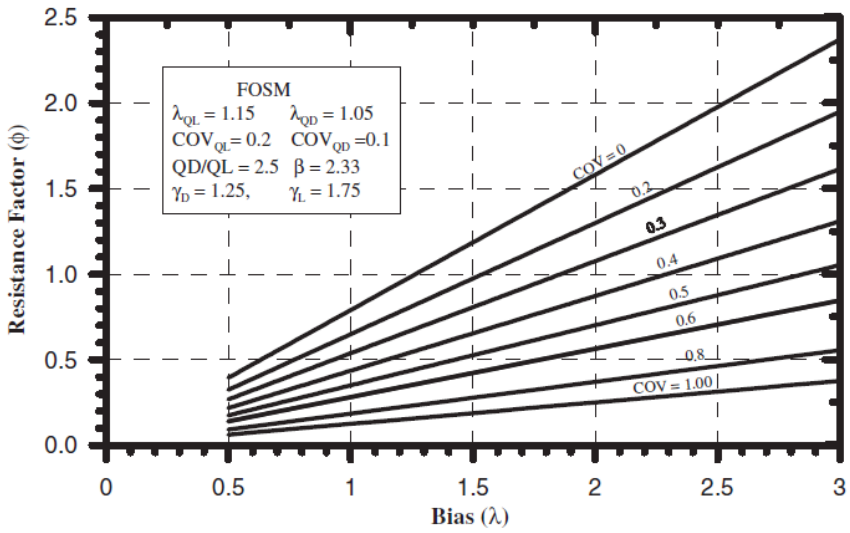

Figure 2-3 Calculated resistance factors as a function of the bias and COV for the chosen load distributions and DD/LL ratio of 2.5 (NCHRP Report 507)

The efficiency or economic performance of the static methods can be evaluated by the ratio of ϕ/λ, indicating the percentage of the measured Davisson capacity that can be utilized for design to reach a predefined structure reliability (McVay et al. 2000). A method/condition combination that has large variability (expressed as COV) results in low resistance factors, the resistance factors alone do not provide a measure of the efficiency of the method. The ratio of ϕ/λ is systematically higher for methods which predict more accurately regardless of the bias. The value of the efficiency factor remains constant for all bias combinations for a given COV, leading to higher values for methods with a lower COV. The efficiency of a given capacity prediction method can therefore, be improved only through a reduction in its variability (COV); alternatively, design methods need to be chosen based on their COV.

Table below presents a summary of the results obtained from the analyses used for static capacity evaluation of pipe piles, compared with the nominal resistance based on Davisson's failure criterion. The information is grouped by soil and pile type and

design method. The table includes statistical parameters and resistance factors for a range of reliability index values, based on the value of DL/LL= 2. The data leading to Table 2-1 were statistically analyzed to remove outliers, and includes only those cases within ±2 standard deviations of the mean.

Table 2-1 Statistical details of static analyses of pipe piles (Paikowsky 2004)

	Total No. of Cases	Design Method	No. of Cases ± 2 SD	β=2.33	β=3.00
				ϕ	ϕ
Clay	20	α-Tomlinson	18	0.25	0.19
	20	α-API	19	0.29	0.20
	13	β-Method	12	0.14	0.10
Sand	20	Nordlund	19	0.56	0.41
	20	β-Method	20	0.36	0.25
	20	Meyerhof	20	0.31	0.22
Mixed soil	13	α-Tomlinson/Nordlund/Thurman	13	0.24	0.17
	34	α-API/Nordland/Thurman	32	0.36	0.26
	31	β-Method/Thurman	29	0.22	0.16

Chapter 3

STEEL PIPE PILE DESIGN AND LOAD TEST DATABASE

This chapter describes steel pipe pile database information and static design methods provided by CALTRANS for predicting axial bearing capacity. The data on the selected 45 steel pipe piles which have the diameter less than 48 inches were collected from California soil. The information and data regarding soil stratification and properties, pile characteristics, load test data, SPT profiles, etc. were processed and transferred from each load test report. In addition, in order to accurately predict bearing capacity of piles, several static design methods were suggested from CALTRANS.

3.1 Pipe Pile Database Interpretation

The piles diameter range from 10.75 to 42 inch, total pile lengths are between 33 and 131.3 ft, embedment lengths range from 28 to 105.2 ft. Among the 45 piles, 11 of those piles are close-ended, 34 are open-ended pipe piles. They were driven into different soil types at different locations within California. 6 piles of those were driven into clay soil, 12 piles were in sandy soil, and the rest 27 piles were driven in layered mixed soils. More than half of piles were ended in sandy soil, 13 out of 45 were in clay, the rest of cases were ended in silt or gravel. Basic diameter, lenth and soil conditions are shown in Table 3-1, Table 3-2, Figure 3-1 and Figure 3-2.

Table 3-1 Investigated pile type distribution

	Open-ended	Close-ended
Sand	9	3
Clay	3	1
Sand and clay	22	7
Total	34	11

Table 3-2 Diameter and soil conditions for investigated piles

Pile Diameter (inch)	Sand	Clay	Sand and clay	Sum
10.75	1	0	0	1
12	1	0	0	1
14	3	0	3	6
16	2	1	2	5
18	1	0	0	1
24	3	3	19	25
42	1	0	5	6
Total	12	4	29	45

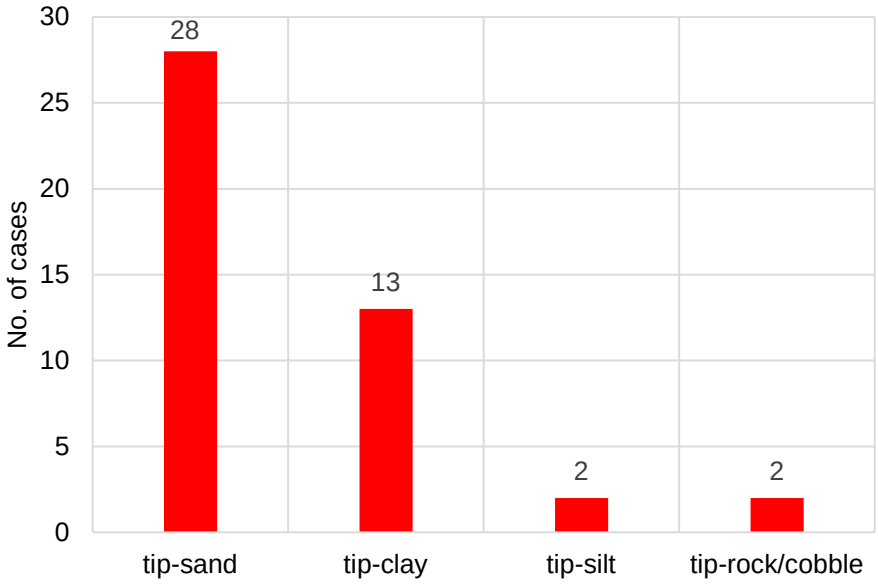

Figure 3-1 Tip soil conditions for investigated pipe pile

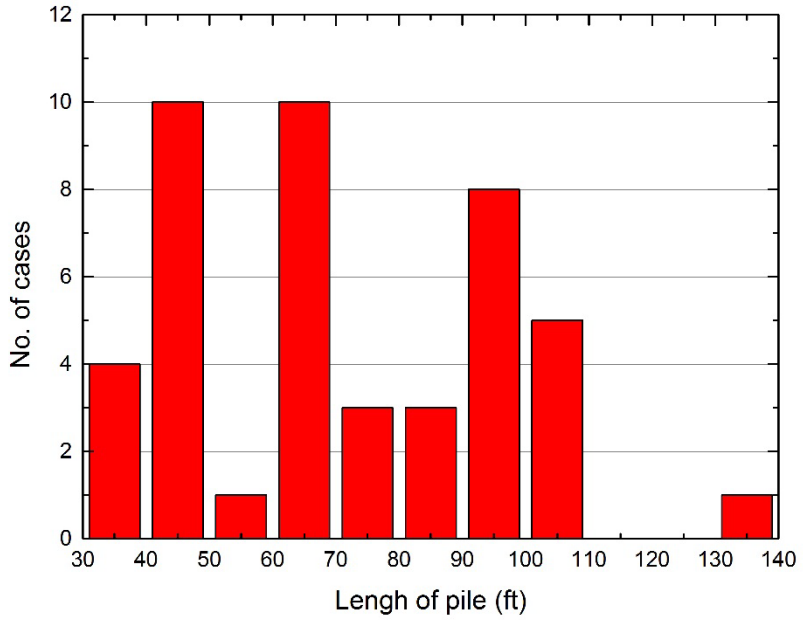

Figure 3-2 Investigated pile length distribution

Table 3-3 presents the summary of investigated pile information, including pile load test report number, pile size, type, length, location of the pile, measured capacities according 1 inch settlement.

Table 3-3 Summary of investigated pile and soil condition

Index	Load report number	Data quality factor	No. of set-up days	Outer Diameter (inch)	Total length (ft)	stick up (ft)	Type	Soil condition	Tip-soil
1	09/03-04	3	15	24	66	2	closed	sand,clay,silt,	tip-sand
2	09-05/06	4	14	24	79.5	4	closed	clay,gravel	tip-clay
3	10-01/02	4	33	42	88.3	2	open	sand,clay	tip-clay
4	11-01/02	3.5	14	24	81.5	2	closed	sand,clay	tip-clay
5	12-01/02	4.5	31	42	97	4	open	sand,clay,gravel	tip-clay
6	12-03/04	3	30	42	103	2	open	sand,clay,gravel	tip-clay
7	12-05/06	4	28	14	98	3	open	sand,clay	tip-sand
8	22-03/04	2.8	6	14	57	5	closed	sand,clay	tip-sand
9	29-01/02	4	30	24	42	2	open	sand,clay	tip-clay
10	29-05/06	4	28	24	42.3	2	open	sand,clay	tip-clay
11	29-08/09	4	16	24	37	2	closed	sand,clay	tip-sand
12	30-01/02	3	26	42	105.5	5	open	sand,clay	tip-clay
13	30-03/04	3	55	42	105.5	5	open	sand,clay	tip-clay
14	31-03/04	4	42	24	65	5	closed	sand,clay	tip-sand
15	31-05/06	4	42	24	69	5	closed	sand,clay	tip-sand
16	31-07/08	4	49	24	61	5	open	sand,clay	tip-sand
17	31-09/10	4	38	24	65	5	closed	sand,clay	tip-sand
18	31-11/12	4	41	24	65	2	open	sand,clay	tip-sand
19	35-01/02	3	1	14	45.6	5	closed	sand	tip-sand
20	37-01/02	2.5	1	14	99.6	5	open	sand,clay	tip-rock
21	40-05	4.5	76	24	33	5	open	sand	tip-sand

Table 3-3—*Continued*

22	40-10/11	4.5	47	24	33	6	open	sand	tip-sand
23	41-01/02	3	6	16	97	6	open	sand	tip-sand
24	41-05/06	3	6	14	91	6	open	sand	tip-sand
25	41-07/08	3.8	2	16	101.5	6	open	sand	tip-sand
26	41-11/12	3.8	4	14	95.5	5	open	sand	tip-sand
27	77-01	3	22	24	40.1	5	open	sand,clay	tip-sand
28	77-02	3	21	24	42.7	5	open	sand,clay	tip-sand
29	79-07/08	3.5	168	16	109.5	5	open	clay	tip-clay
30	83-01	3	67	18	40.5	7.5	open	sand	tip- sand
31	85-01/02	3.5	10	24	47	5	open	sand,clay	tip-sand
32	86-01/02	3	25	24	43.5	0	open	sand,clay	tip-sand
33	95-03/04	3	13	24	68.5	5	open	sand,clay	tip-sand
34	96-01/02	3	50	16	64.4	5	open	sand,clay	tip-sand
35	96-03/04	3	50	16	63.9	5	open	sand,clay	tip-sand
36	97-03/04	2	17	24	66	3	open	sand,clay	tip-sand
37	98-01/02	4	35	24	97.7	5	open	sand,clay	tip-clay
38	98-03/04	4	33	24	96.7	5	open	clay	tip-clay
39	99-01/02	4.5	30	24	73.1	5	open	sand,clay	tip-sand
40	99-03/04	4.5	34	24	71.6	5	open	sand,clay	tip-sand
41	100-01/02	3.5	15	24	87	6	open	clay	tip-clay
42	109-01	3	5	10.75	35.5	3	closed	sand	tip-sand
43	114-02	2.8	7	12	43.1	4	closed	sand,silt	tip-silt
44	130-01	3.3	8	42	48.7	3	open	sand,silt	tip-silt
45	131-01	3	11	24	131.3	3	open	sand,gravel,cobbles	tip-gravel

For each investigated pile selected from the database, information provided from CALTRANS mainly focus on “key words”, “pile data”, “soil profile”, “soil properties” and “capacity”.

“key words” consists load test report number, data qualify factor, set-up days, specified pile type and soil type. “pile data” consists of pile length, stick-up length, diameter, wall thickness, Young’s modulus, sectional area and installation method. “soil profile” consist of soil stratification, soil type, water table depth, surface elevation, unit weight of excavation soil. “soil properties” includes undrained shear stress (for cohesion soil), SPT number (for cohesionless soil) for each layer. In addition, pile load tests were performed, corresponding data were included in “capacity”. During the pile load-settlement test, increasing load was applied on the pile head, and corresponding pile head settlement was measured and recorded. The ultimate load capacity of the pile was determined as measured capacity Q_m with corresponding pile settlement equals to 1 inch.

For example, one selected driven pile has a total length of 88.3 ft, 2 ft of which is stickup length above the ground surface, water table is met 5.7 ft below the ground surface, first 13.5 ft length below the ground surface is for casing. The soil profile where the pile has been driven can be plotted in Figure 3-3, each layered depth is shown in absolute depth below the ground surface and elevation heights. Also the parameters of soil layer are included, such as undrained shear strength $S_u$for clay layer, standard penetration blow counts N number for sandy soil layer and total unit weight. Those soil parameters can be used to calculate ultimate pile bearing capacities for different predicting methods.

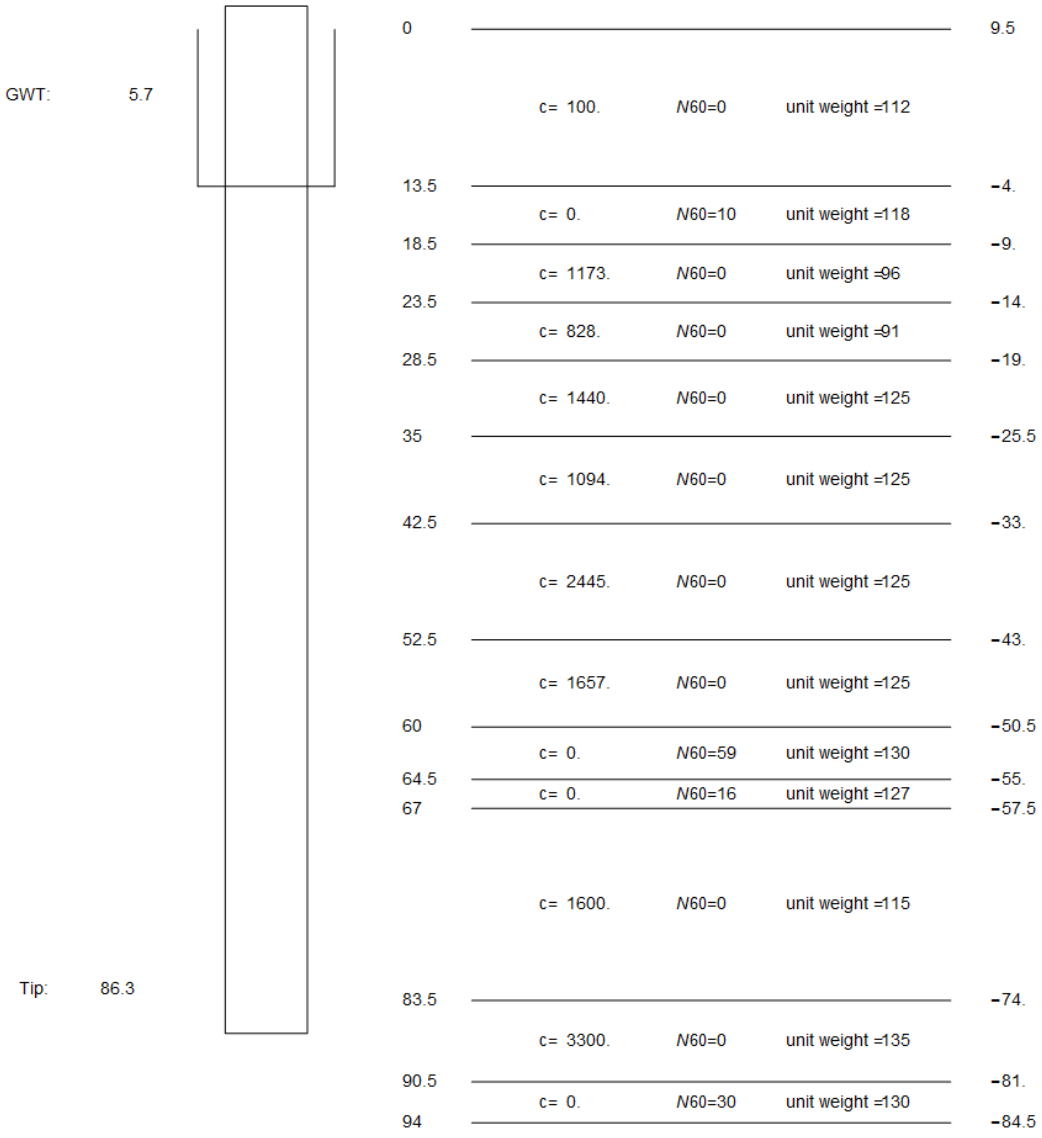

Figure 3-3 Example of a selected pile and corresponding soil condition from CALTRANS database

3.2 26 Pile Capacity Predicting Methods From CALTRANS

There have been several methods applied in geotechnical field for predicting ultimate axial bearing capacity, including traditional static methods, pile load tests, and dynamic analysis methods. In this thesis, static analysis, which based on soil properties obtained from local soil, has been selected to estimate pile resistance. Accordingly, In the Mathematica file which from CALTRANS, 6 methods are selected and used for calculating clay skin friction for pipe piles, 4 methods for skin friction in sand, 1 method for tip resistance in clay, 2 methods for tip resistance in sand. All the methods are tabulated as follows:

Table 3-4 Predicting methods used in Mathematica from CALTRANS

skin friction	clay	1	2	3	4	5	6
		Api25	Api33	Dennis	Tomlinson	Kraft	Karlsrud(β)
	sand	1	2	3	4		
		Nordlund	Apisand	Decourt	Olson		
tip	clay	API					
	sand	Nordlund	API				

Nordlund method for tip resistance calculation is preferred only when this method is conducted in sand layers for skin friction, otherwise, using API method for tip resistance in sand. Those methods above generates 24 different ways to predict capacity. In addition, CATRANS currently prefers Tomlinson and Nordlund methods for small diameter piles, API method for large diameter piles, recommended diameter threshold 16 inch and 24 inch will be checked, a summary of the design methods is presented below:

Table 3-5 Predicting methods combination from CALTRANS

NO.	Skin		Tip	
	sand	clay	sand	clay
1	Nordlund	Api25	Nordlund	API
2	Nordlund	Api33	Nordlund	API
3	Nordlund	Dennis	Nordlund	API
4	Nordlund	Tomlinson	Nordlund	API
5	Nordlund	Kraft	Nordlund	API
6	Nordlund	Karlsrud	Nordlund	API
7	Api	Api25	API	API
8	Api	Api33	API	API
9	Api	Dennis	API	API
10	Api	Tomlinson	API	API
11	Api	Kraft	API	API
12	Api	Karlsrud	API	API
13	Decourt	Api25	API	API
14	Decourt	Api33	API	API
15	Decourt	Dennis	API	API
16	Decourt	Tomlinson	API	API
17	Decourt	Kraft	API	API
18	Decourt	Karlsrud	API	API
19	Olson	Api25	API	API
20	Olson	Api33	API	API
21	Olson	Dennis	API	API
22	Olson	Tomlinson	API	API
23	Olson	Kraft	API	API
24	Olson	Karlsrud	API	API
25	D≤16 in, method 4; D>16 in, method 7			
26	D≤24 in, method 4; D>24 in, method 7			

CALTRANS 16 (method 25) is using Tomlinson and Nordlund methods (method 4) when pile diameter is equal or less than 16 inch, otherwise, API method (method 7) will be used. CALTRANS 24 (method 26) increases threshold diameter from 16 inch to 24 inch.

3.3 Static Capacity Methods for Pile Design

The ultimate axial resistance (Q_u) of a driven pile consists of the end-bearing resistance (Q_b) and the skin frictional resistance (Q_s). The ultimate driven pile resistance can then be calculated using the following equation:

$$Q_u = Q_b + Q_s = q_b \cdot A_b + \sum_{i=1}^{n} f_i A_{si} \quad (3\text{-}1)$$

Where, q_b is the unit tip bearing resistance, A_b is the cross section area of the pile tip, f_i is the average unit skin friction of the soil layer i, A_{si} is the area of the pile shaft area interfacing with layer i, and n is the number of soil layers along the pile.

3.3.1 Skin friction and end bearing in cohesive soil

3.3.1.1 Tomlinson 1980 (α-Method)

For driven pile in cohesive soil, compute the unit skin resistance f_s in ksf

$$f_s = Ca = \alpha * c_u \quad (3\text{-}2)$$

In which α is an empirical adhesion factor for reduction of the average undrained shear strength C_u, of undisturbed clay along the embedded length of the pile. The coefficient α depends on the nature and strength of the clay, pile dimension, method of pile installation, and time effects. The values of α vary within wide limits and decrease rapidly with increasing shear strength.

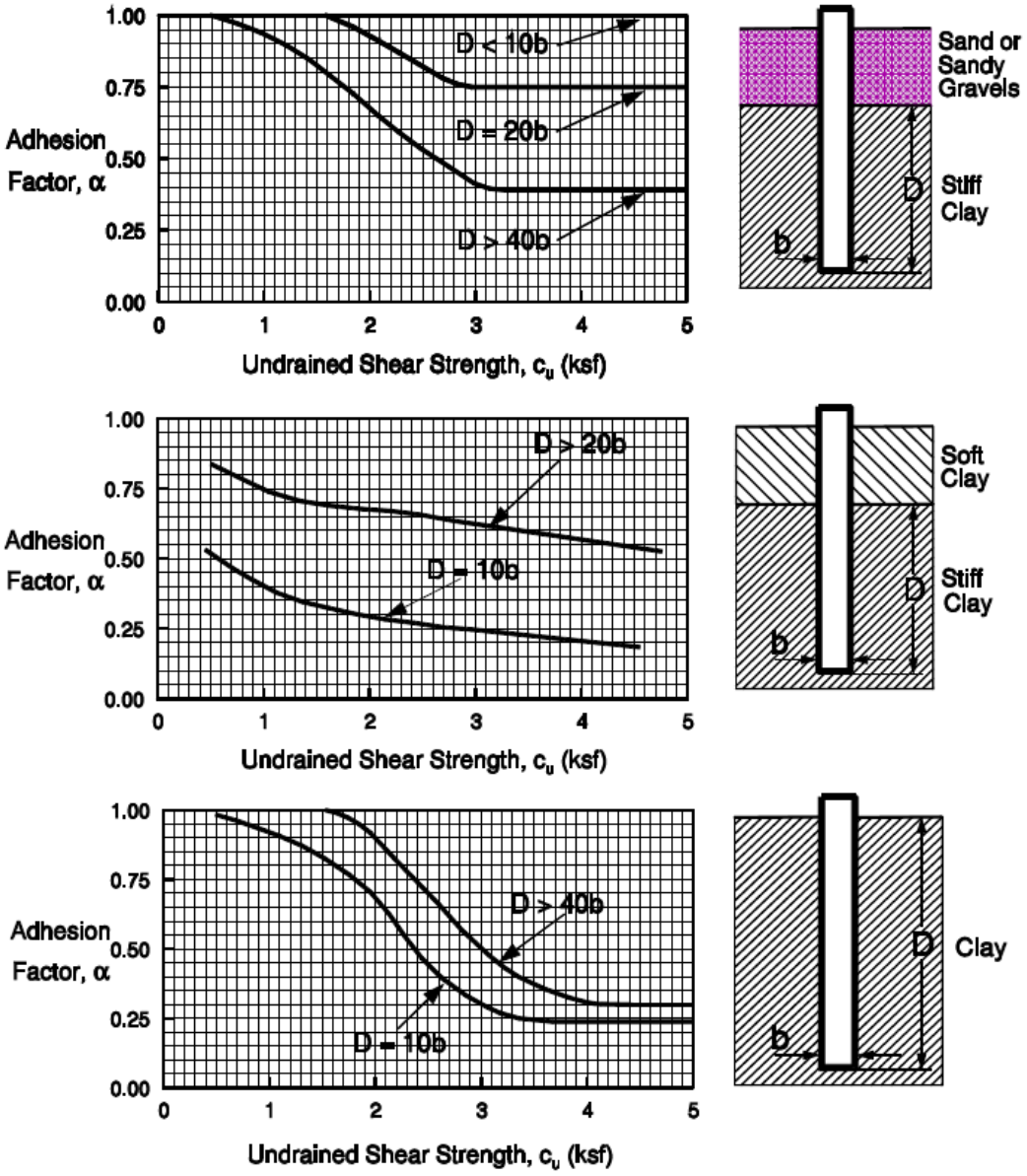

Figure 3-4 Adhesion Factors for Driven Piles in Clay- US Unis (Tomlinson 1980)

3.3.1.2 API 25 and API 33

In the API method, α is correlated with S_u/σ'_{vo} rather than Su as in Tomlinson's α-methods. For driven piles in cohesive soil, side resistance, f, in lb/ft^2 (kPa) at any point along the pile may be calculated by following equations (API 2005):

$$f = \alpha s_u \quad (3\text{-}3)$$

Where

α = a dimensionless factor,

s_u = undrained shear strength of the soil at the point in question.

The factor, α, can be computed by the equations:

$$\alpha = {\varphi_{nc}}^{0.5} * \varphi^{-0.5} \varphi \leq 1$$

$$\alpha = {\varphi_{nc}}^{0.5} * \varphi^{-0.25} \varphi > 1 \quad (3\text{-}4)$$

$\varphi = \frac{Su}{\sigma'_{vo}}$ for the point of interest

In API 25 method, φ_{nc} is assumed to be 0.25, in API 33 method, φ_{nc} is assumed to be 0.33.

3.3.1.3 Dennis method

The side resistance in clay in Dennis method is calculated in the similar function as the Tomlinson method in which α is correlated to S_u. Unit side resistance is calculated using the equation below:

$$f = \alpha s_u F_L \quad (3\text{-}5)$$

α is determined from Figure 3-5.

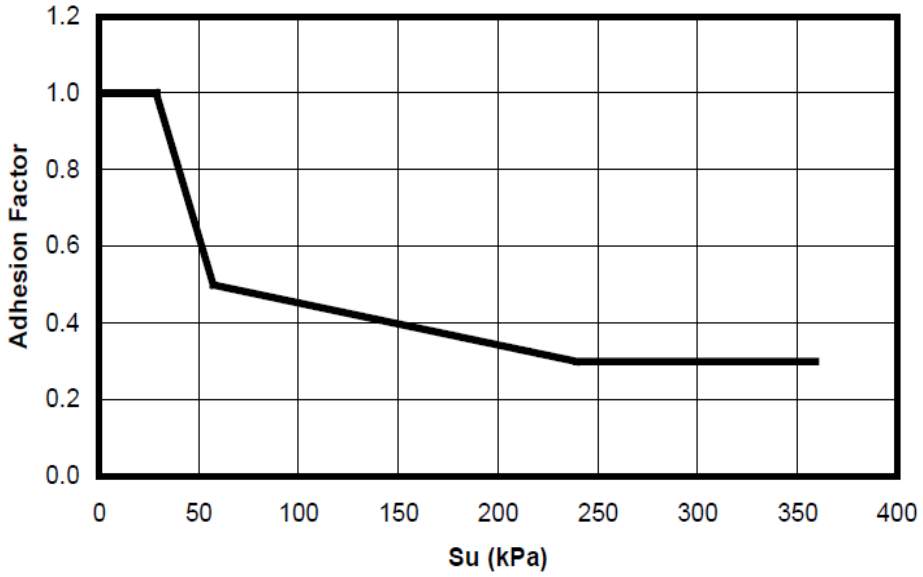

Figure 3-5 Adhesion Factors for Piles in Clay (Dennis and Olson 1983a)

F_L is a correction factor for pile penetration which can be obtained from Figure 3-6

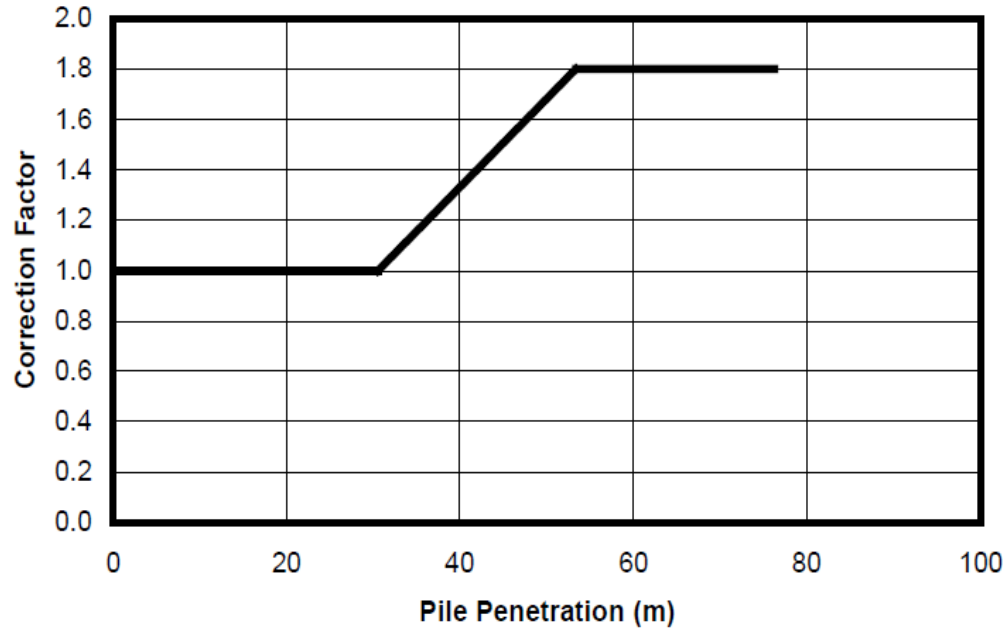

Figure 3-6 Correction Factor for Pile Penetration (Dennis and Olson 1983a)

3.3.1.4 Kraft et al. 1981(λ- Method)

Unit side resistance is calculated using equation (Kraft et al. 1981) below:

$$f = \lambda\,(\sigma'_{vo} + 2s_u) \qquad (3\text{-}6)$$

$\lambda = 0.296 - 0.032\ln(L)$, for $s_u/\sigma'_{vo} \leq 0.4$

$\lambda = 0.488 - 0.078\ln(L)$, for $s_u/\sigma'_{vo} > 0.4$

In which L is pile penetration depth.

3.3.1.5 Karlsrud 1999 (β-Method)

The method for piles in clay currently recommended by Norwegian Geotechnical Institute (NGI) is a β-Method(Karlsrud 1999), in which unit side resistance is defined as:

$$f = \beta\sigma'_{vo} \qquad (3\text{-}7)$$

β is determined from OCR using the relationship in figure below:

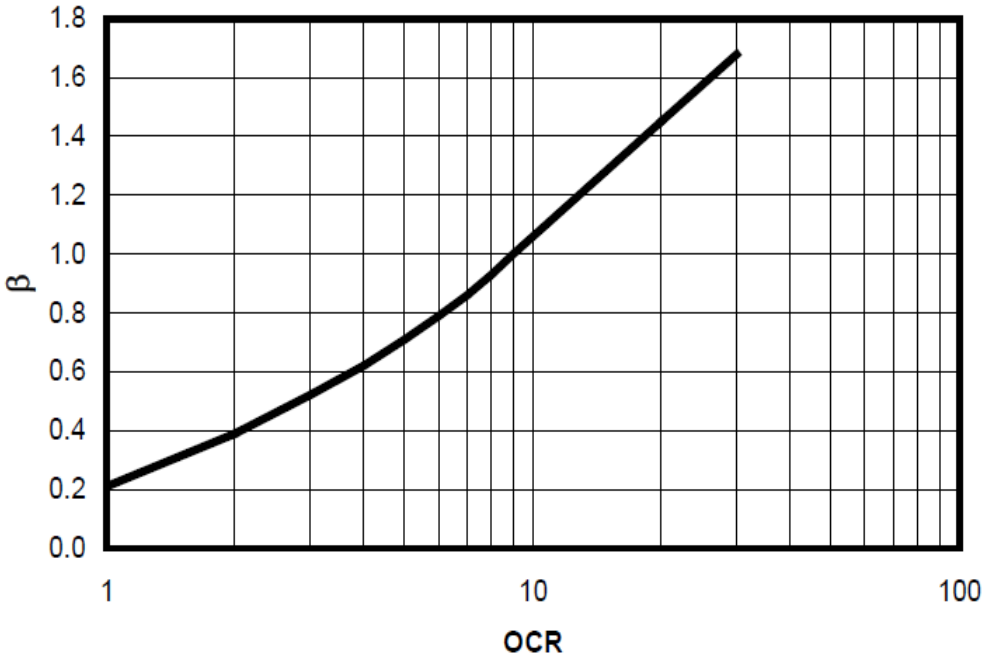

Figure 3-7 Relationship between β and OCR (Karlsrud 1999)

OCR is determined from the correlations with s_u/σ'_{vo} using equation:

$$OCR = \left(\frac{s_u/\sigma'_{vo}}{0.32}\right)^{1.25} \quad (3\text{-}8)$$

3.3.1.6 API method for tip resistance:

The American Petroleum Institute (API) (2005) provides design recommendations for piles end bearing in cohesive soils, the unit end bearing q, in lbs/ft^2 (kPa), may be computed by the equation

$$q = 9\, s_u \quad (3\text{-}9)$$

3.3.2 Skin friction and end bearing in cohesionless soil

3.3.2.1 API method

Unit side resistance is calculated using equation followed by American Petroleum Institute (API) (2005):

$$f = K\sigma'_{vo}\tan(\delta) \leq f_{lim} \quad (3\text{-}10)$$

Where

K = coefficient of lateral earth pressure (ratio of horizontal to vertical normal effective stress),

σ'_{vo} = effective overburden pressure lb/ft^2 (kPa) at the point in question,

δ = friction angle between the soil and pile wall.

For open-ended pipe piles driven unplugged, it is usually appropriate to assume K_{as} equals to 0.8 for both tension and compression loadings. Values of K for full displacement piles (plugged or closed end) may be assumed to be 1.0. The values of δ and f_{lim} are determined in Table 3-6.

Table 3-6 Design Parameters for Cohesionless Siliceous Soil (API 2005)

Soil Type	Range of N_{corr} (blows/305 mm)	δ(degrees)	$f_{s,lim}$(kPa)
Gravel	0 – 4	20	67
	5 – 10	25	81.3
	11 – 30	30	95.7
	over 30	35	114.8
Sand	0 – 4	15	47.8
	5 – 10	20	67
	11 – 30	25	81.3
	31 – 50	30	95.7
	over 50	35	114.8

3.3.2.2 Olson method(Olson 1990)

Olson's 1990 method is actually a revision of the API method for piles in sand, follows the same pattern as the API method for the calculation of unit side resistance.

$$f = K\sigma'_{vo}\tan(\delta) \leq f_{lim} \qquad (3\text{-}11)$$

K is determined as a function of N_{corr} using equations:

$K = 0.16 + 0.015N_{corr}$ for non-displacement piles

$K = 0.70 + 0.015N_{corr}$ for full-displacement piles

The values of δ and f_{lim} are determined as

Table 3-7 Soil Properties (Olson 1990)

Soil Type	Range of N_{corr} (blows/305 mm)	δ(degrees)	$fs_{,lim}$(kPa)
Gravel	0 – 4	20	67
	5 – 10	25	81.3
	11 – 30	30	95.7

Table 3-7—*Continued*

	over 30	35	114.8
Sand	0 – 4	20	47.8
	5 – 10	30	52.7
	11 – 30	35	91
	31 – 50	40	124.5
	50 – 100	40	177.2
	over 100	40	181.9

3.3.2.3 Decourt method

Decourt (Decourt 1982) presents a simple SPT-based method for the prediction of side resistance in both clay and sand. Unit side resistance is calculated using:

$$f = 68.9N + 208.8\ (psf) \quad (3 \leq N \leq 50) \qquad (3\text{-}12)$$

3.3.2.4 Nordlund Method

For a pile of uniform cross section (ω=0), the Nordlund equation(Nordlund 1963) for skin friction in sand layer becomes:

$$\mathrm{f} = \mathrm{K_\delta p_d C_F}\ \sin\delta \qquad (3\text{-}13)$$

In which

K_δ = Coefficient of lateral earth pressure at depth d.

C_F = Correction factor for K_δ when $\delta \neq \varphi$.

δ = Friction angle between pile and soil.

p_d = Effective overburden pressure at the center of depth increment d.

The soil friction angle φ influences most of the calculations in the Nordlund method. In the absence of laboratory test data, φ can be estimated from corrected SPT N' values.

Table 3-8 Empirical values for φ, Dr, and unit weight of granular soil based on N'(Nordlund 1963)

Description	Very Loose	Loose	Medium	Dense	Very Dense
Relative density D_r	0 - 0.15	0.15 - 0.35	0.35 - 0.65	0.65 - 0.85	0.85 - 1.00
Corrected Standard Penetration N' value	0 to 4	4 to 10	10 to 30	30 to 50	50+
Approximate angle of internal friction ϕ *	25 - 30°	27 - 32°	30 – 35°	35 - 40°	38 - 43°
Range of approximate moist unit weight γ kN/m^3 (lb/ft^3)	11.0 - 15.7 (70 - 100)	14.1 - 18.1 (90 - 115)	17.3 - 20.4 (110 - 130)	17.3 - 22.0 (110 - 140)	20.4 - 23.6 (130 - 150)

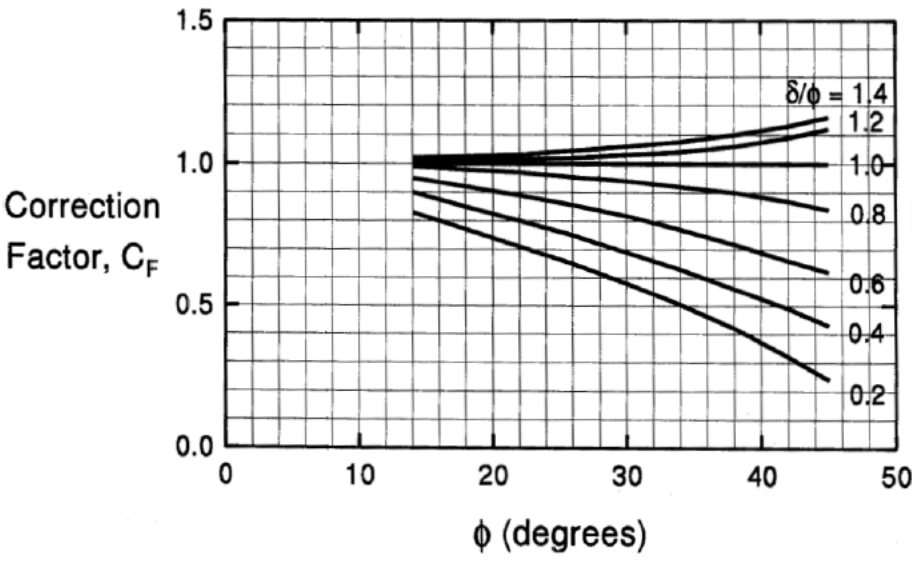

Figure 3-8 Correction factors (C_f) for coefficient of lateral stress **(K_δ)** (after Nordlund, 1979)

Table 3-9 K_δ for non-tapered piles (Nordlund 1963)

φ	Volume of soil displaced per unit length (ft^3/ft)								
	0.1	0.3	0.5	0.7	1	3	5	7	10
25	0.70	0.77	0.80	0.83	0.85	0.92	0.95	0.98	1.00
26	0.73	0.82	0.86	0.88	0.91	1.00	1.04	1.06	1.09
27	0.76	0.86	0.91	0.94	0.97	1.07	1.12	1.15	1.18
28	0.79	0.9	0.96	0.99	1.03	1.14	1.2	1.23	1.27
29	0.82	0.95	1.01	1.05	1.09	1.22	1.28	1.32	1.36
30	0.85	0.99	1.06	1.10	1.15	1.29	1.36	1.40	1.45
31	0.91	1.08	1.16	1.21	1.27	1.44	1.52	1.57	1.63
32	0.97	1.17	1.26	1.32	1.39	1.59	1.68	1.74	1.81
33	1.03	1.26	1.37	1.44	1.51	1.74	1.85	1.92	1.99
34	1.09	1.35	1.47	1.55	1.63	1.89	2.01	2.09	2.17
35	1.15	1.44	1.57	1.66	1.75	2.04	2.17	2.26	2.35
36	1.26	1.61	1.78	1.89	2.00	2.35	2.52	2.63	2.74
37	1.37	1.79	1.99	2.11	2.25	2.67	2.87	2.99	3.13
38	1.48	1.97	2.19	2.34	2.50	2.99	3.21	3.36	3.52
39	1.59	2.14	2.4	2.57	2.75	3.30	3.56	3.73	3.91
40	1.7	2.32	2.61	2.800	3.00	3.62	3.91	4.10	4.30

3.3.2.5 Tip Nordlund method

Tip resistance using Nordlund method can be presented as:

$$q_b = \alpha_t \mathrm{N'}_q \mathrm{p_t} \qquad (3\text{-}14)$$

α_t = Dimensionless factor (dependent on pile depth-width relationship)

N'_q = Bearing capacity factor.

p_t = Effective overburden pressure at the pile toe.

α_t coefficient can be determined based on pile length to diameter ratio, N'_q can be determined by φ angle near pile toe:

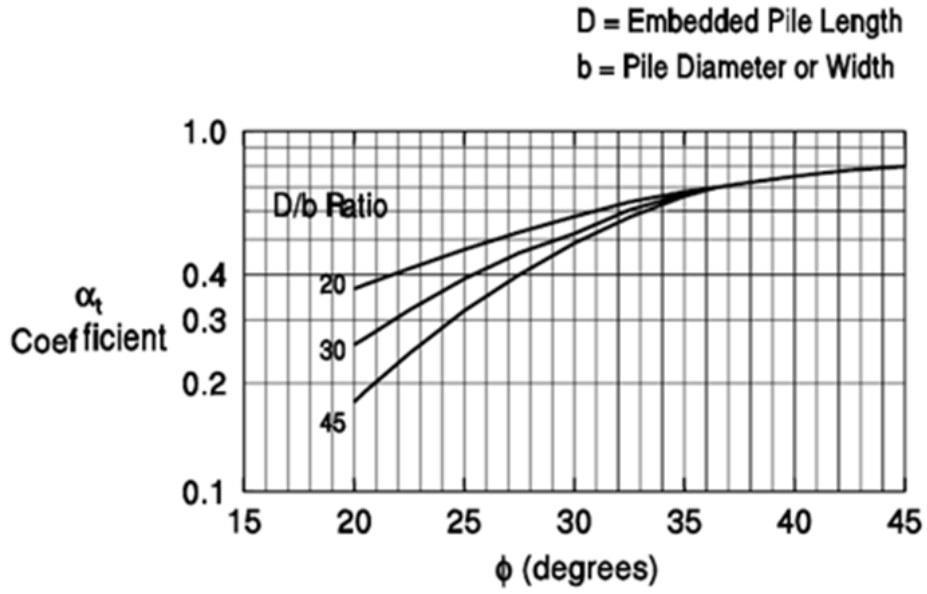

Figure 3-9 Chart for Estimating α_t Coefficient and Bearing Capacity Factor N'_q (Chart modified from Bowles, 1977)

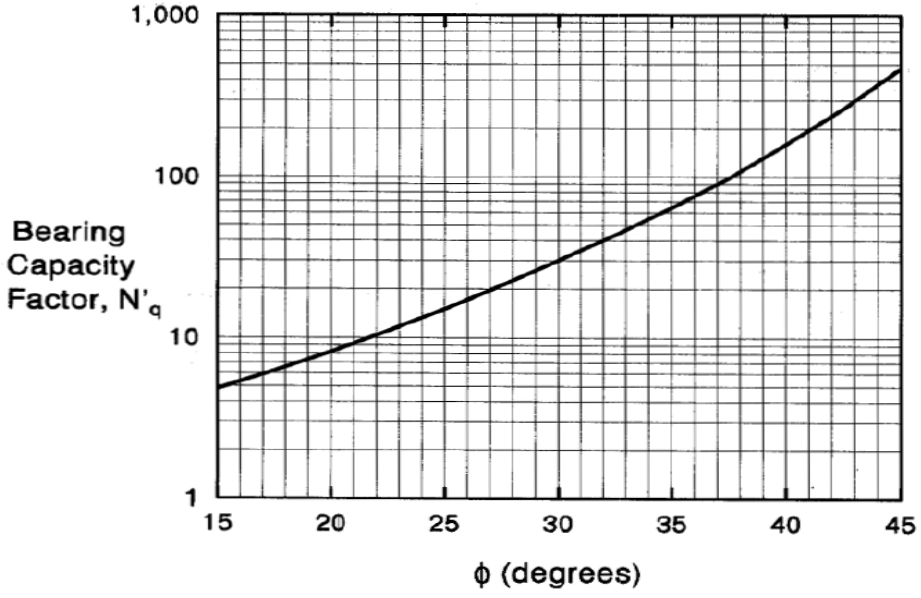

Figure 3-10 Chart for Estimating α_t Coefficient and Bearing Capacity Factor N'_q (Chart modified from Bowles, 1977)

3.3.2.6 API method for Tip resistance in sand

$$q_b = N_q \sigma'_{vo} \leq q_{lim} \quad (3\text{-}15)$$

N_q and q_{lim} can be determined from Table 3-10.

Table 3-10 API recommendations for tip resistance in siliceous soil (API 1993)

Soil Type	Range of N_{corr}(blows/305 mm)	δ(degrees)	N_q	q_{lim}(kips)
Sand	0 – 4	15	8	40
	5 – 10	20	12	60
	11 – 30	25	20	100
	31 – 50	30	40	200
	over 50	35	50	250

Chapter 4

EVALUATION OF 26 DESIGN METHODS FOR AXIL PILE CAPACITY

This chapter presents an evaluation of the performance of 26 methods in predicting bearing capacity of steel pipe piles driven into California soil. In this thesis, predicted bearing capacity Q_c is obtained from static analysis, measured bearing capacity Q_m is coming from pile load test. All these pile, soil, load test information are collected from CALTRANS database in a proper format of Mathematica file.

In order to assess the performance of design methods, pile capacity predicted from the 26 static prediction methods can be compared with measured pile capacity from load test. A systematic evaluation method based on statistical analysis of predicted and measured pile capacity was used to rank the 26 static predicting methods. This evaluation method considers the best fit line of Q_c and Q_m, the arithmetic mean and standard deviation of Q_c/Q_m, the cumulative probability of Q_c/Q_m, and the histogram and log-normal distribution of Q_c/Q_m.

4.1 Evaluation Criteria

The primary objective of this evaluation study is to make an assessment of the 26 predict methods based on their accuracy of predicting ultimate bearing capacity of pipe piles. In order to achieve this goal, the relationship between Q_c and Q_m is analyzed for each predicting method.

Generally, the accuracy of a prediction method can be estimated by the ratio of predicted capacity to the measured capacity, which is always greater than 0. The predict method under-predicts the measured capacity when $Q_c/Q_m<1$, and over-predicts the measured capacity when $Q_c/Q_m>1$ (Abu-Farsakh and Titi 2004). It is considered to be a perfect fit when $Q_c/Q_m =1$. In statistical analyses, the mean μ and standard deviation σ are the important indicators of accuracy and precision of each prediction method. An

ideal situation will give mean of Q_c/Q_m equals to 1, and standard deviation σ equals to 0, respectively, showing the predicted capacity is exactly same as the measured pile capacity for each single pile. In reality, however, the predicting method with mean of Q_c/Q_m closer to 1 and standard deviation σ closer to 0 would be considered a good prediction. Log-normal distribution is imposed in this study (Briaud and Tucker 1988) to analysis the distribution of Q_c/Q_m values of each method since the value range of Q_c/Q_m is not symmetric around 1. Also the probability was determined and calculated based on the area covered underneath the log-normal probability density function (PDF) curve within Q_c/Q_m range from 0.8 to 1.2.

In order to rank the performance of 26 different methods for predicting the compression axial capacity of pipe piles, an evaluation scheme using 4 different criteria has been introduced in this study. All the predicting methods were ranked under each single criterion based on their prediction accuracy, then an overall rank index (RI) was introduced to quantify the overall performance of each predicting method. The final rank would be made based on rank index RI with corresponding to performances in all these 4 criteria. Rank index RI is defined as the sum of the ranks from those four criteria (RI=R1+R2+R3+R4), the lower the rank index, the better and more accurate the performance of the predicting method. The following evaluation criteria were used in this study (Abu-Farsakh and Titi 2004):

The parameters from equations of the best-fit line of estimated Q_c versus measured capacity Q_m with the corresponding coefficient of determination (R^2);

The arithmetic mean (μ) and standard deviation (σ) for Q_c/Q_m values;

The 50 and 90% cumulative probabilities (P_{50} and P_{90}) of Q_c/Q_m values;

The 20% accuracy level obtained from the histogram and log-normal distribution of Q_c/Q_m values.

4.1.1 Criterion 1

The estimated pile capacity Q_c were plotted against the measured capacity Q_m in Figure 4-1 to Figure 4-24. For each predicting method, regression analysis was conducted to obtain best-fit line for Q_c/Q_m. The fitting relationship Q_c/Q_m which was presented as slope of the fitting line, and the corresponding coefficient of determination (R^2) which shows how well data fit this statistical model can be determined for each capacity estimating method. A method with a best fitting slope close to 1 and R^2 also close to 1 is considered a good predicting method.

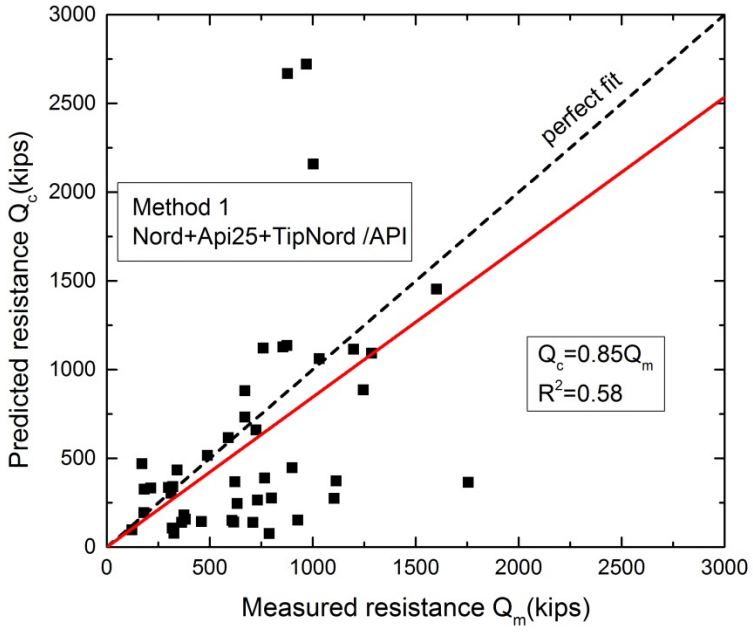

Figure 4-1 Estimated Q_c versus measured Q_m in Method 1

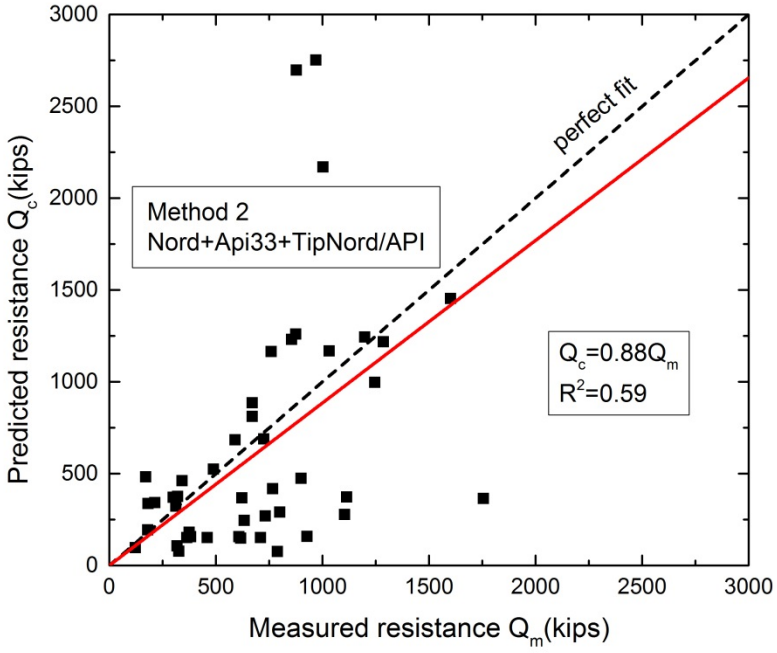

Figure 4-2 Estimated Q_c versus measured Q_m in Method 2

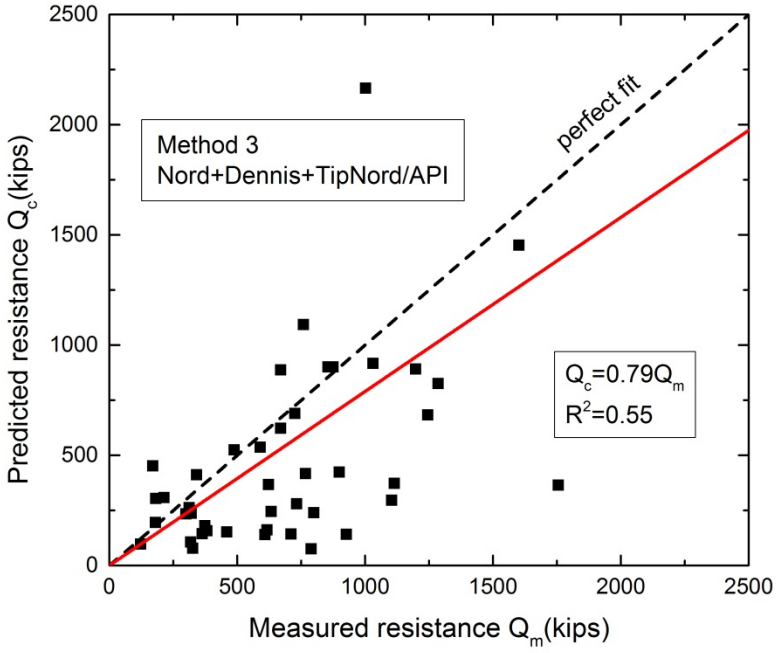

Figure 4-3 Estimated Q_c versus measured Q_m in Method 3

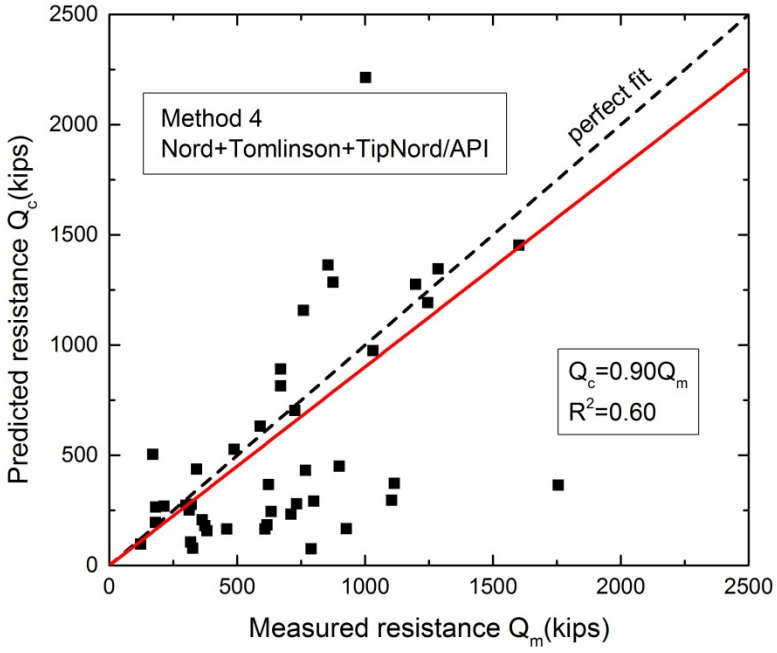

Figure 4-4 Estimated Q_c versus measured Q_m in Method 4

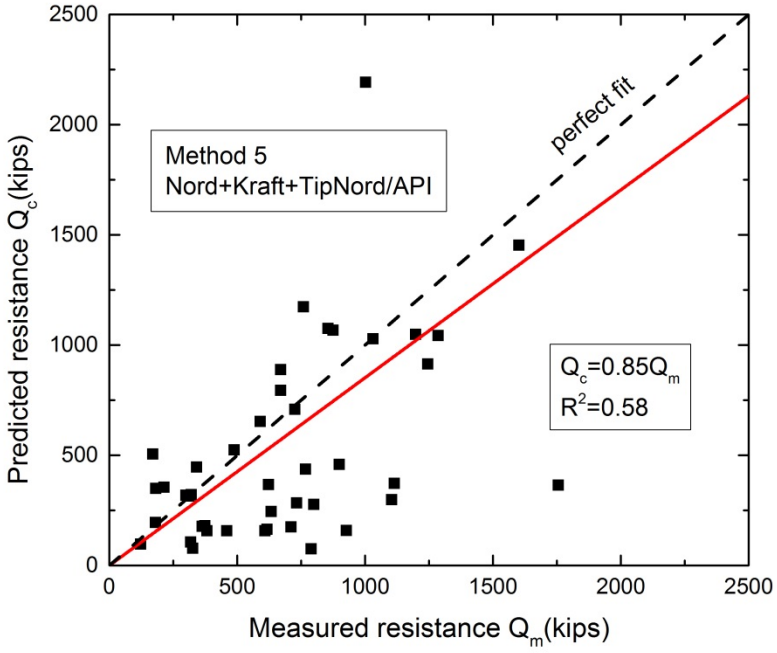

Figure 4-5 Estimated Q_c versus measured Q_m in Method 5

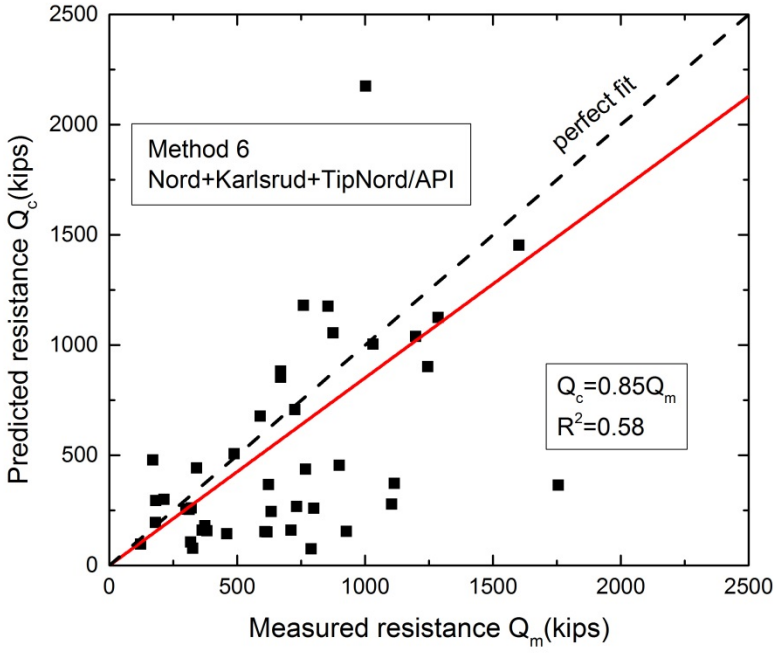

Figure 4-6 Estimated Q_c versus measured Q_m in Method 6

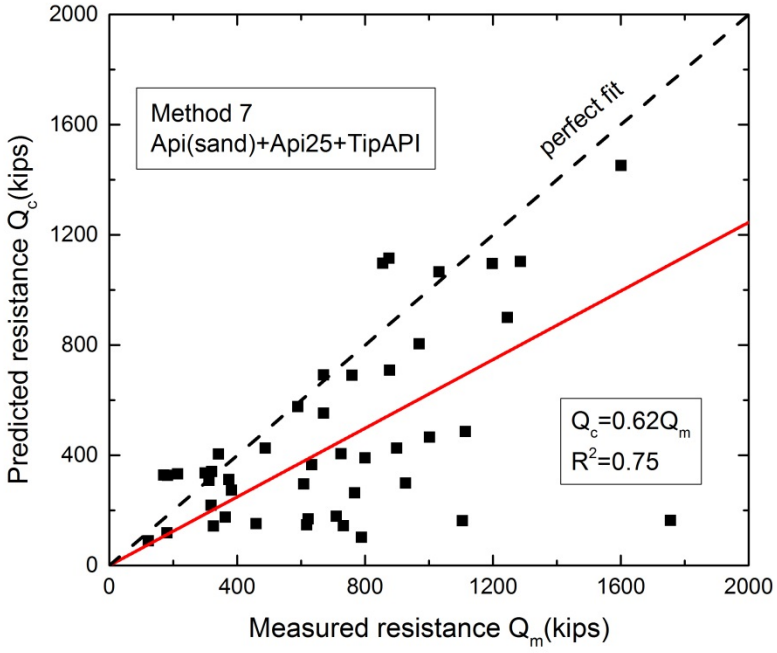

Figure 4-7 Estimated Q_c versus measured Q_m in Method 7

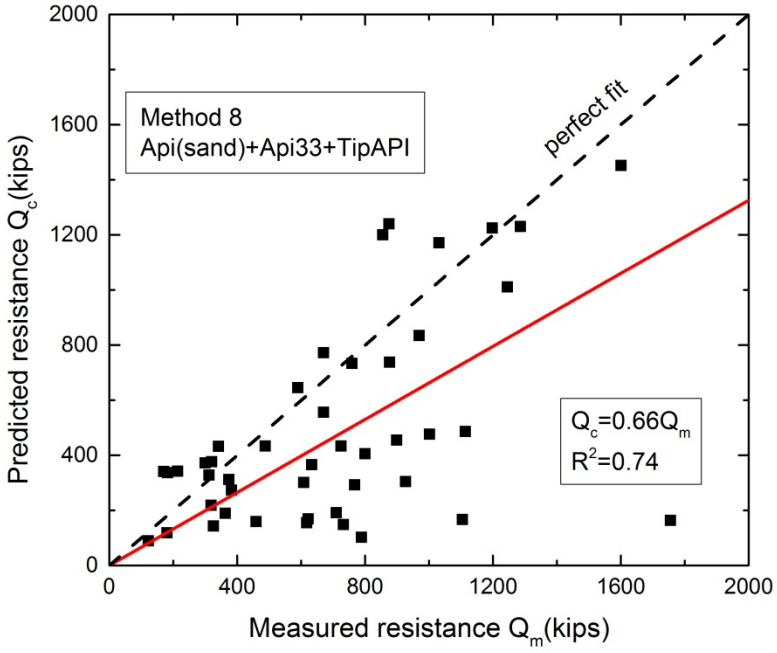

Figure 4-8 Estimated Q_c versus measured Q_m in Method 8

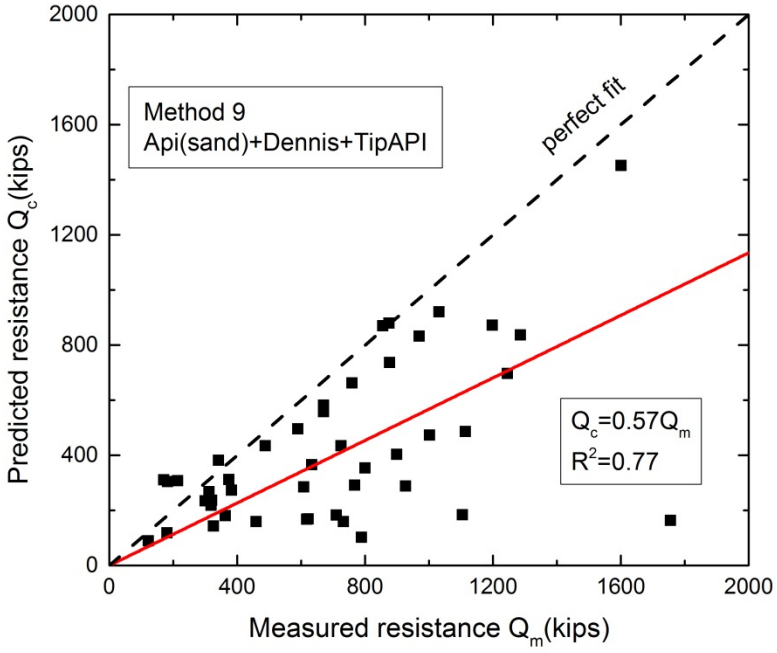

Figure 4-9 Estimated Q_c versus measured Q_m in Method 9

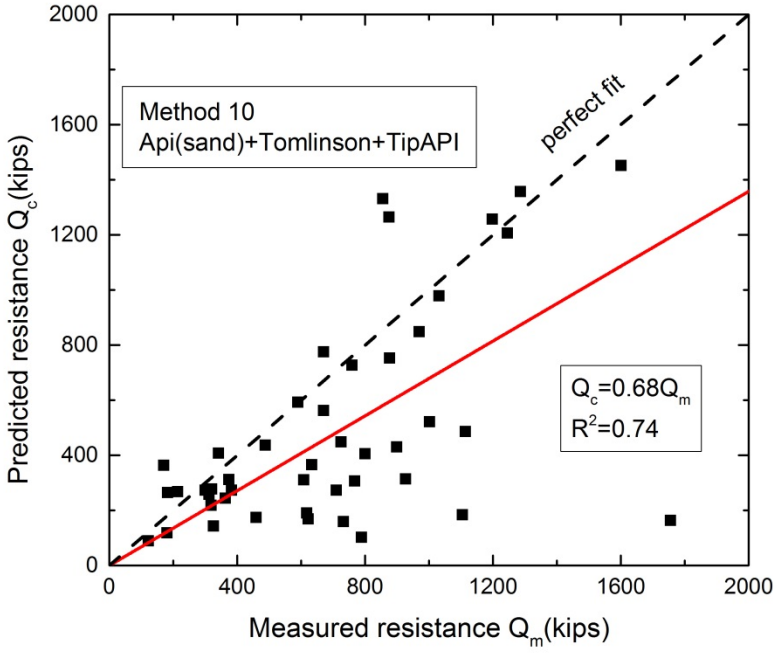

Figure 4-10 Estimated Q_c versus measured Q_m in Method 10

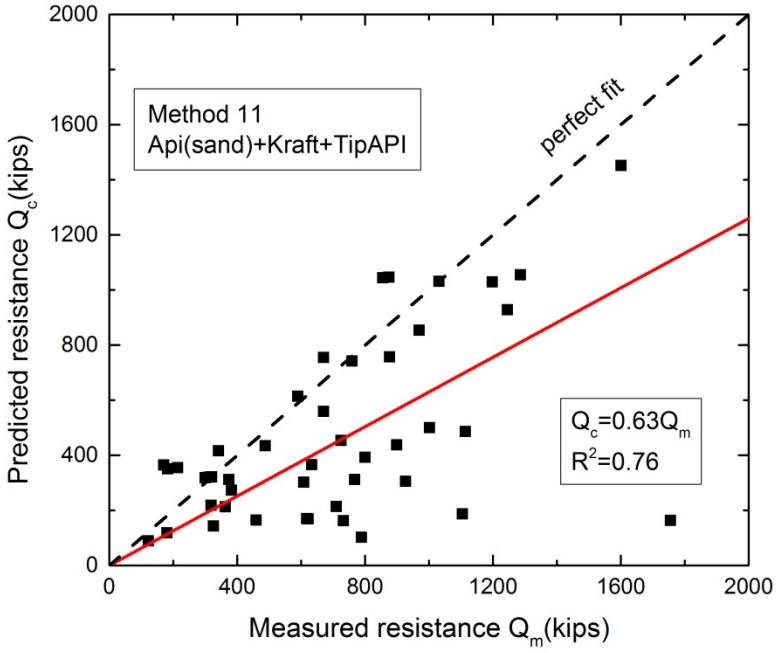

Figure 4-11 Estimated Q_c versus measured Q_m in Method 11

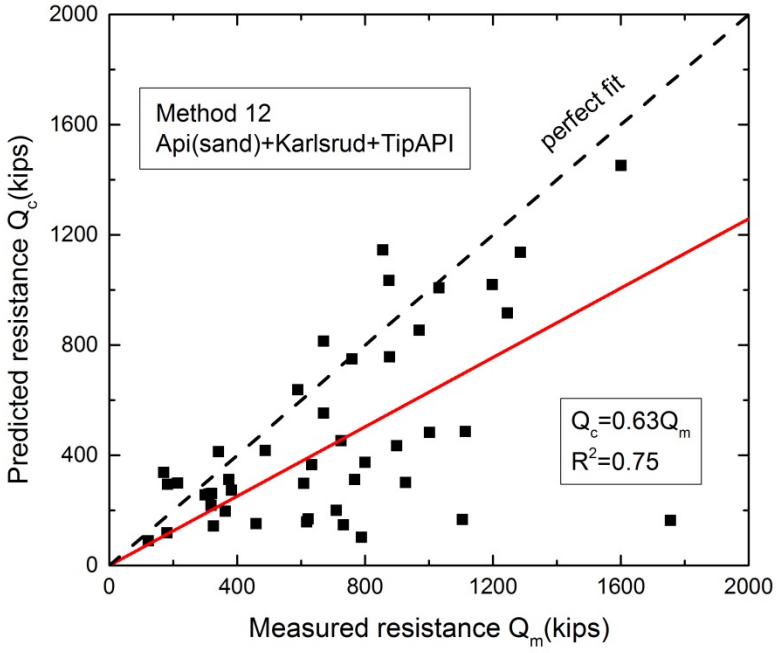

Figure 4-12 Estimated Q_c versus measured Q_m in Method 12

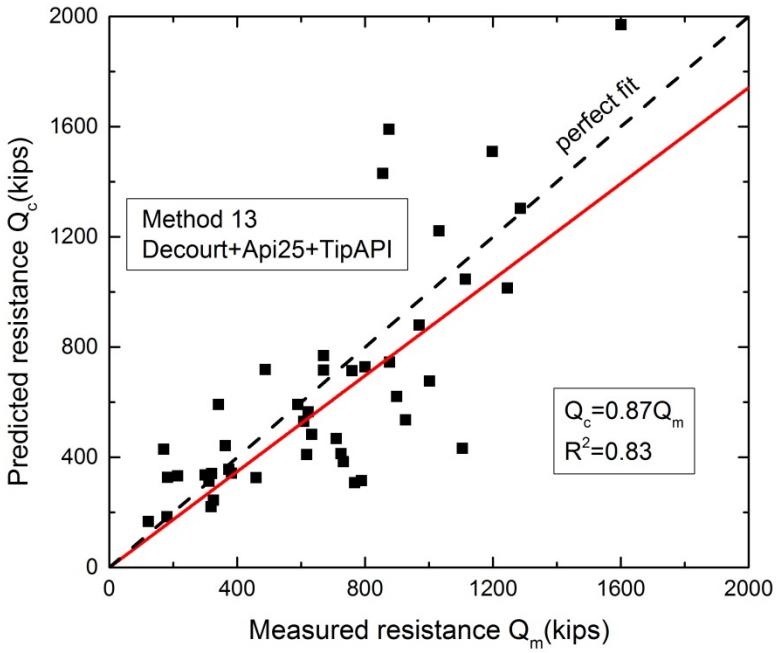

Figure 4-13 Estimated Q_c versus measured Q_m in Method 13

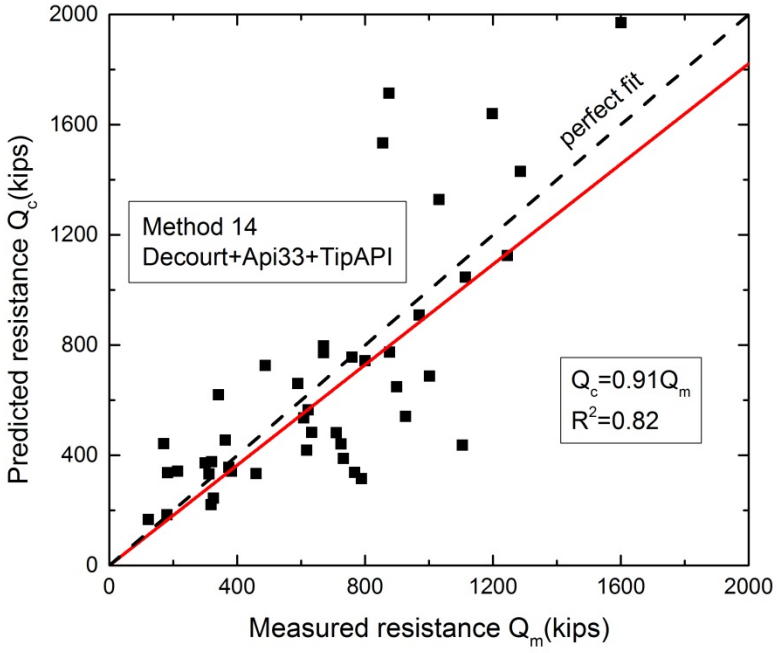

Figure 4-14 Estimated Q_c versus measured Q_m in Method 14

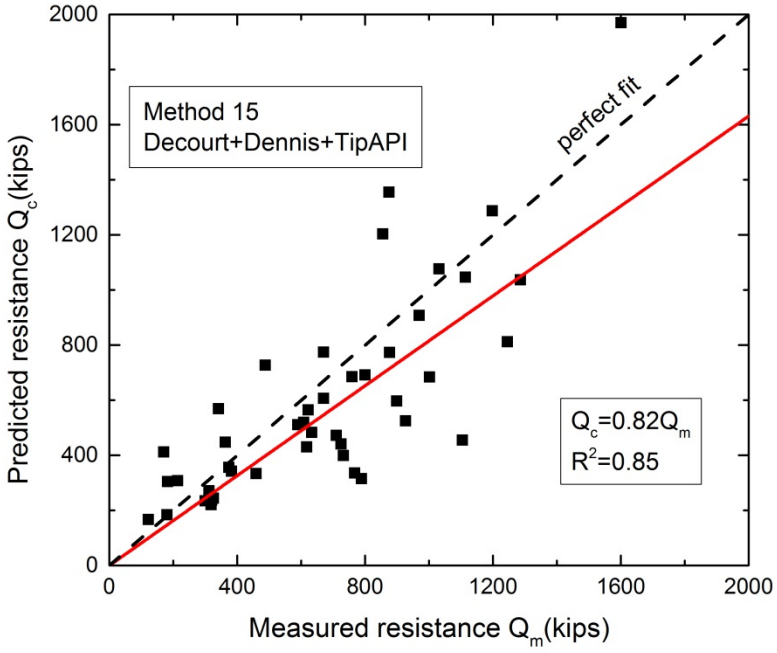

Figure 4-15 Estimated Q_c versus measured Q_m in Method 15

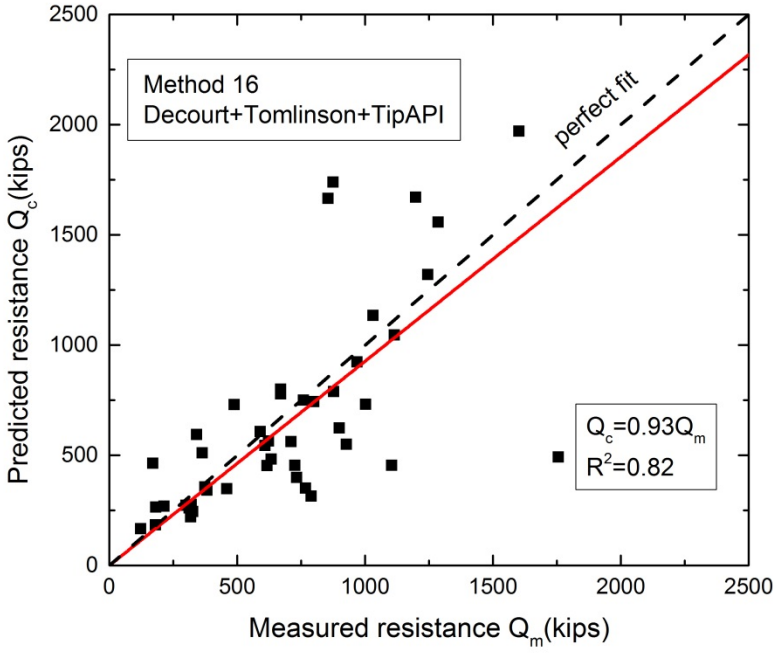

Figure 4-16 Estimated Q_c versus measured Q_m in Method 16

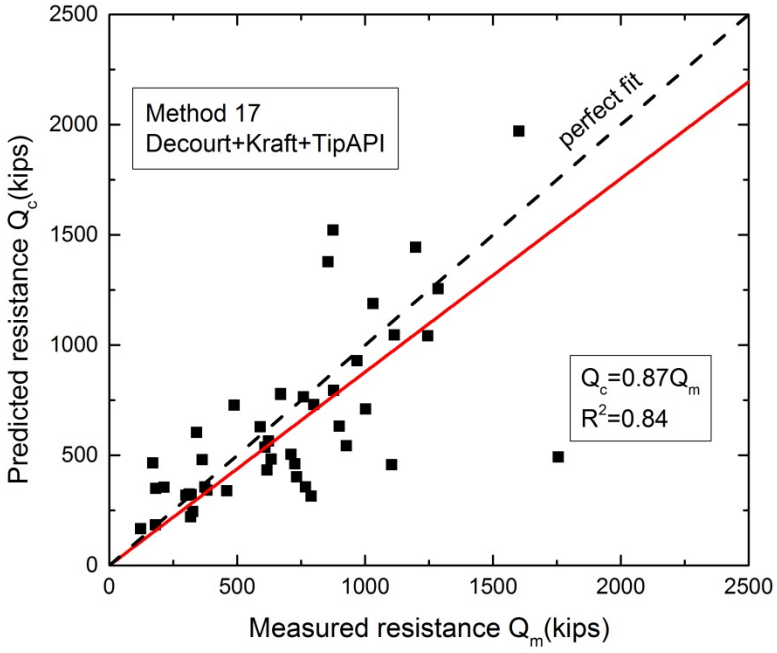

Figure 4-17 Estimated Q_c versus measured Q_m in Method 17

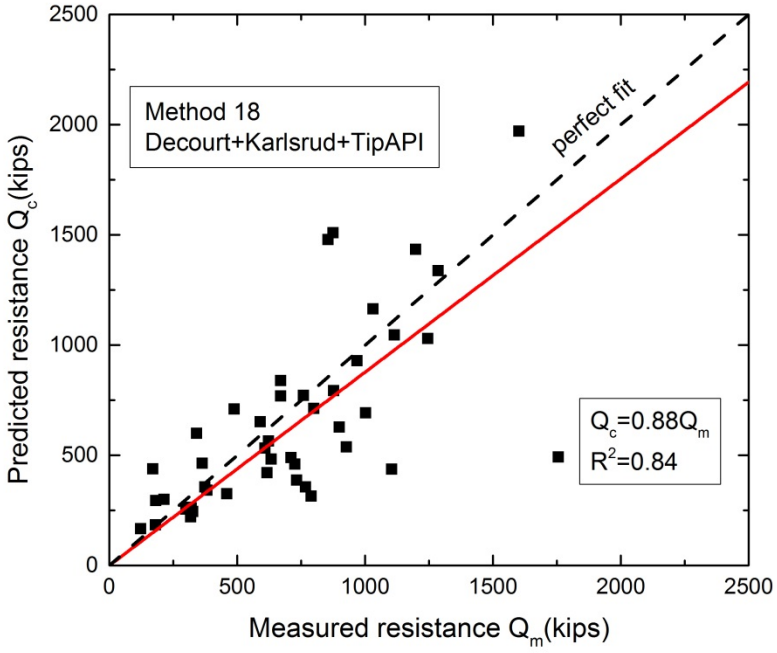

Figure 4-18 Estimated Q_c versus measured Q_m in Method 18

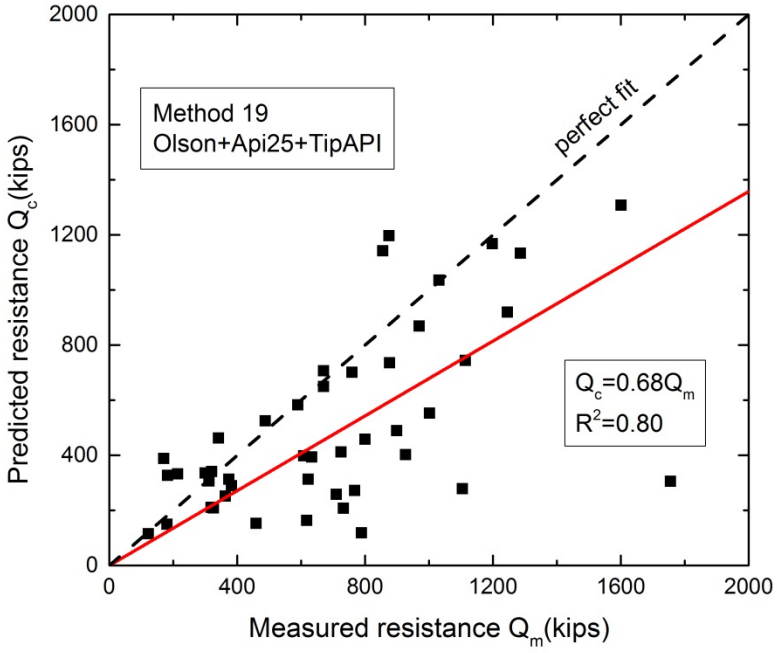

Figure 4-19 Estimated Q_c versus measured Q_m in Method 19

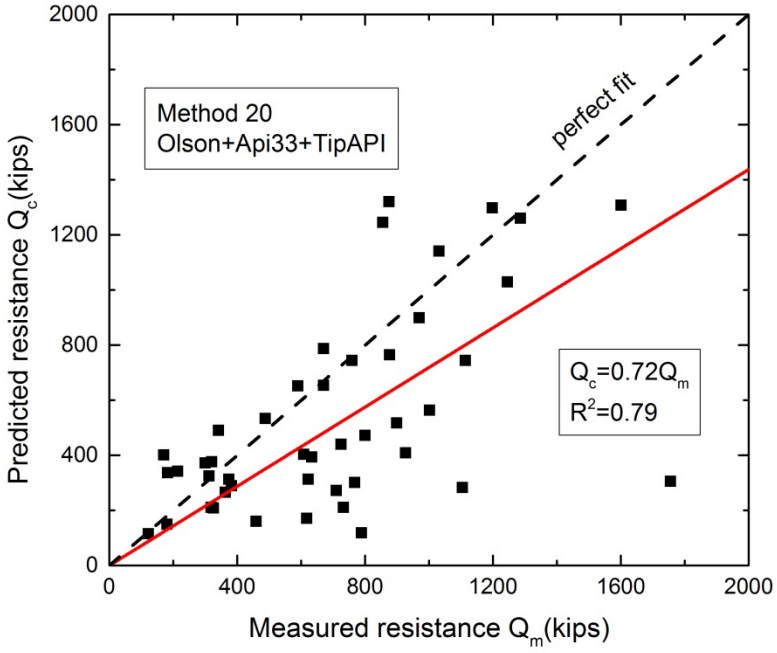

Figure 4-20 Estimated Q_c versus measured Q_m in Method 20

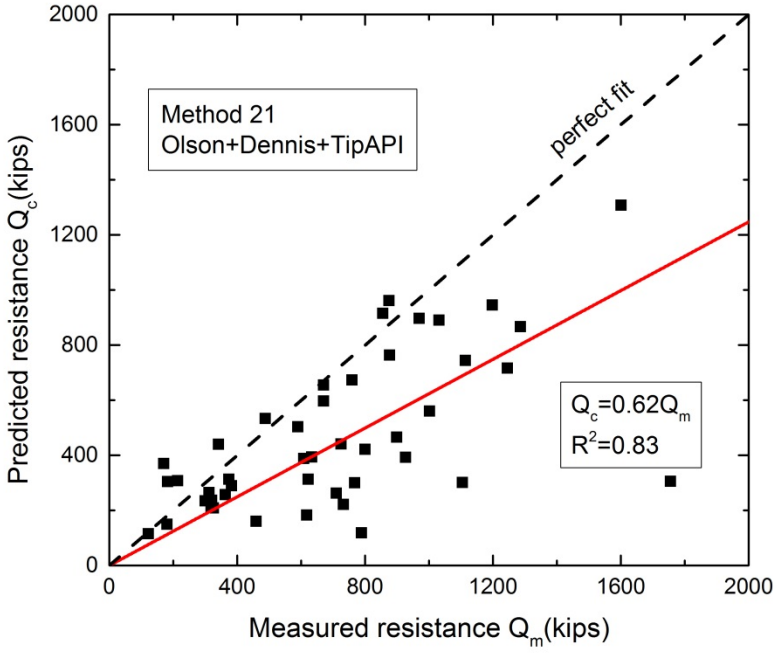

Figure 4-21 Estimated Q_c versus measured Q_m in Method 21

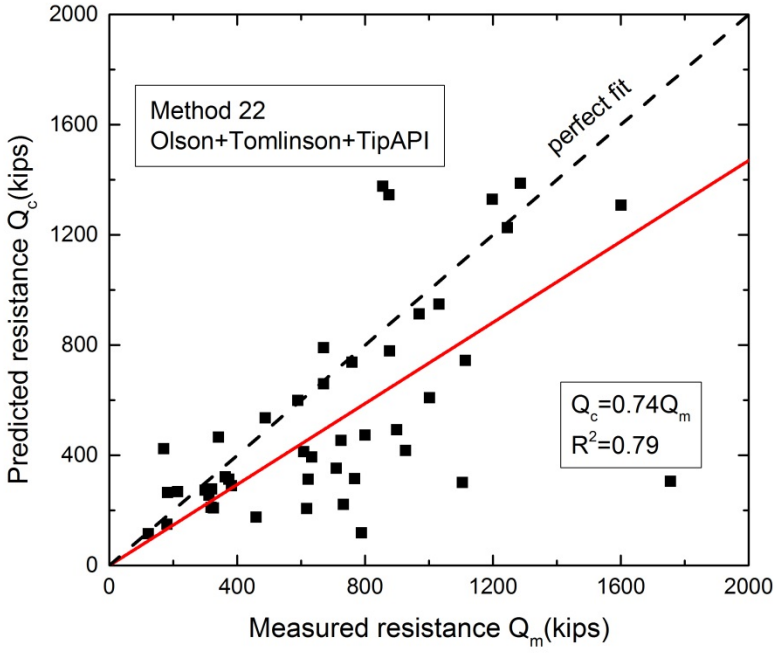

Figure 4-22 Estimated Q_c versus measured Q_m in Method 22

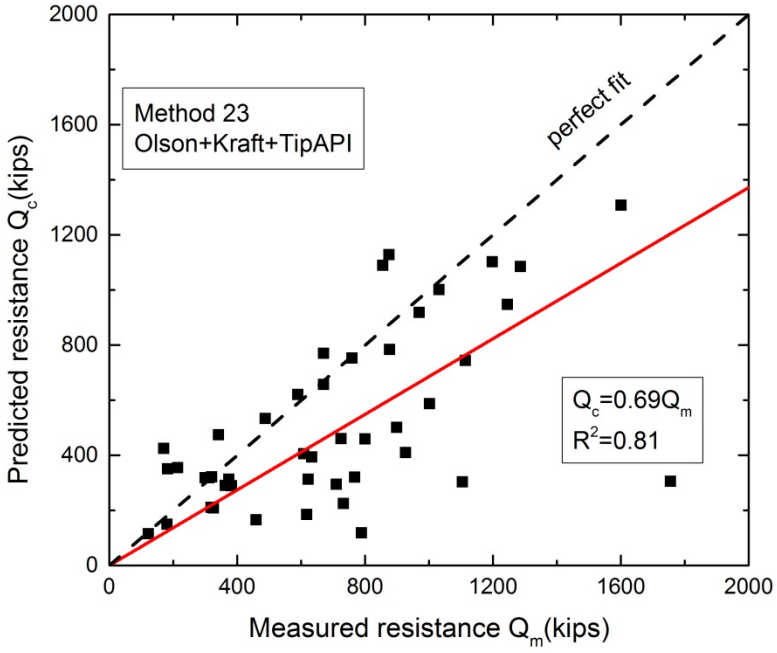

Figure 4-23 Estimated Q_c versus measured Q_m in Method 23

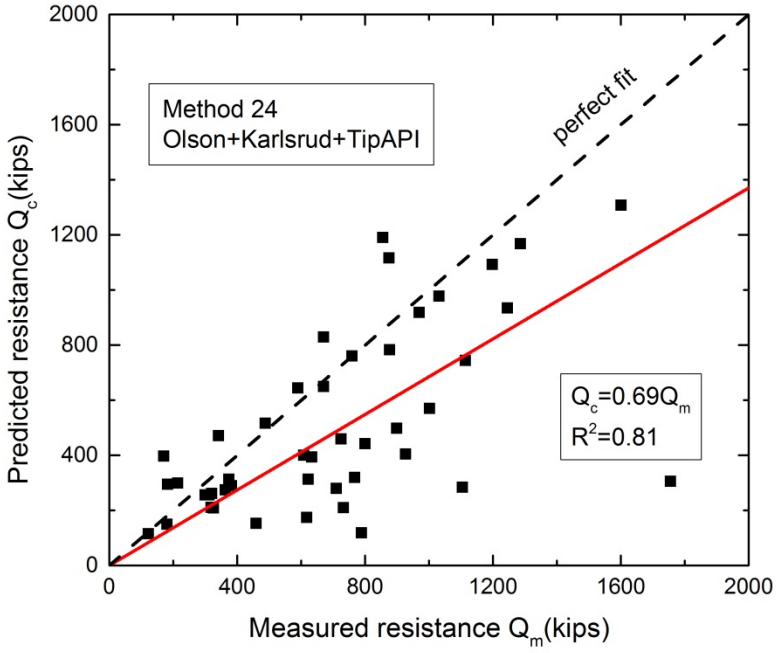

Figure 4-24 Estimated Q_c versus measured Q_m in Method 24

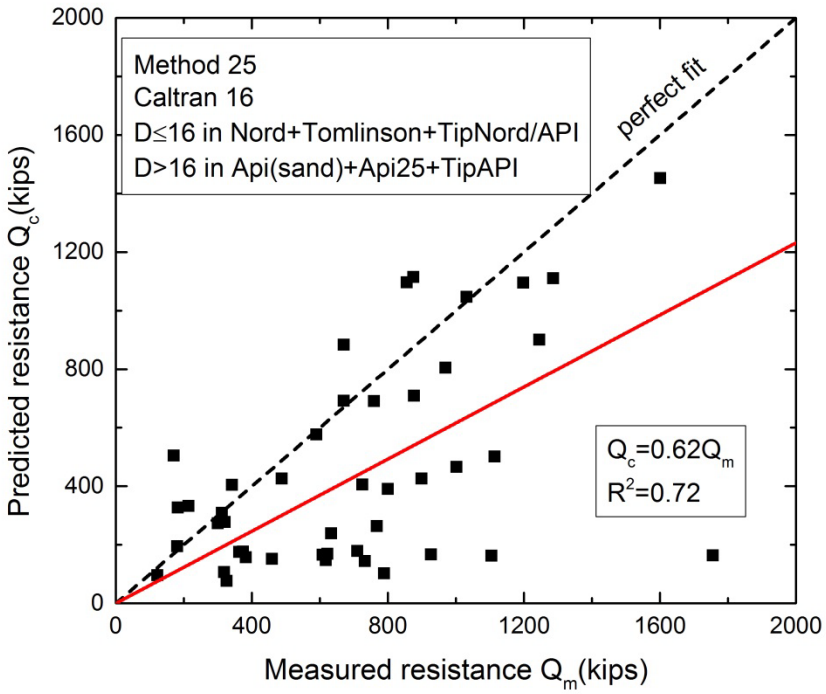

Figure 4-25 Estimated Q_c versus measured Q_m in CALTRANS 16 (Method 25)

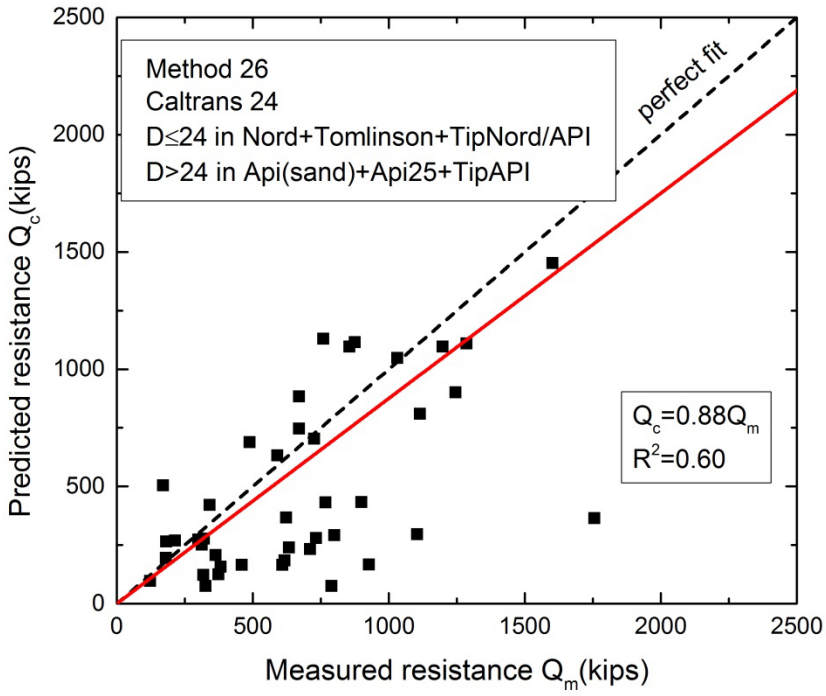

Figure 4-26 Estimated Q_c versus measured Q_m in CALTRANS 24 (Method 26)

The fitting slope calculated from figures above and R^2 (coefficient of determination) for 26 capacity predicting methods are summarized as below:

Table 4-1 Evaluation of performance of 26 methods according to criterion 1

Criterion 1 Best fit calculations			
Method	Q_c/Q_m	R^2	R1
1	0.85	0.58	16
2	0.88	0.59	14
3	0.79	0.55	24
4	0.90	0.60	9
5	0.85	0.58	17
6	0.85	0.58	18
7	0.62	0.75	23
8	0.66	0.74	20
9	0.57	0.77	25
10	0.68	0.74	19

Table 4-1—*Continued*

11	0.63	0.76	21
12	0.63	0.75	22
13	0.87	0.83	5
14	0.91	0.82	2
15	0.82	0.85	6
16	0.93	0.82	1
17	0.87	0.84	4
18	0.88	0.84	3
19	0.68	0.80	12
20	0.72	0.79	8
21	0.62	0.83	15
22	0.74	0.79	7
23	0.69	0.81	10
24	0.69	0.81	11
25	0.62	0.72	26
26	0.88	0.6	13

From the table above, Method 16, Decourt(sand)+Tomlinson(clay)+TipAPI shows the best-fit equation $Q_c=0.93Q_m$ ($R^2=0.82$), which tends to under-predict the measured bearing capacity for piles by an average of 7 percent. Considering both slope and R^2 close to 1, method 16 is ranked as NO.1 in criterion 1, and is given RI=1. Method 14 with $Q_c=0.91Q_m$ ($R^2=0.82$) tends to under-estimate measured capacity by 9 percent, ranked as NO.2. It can be seen that all the best fitting slopes are under than 1, which means the predicted bearing capacity for those selected pipe piles has been under-estimated.

4.1.2 Criterion 2

The arithmetic mean (μ) and standard deviation (σ) of the ratio Q_c/Q_m values are important factors affecting the accuracy of prediction. A good prediction method would have a mean value of Q_c/Q_m close to 1, and a small standard deviation. μ and σ of the Q_c/Q_m values for each method were calculated and considered as second evaluation criterion, then the 26 methods were ranked based on μ and σ as summarized below:

Table 4-2 Evaluation of performance of 26 methods according to criterion 2

Criterion 2 Arithmetic Calculations			
Method	Arithmetic Mean (Q_c/Q_m)	Standard Deviation σ (Q_c/Q_m)	R2
1	0.91	0.72	24
2	0.95	0.73	19
3	0.85	0.70	26
4	0.93	0.72	20
5	0.93	0.74	23
6	0.90	0.72	25
7	0.74	0.42	17
8	0.78	0.45	14
9	0.68	0.37	18
10	0.76	0.42	13
11	0.76	0.44	16
12	0.73	0.41	15
13	1.00	0.44	2
14	1.04	0.47	6
15	0.94	0.40	3
16	1.02	0.46	5
17	1.02	0.46	4
18	0.99	0.43	1
19	0.82	0.43	11
20	0.86	0.46	8
21	0.76	0.38	12
22	0.84	0.43	7
23	0.84	0.45	10
24	0.81	0.41	9
25	0.74	0.53	22
26	0.92	0.71	21

According to this criterion, method 18, which is Decourt(sand)+ Karlsrud (clay)+Tip API, shows best predicting performance. Therefore, this method 18 with

μ=0.99, σ =0.43 ranks as NO.1, and is given R2=1. Then followed by method 13, which is second best performance method according to this criterion. From the results above, only methods 14, 16 and 17 have mean values greater than 1, which means these three methods are slightly overestimating pipe pile capacity on average. The rest of predicting methods give the mean values of Q_c/Q_m below 1, which means the bearing capacity has been under-predicted.

4.1.3 Criterion 3

The third evaluation criterion is based on 50 and 90% cumulative probabilities, P_{50} and P_{90}, showing in Figure 4-27 to Figure 4-34. The concept is to sort Q_c/Q_m values for each method in an ascending order (1,2,3,…,n), and then estimate the cumulative probability P from the following equation:

$$P = \frac{i}{n+1} \qquad (4\text{-}1)$$

Where i=order number given for Q_c/Q_m values in each single method; and n= total number of selected piles from database. The 50% and 90% cumulative probabilities (P_{50} and P_{90}) were determined based on the rule above, and used to evaluate the ability of the method for predicting bearing capacity of pipe piles. P_{50} is also called median, which means within each method, 50% of Q_c/Q_m values are less than this certain value, and another 50% of values are greater than it. P_{90} is the threshold for 90% of Q_c/Q_m values sorted by ascending order within each method. Then the range of difference between P_{50} and P_{90} can be calculated, in which large range means Q_c/Q_m values are dispersed. The pile capacity prediction method with a P_{50} value close to 1 and a low P_{90}-P_{50} range is considered good predicting way.

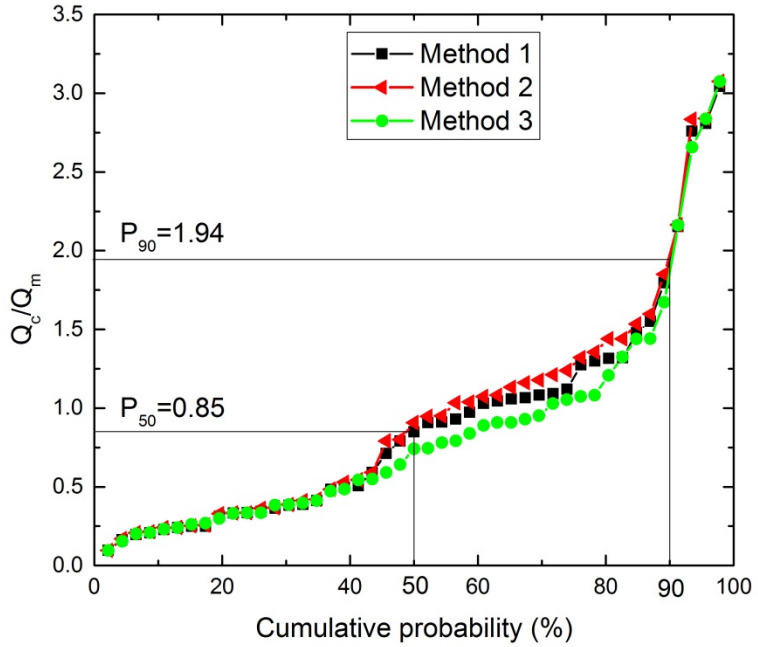

Figure 4-27 Cumulative probability of Q_c/Q_m for method 1, 2 and 3

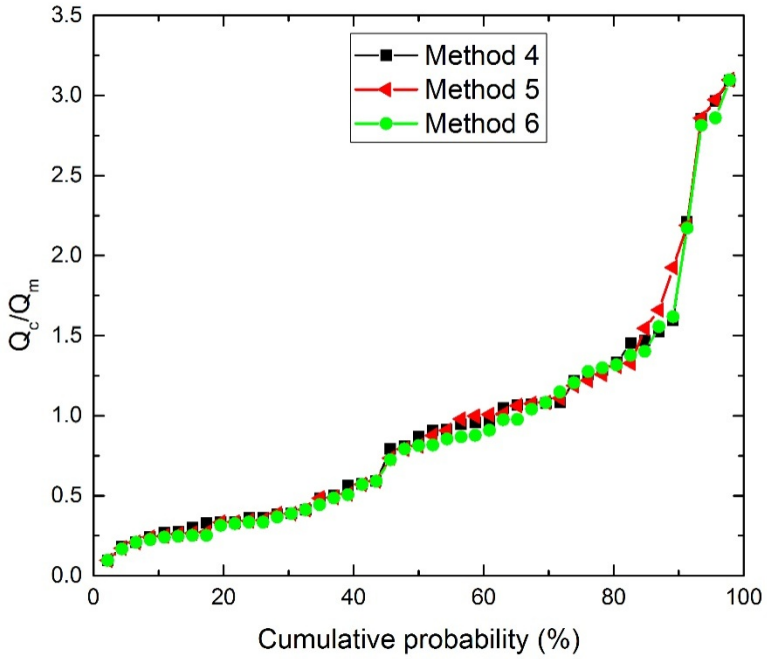

Figure 4-28 Cumulative probability of Q_c/Q_m for method 4, 5 and 6

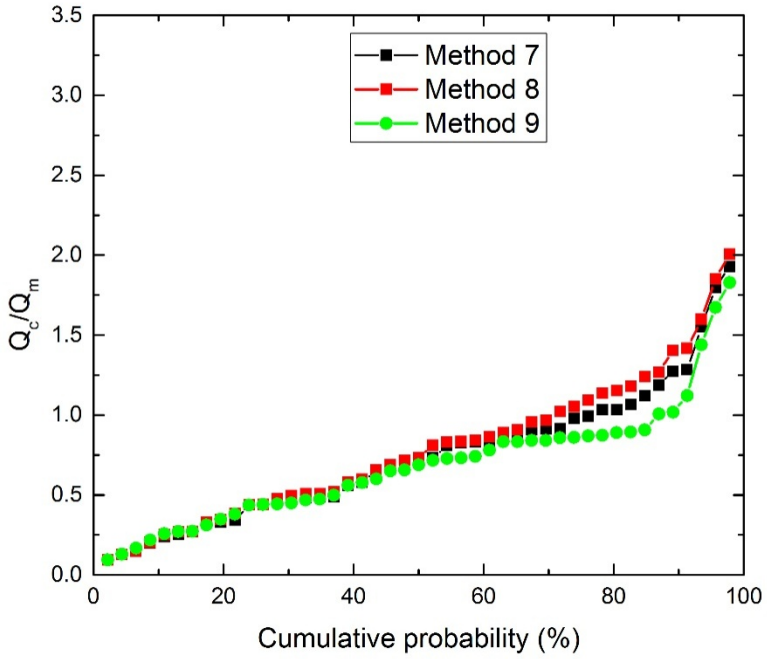

Figure 4-29 Cumulative probability of Q_c/Q_m for method 7, 8 and 9

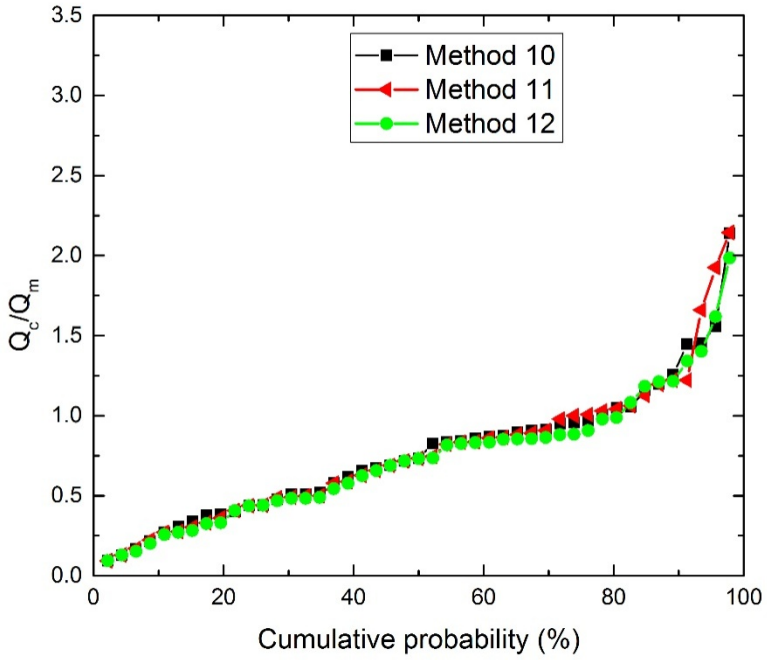

Figure 4-30 Cumulative probability of Q_c/Q_m for method 10, 11 and 12

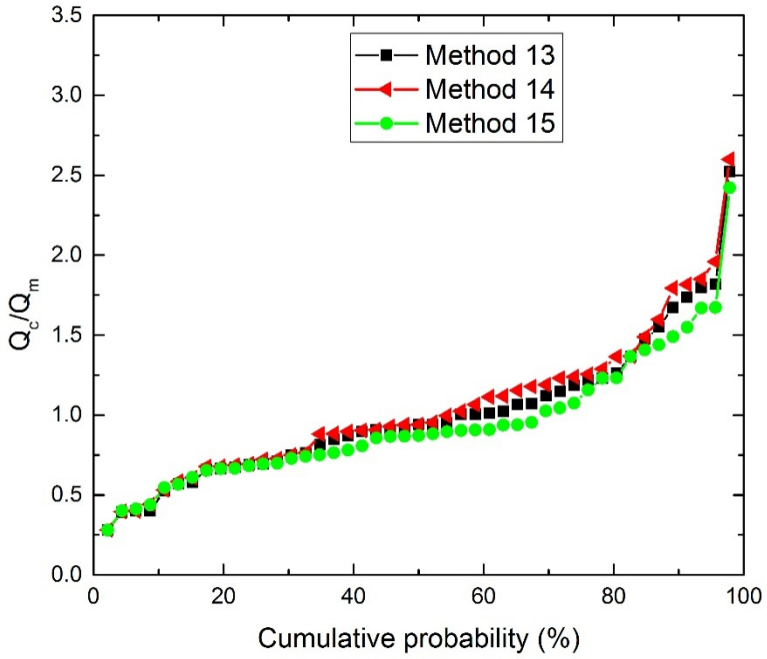

Figure 4-31 Cumulative probability of Q_c/Q_m for method 13, 14 and 15

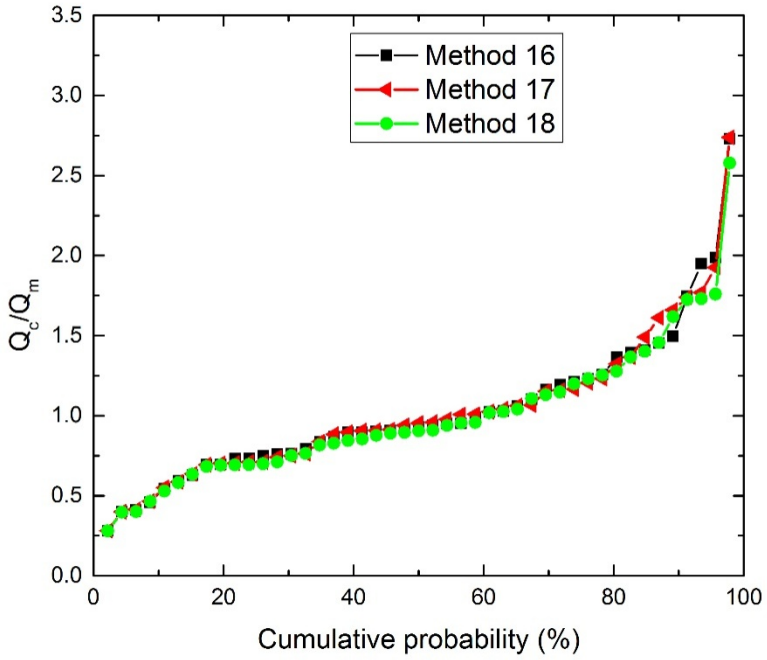

Figure 4-32 Cumulative probability of Q_c/Q_m for method 16, 17 and 18

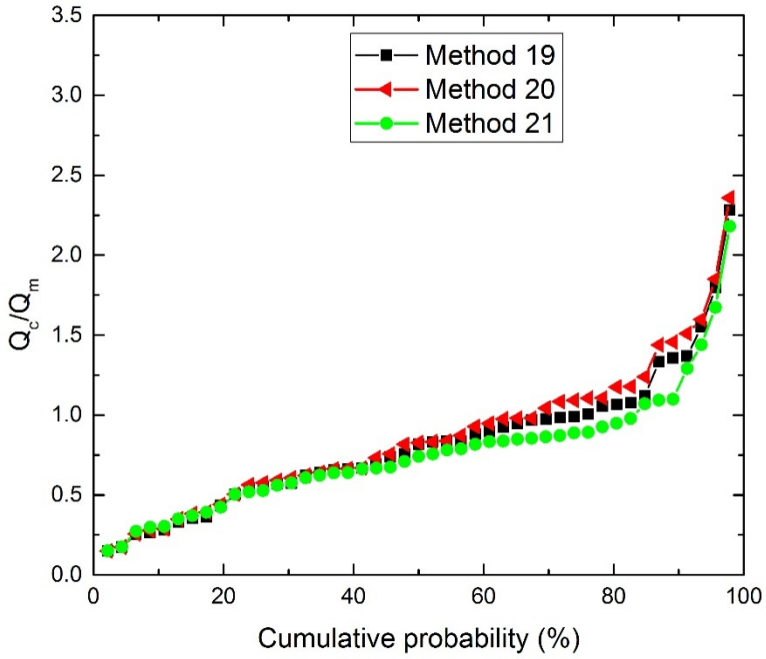

Figure 4-33 Cumulative probability of Q_c/Q_m for method 19, 20 and 21

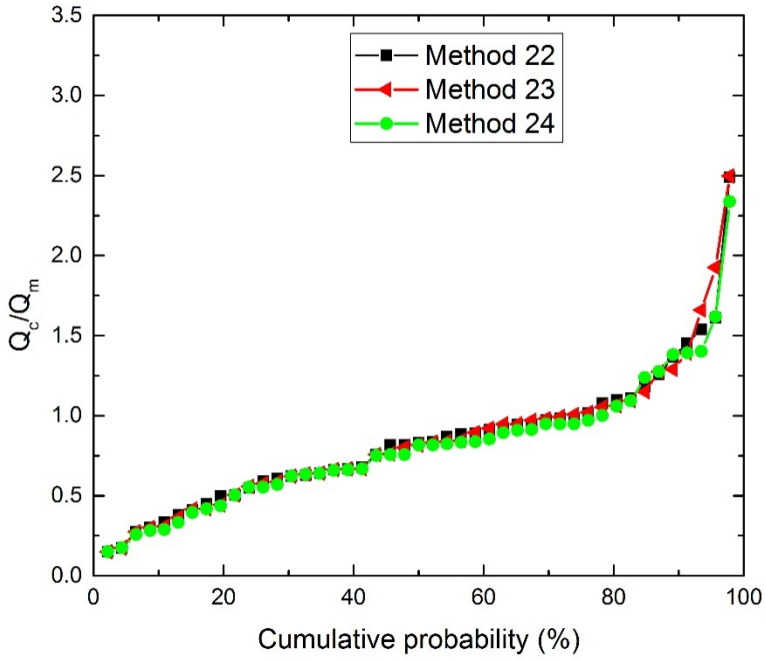

Figure 4-34 Cumulative probability of Q_c/Q_m for method 22, 23 and 24

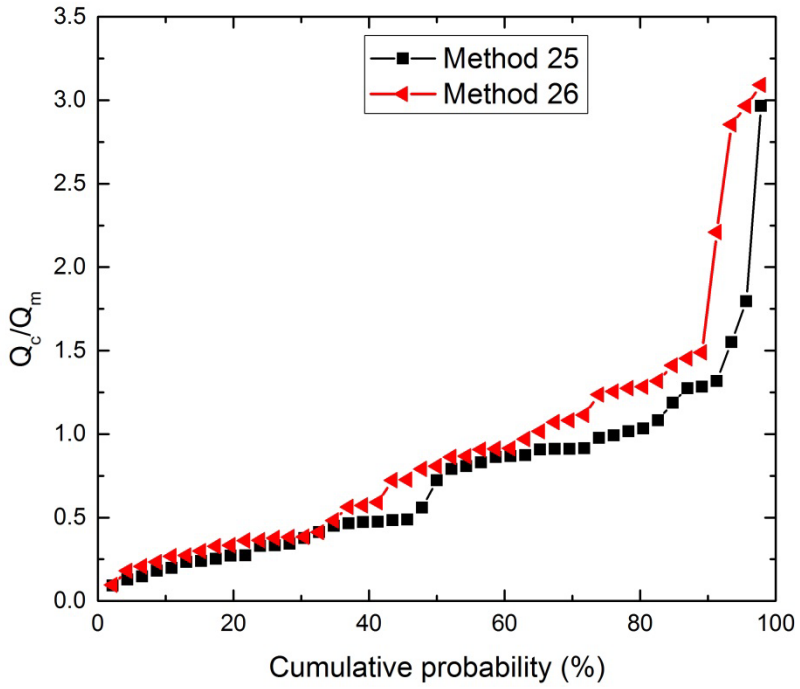

Figure 4-35 Cumulative probability of Q_c/Q_m for CALTRANS 16 and 24 (Method 25 and 26)

P_{50}, P_{90} values were determined from Figure 4-27 to Figure 4-35 above, and ranking numbers have been given based on the two parameters. Summarized characteristics can be presented below:

Table 4-3 Evaluation of performance of 26 methods according to criterion 3

Criterion 3 Cumulative probability			
Method	Q_c/Q_m at P_{50}	P_{90}	R3
1	0.85	1.94	24
2	0.91	1.98	23
3	0.74	1.86	25
4	0.87	1.87	18
5	0.81	2.04	26
6	0.81	1.87	22

Table 4-3—*Continued*

7	0.72	1.27	16
8	0.73	1.41	21
9	0.69	1.04	3
10	0.73	1.32	12
11	0.73	1.22	11
12	0.73	1.26	9
13	0.94	1.71	13
14	0.94	1.83	20
15	0.87	1.52	8
16	0.93	1.59	2
17	0.95	1.71	10
18	0.90	1.67	15
19	0.82	1.36	6
20	0.83	1.50	14
21	0.74	1.16	1
22	0.83	1.41	5
23	0.82	1.34	4
24	0.82	1.37	7
25	0.72	1.28	17
26	0.81	1.49	19

Under this criterion, best prediction method is considered the one with P_{50} closer to 1, and smaller value range between P_{50} and P_{90}. Based on this rule, estimating method 21 ranks No. 1 and is assigned R3=1. Although P_{50}=0.69 is relatively low when compared to 1, the difference between P_{50} and P_{90} is the smallest among those 26 methods. As mentioned before, predicting method with less scatter would be preferred. Method 16 ranks No. 2 with P_{50}=0.93, P_{90}-P_{50}=0.66. It can be seen from all results under this criterion, values of P_{50}, which are medians of the values Q_c/Q_m in each predicting method, are less than 1, showing the bearing capacity for piles has been under-estimated.

4.1.4 Criterion 4

The forth criterion used to evaluate the predicting methods is based on the histogram and log-normal distribution of Q_c/Q_m. The reason log-normal distribution was chosen as the model of this case is because Q_c/Q_m ranges from 0 to an unlimited upper value with an optimum value of one, resulting a non-symmetric distribution of Q_c/Q_m around the mean. The probability of density curve for log-normal distribution is defined as:

$$f(x) = \frac{1}{\sqrt{2\pi}\sigma_{ln}x} exp\left[-\frac{1}{2}\left(\frac{\ln(x) - \mu_{ln}}{\sigma_{ln}}\right)^2\right] \quad (4\text{-}2)$$

Where

$x=Q_c/Q_m$;

μ_{ln}=mean of $\ln(Q_c/Q_m)$;

and σ_{ln}=standard deviation of $\ln(Q_c/Q_m)$.

First, the ratio Q_c/Q_m and the natural logarithm of the ratio $\ln(Q_c/Q_m)$ for each pile was calculated. Then, the log mean(μ_{ln}), log standard deviation (σ_{ln}), were determined and used to identify probability density function (PDF) of log-normal distribution for each method.

For the histogram using here, the ratios of Q_c to Q_m have been grouped, which are increasing as a unit of 0.2. Relative frequency is defined as the number of Q_c/Q_m values falls into a specific interval over total number of Q_c/Q_m values. Generated PDF and histograms are showing in Figure 4-36 to Figure 4-61.

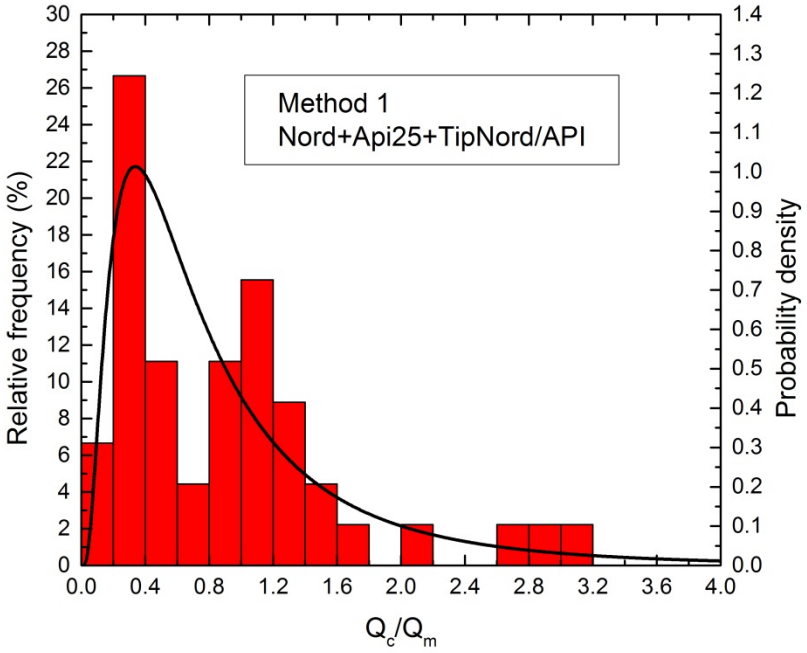

Figure 4-36 Histogram and PDF curve of Q_c/Q_m for method 1

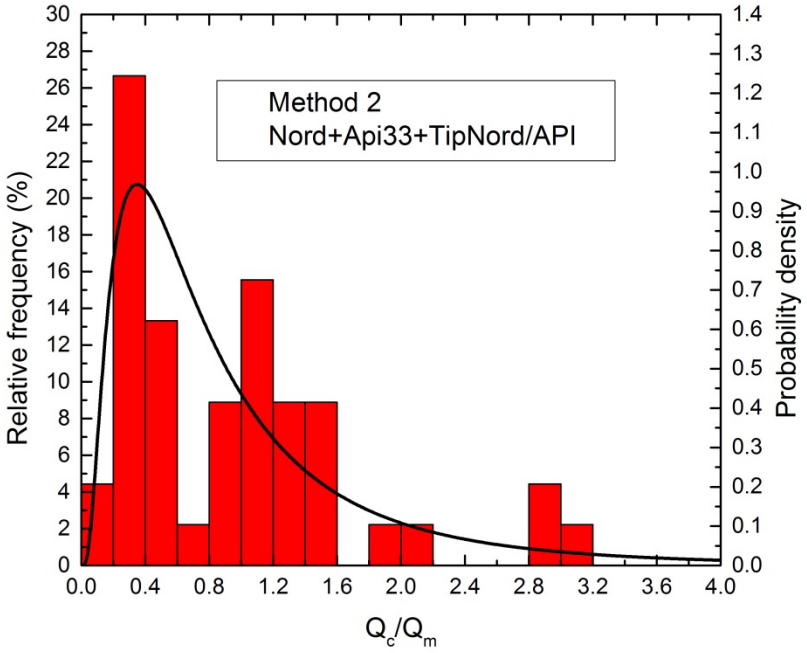

Figure 4-37 Histogram and PDF curve of Q_c/Q_m for method 2

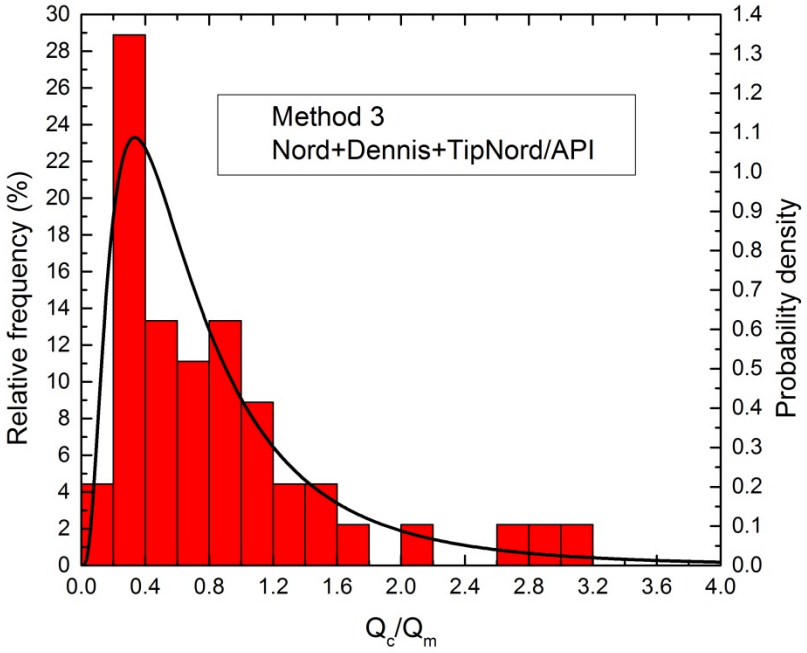

Figure 4-38 Histogram and PDF curve of Q_c/Q_m for method 3

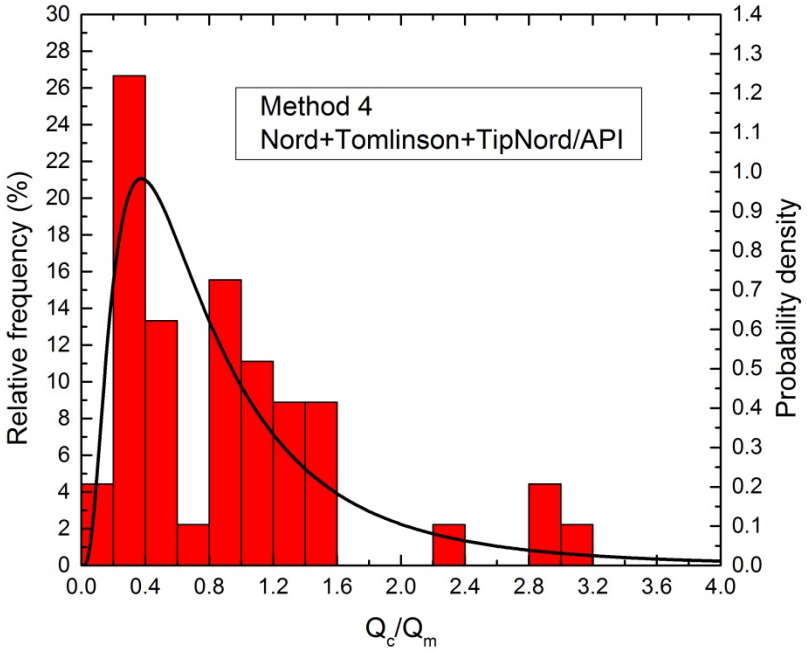

Figure 4-39 Histogram and PDF curve of Q_c/Q_m for method 4

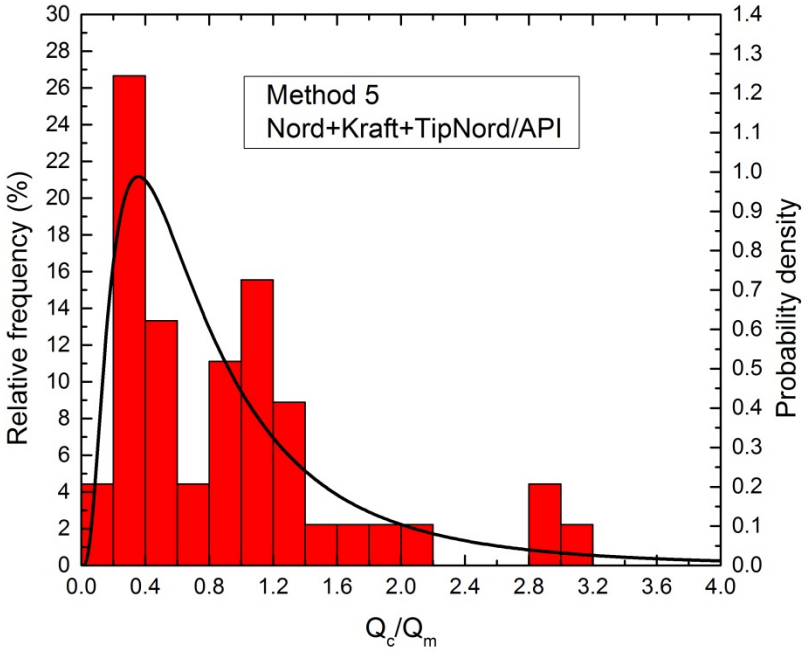

Figure 4-40 Histogram and PDF curve of Q_c/Q_m for method 5

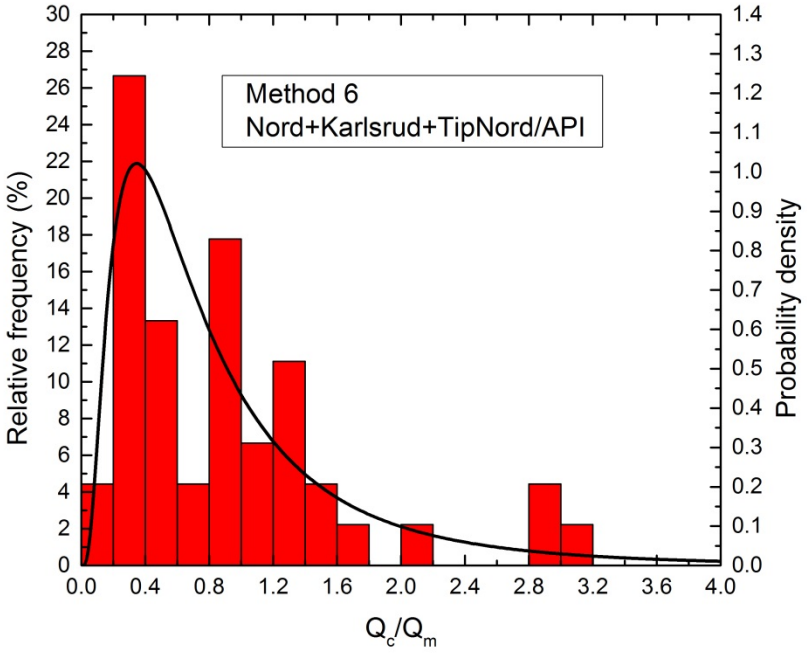

Figure 4-41 Histogram and PDF curve of Q_c/Q_m for method 6

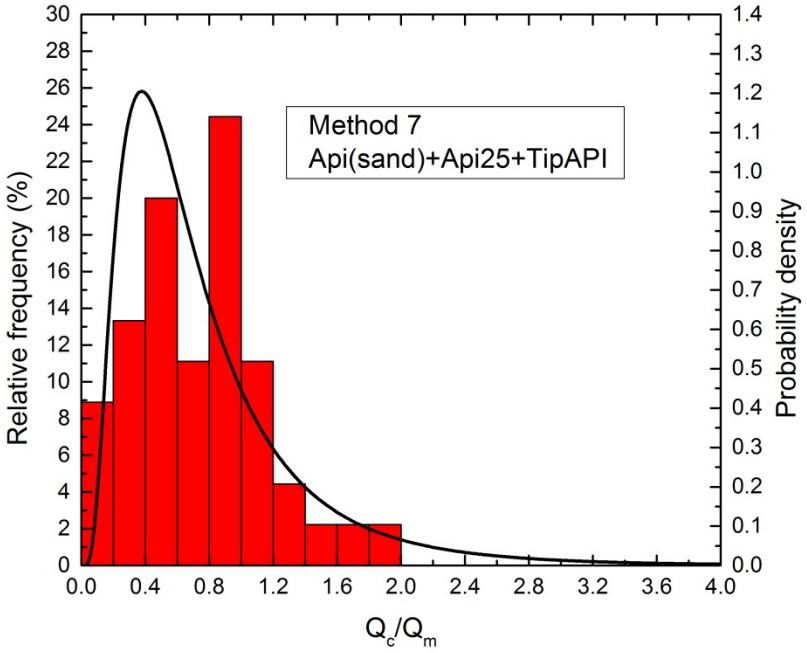

Figure 4-42 Histogram and PDF curve of Q_c/Q_m for method 7

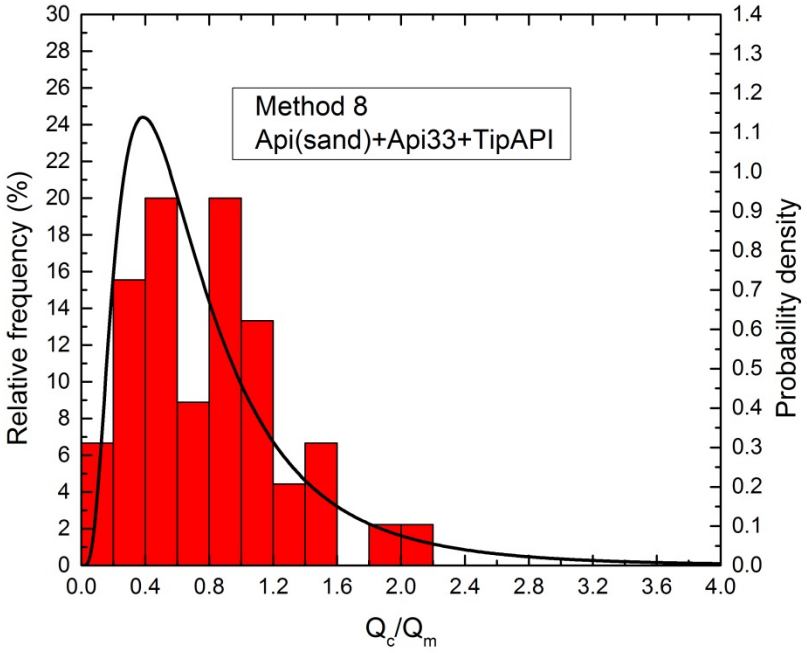

Figure 4-43 Histogram and PDF curve of Q_c/Q_m for method 8

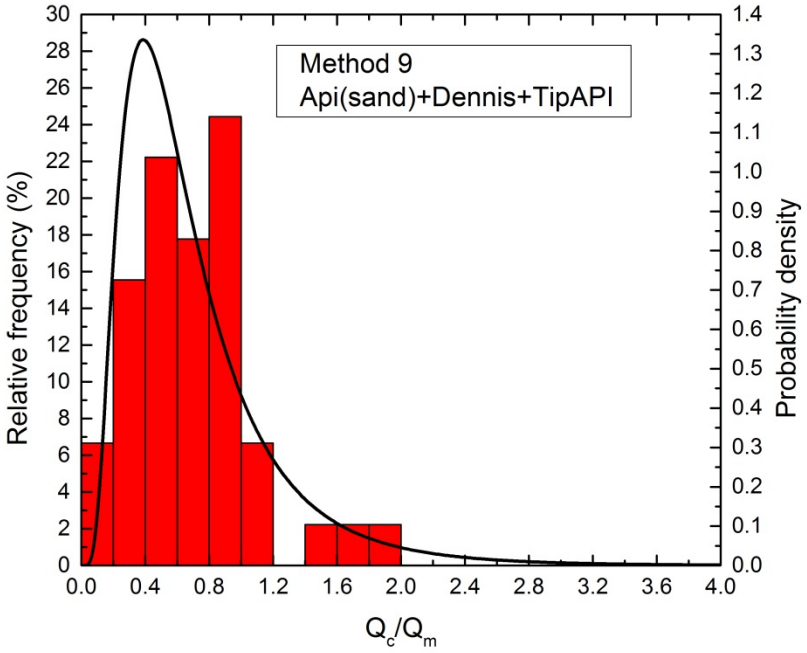

Figure 4-44 Histogram and PDF curve of Q_c/Q_m for method 9

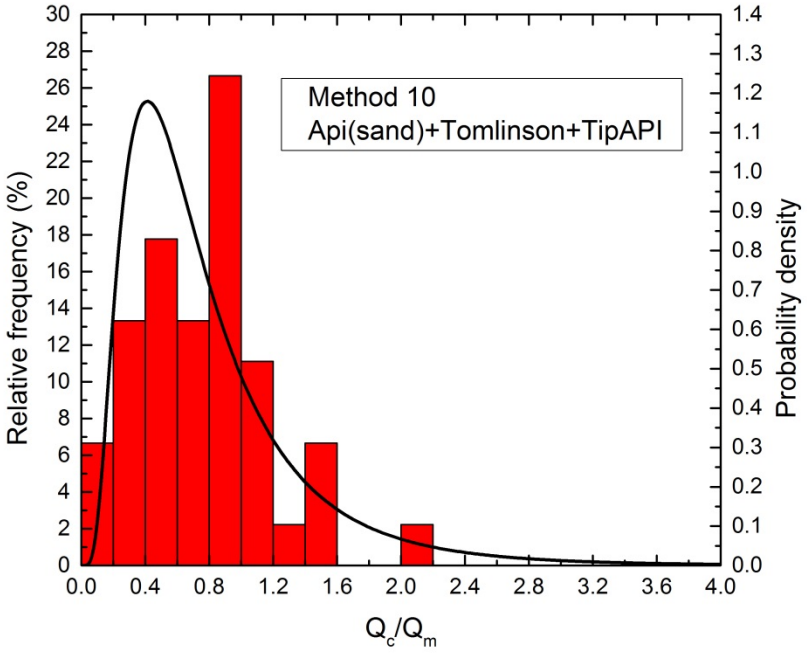

Figure 4-45 Histogram and PDF curve of Q_c/Q_m for method 10

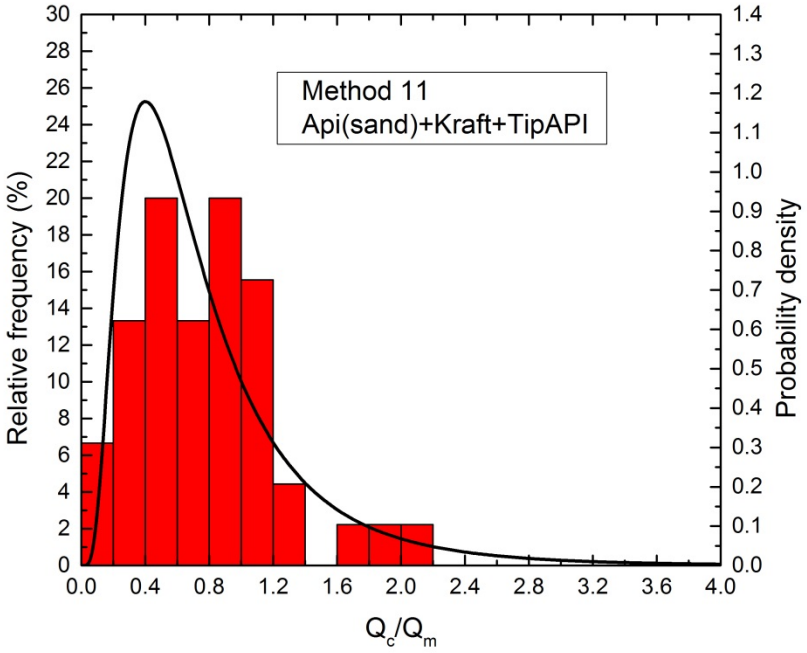

Figure 4-46 Histogram and PDF curve of Q_c/Q_m for method 11

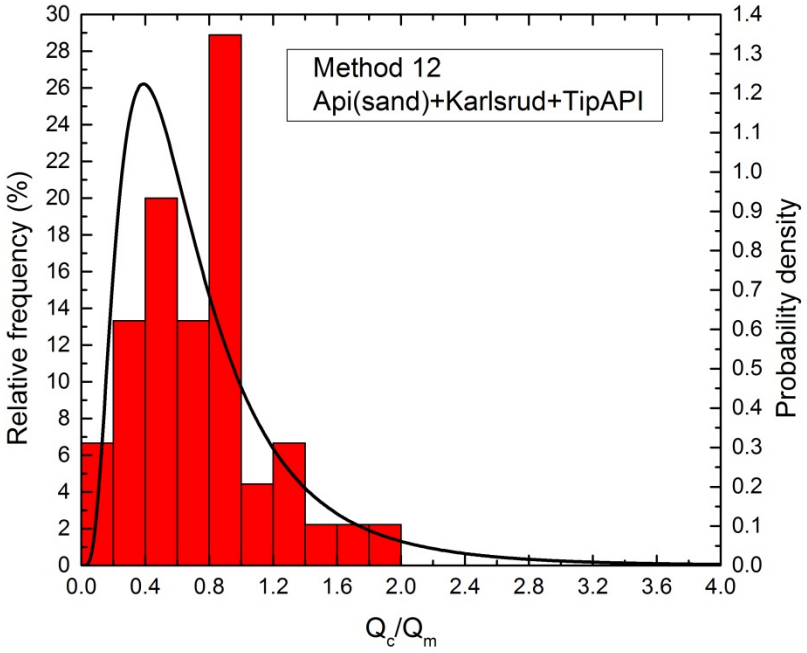

Figure 4-47 Histogram and PDF curve of Q_c/Q_m for method 12

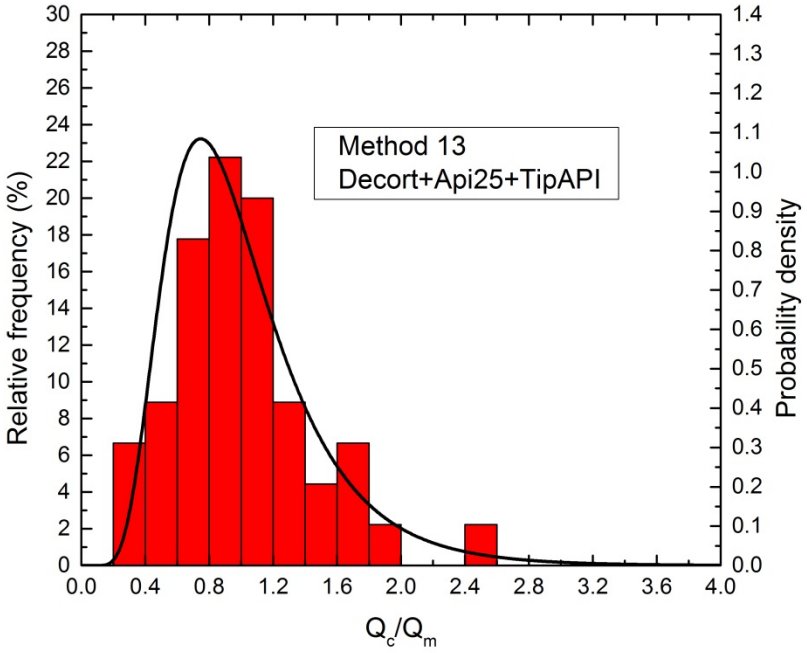

Figure 4-48 Histogram and PDF curve of Q_c/Q_m for method 13

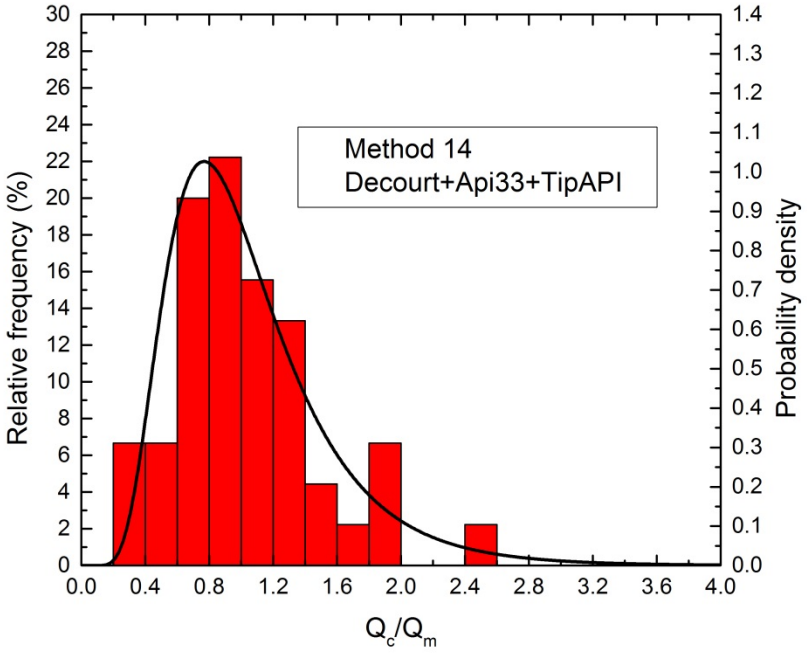

Figure 4-49 Histogram and PDF curve of Q_c/Q_m for method 14

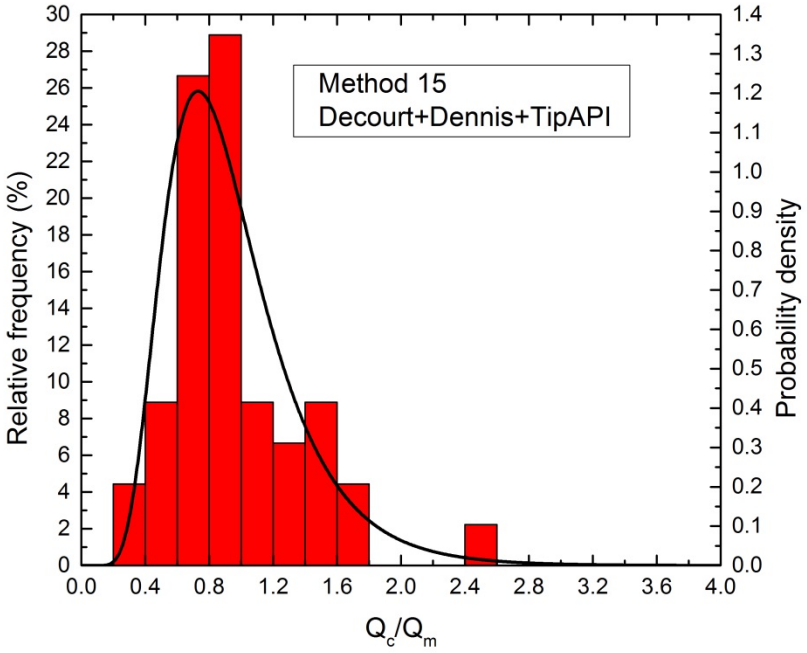

Figure 4-50 Histogram and PDF curve of Q_c/Q_m for method 15

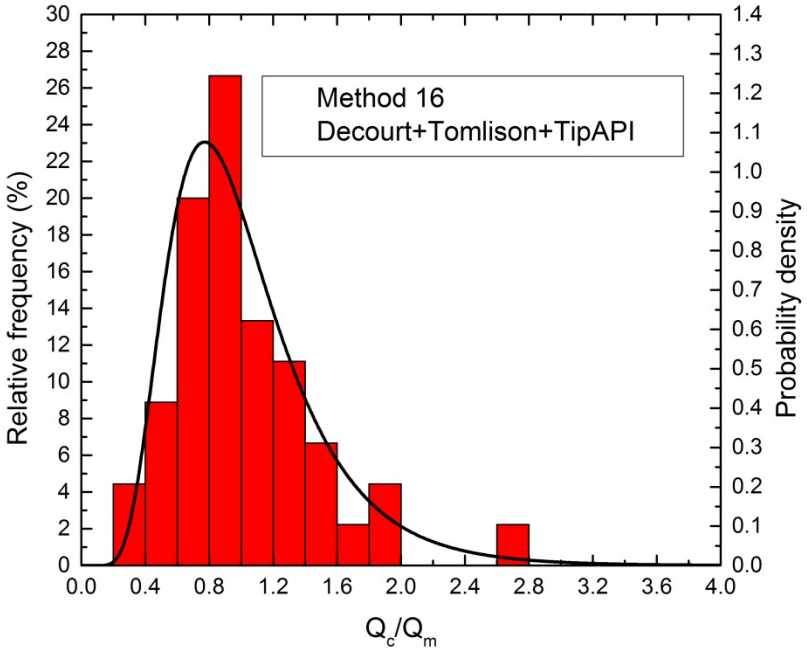

Figure 4-51 Histogram and PDF curve of Q_c/Q_m for method 16

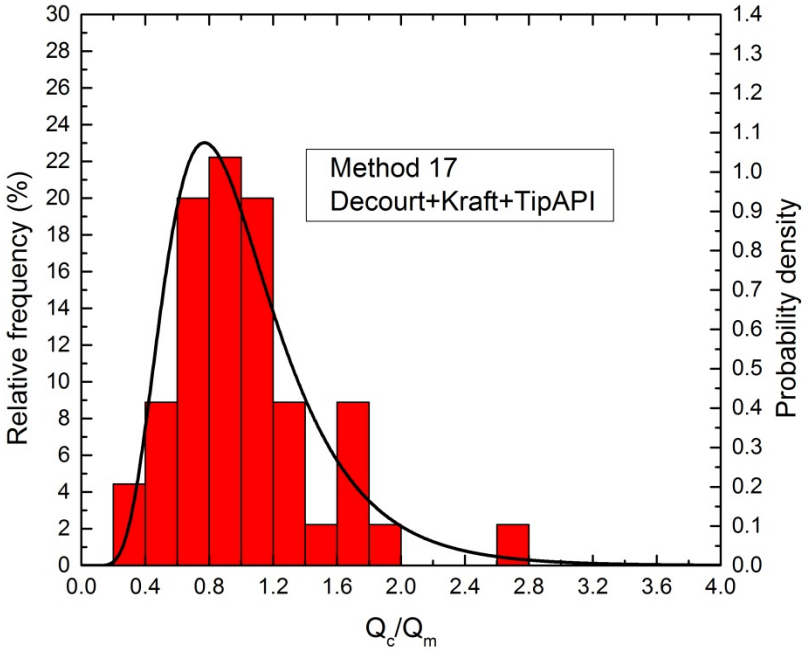

Figure 4-52 Histogram and PDF curve of Q_c/Q_m for method 17

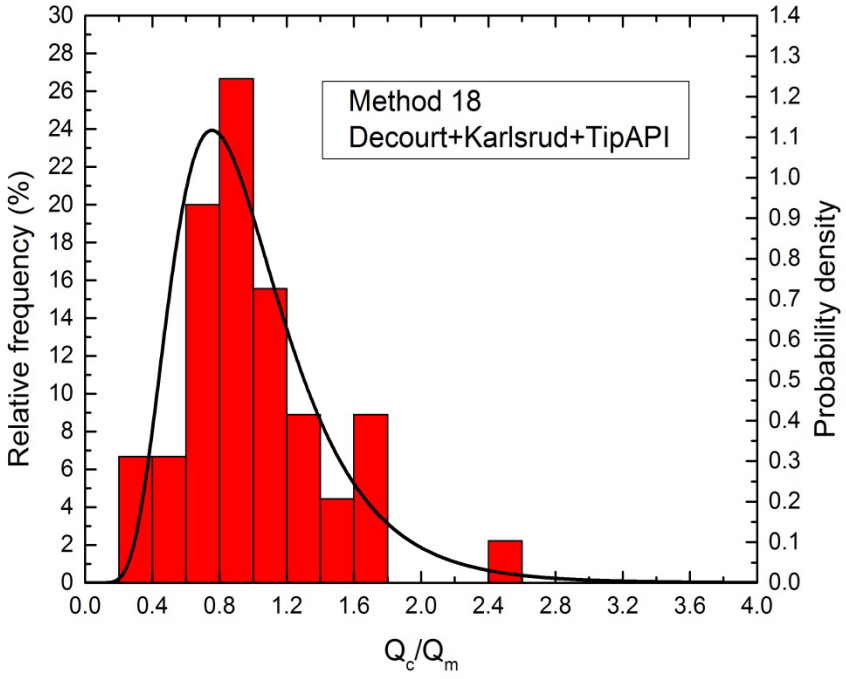

Figure 4-53 Histogram and PDF curve of Q_c/Q_m for method 18

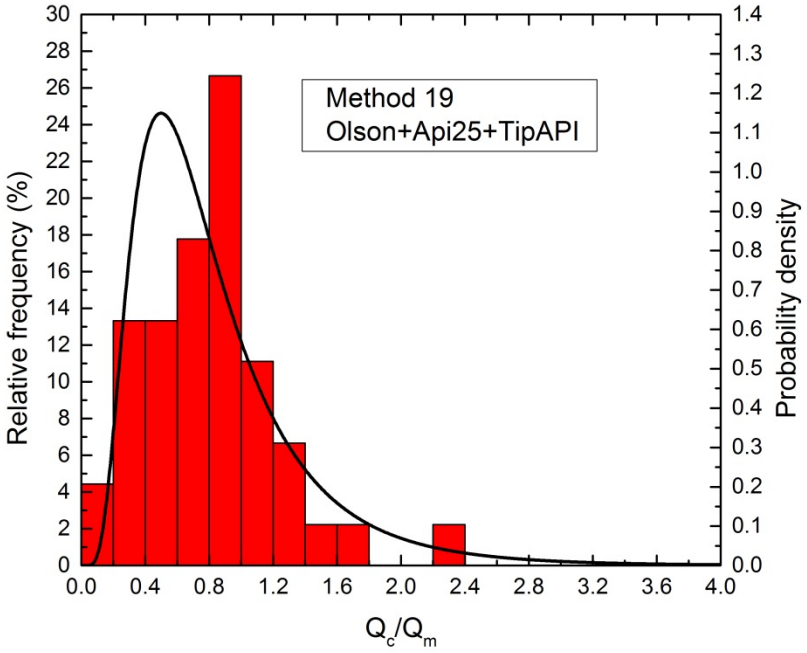

Figure 4-54 Histogram and PDF curve of Q_c/Q_m for method 19

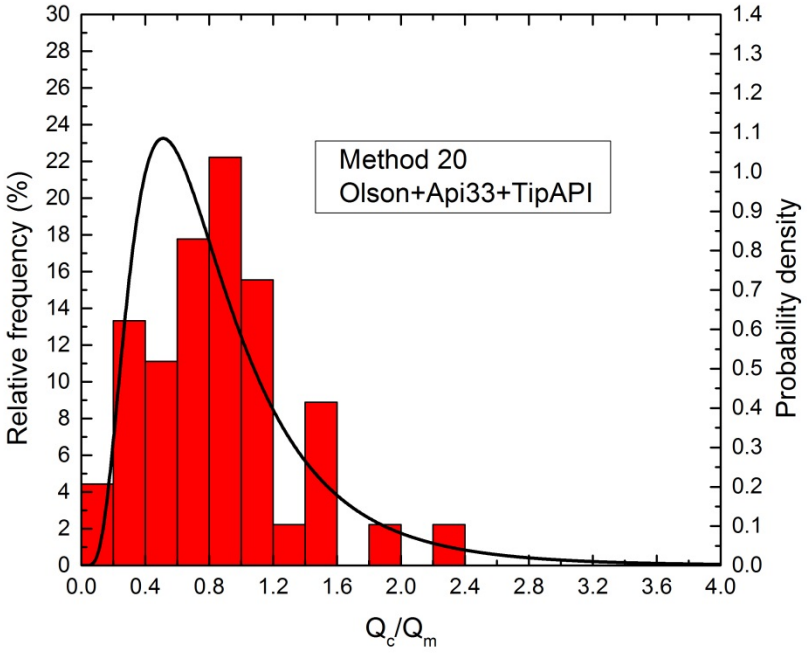

Figure 4-55 Histogram and PDF curve of Q_c/Q_m for method 20

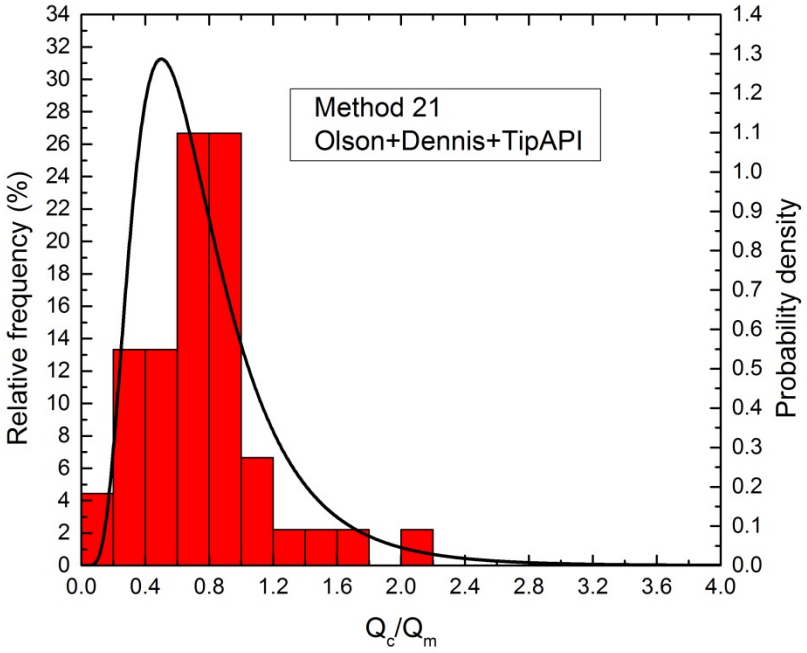

Figure 4-56 Histogram and PDF curve of Q_c/Q_m for method 21

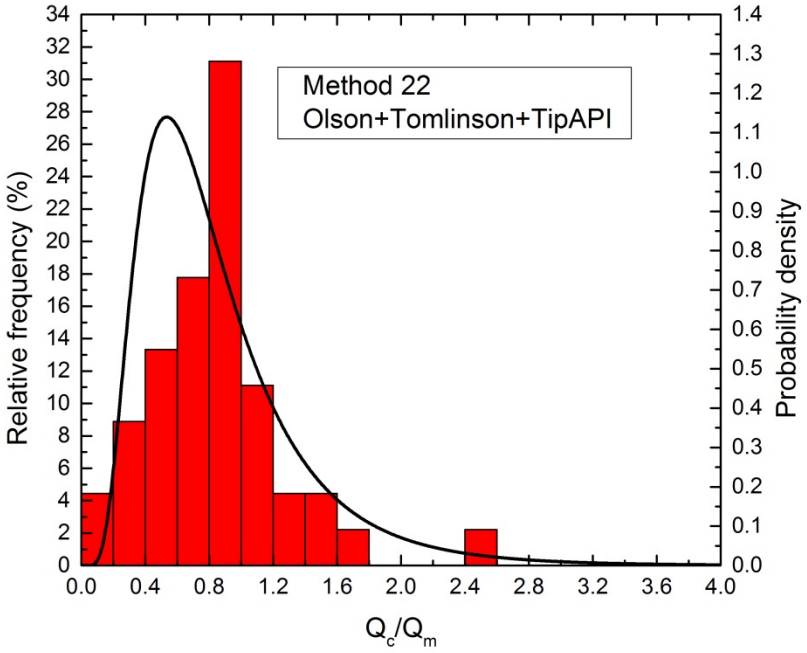

Figure 4-57 Histogram and PDF curve of Q_c/Q_m for method 22

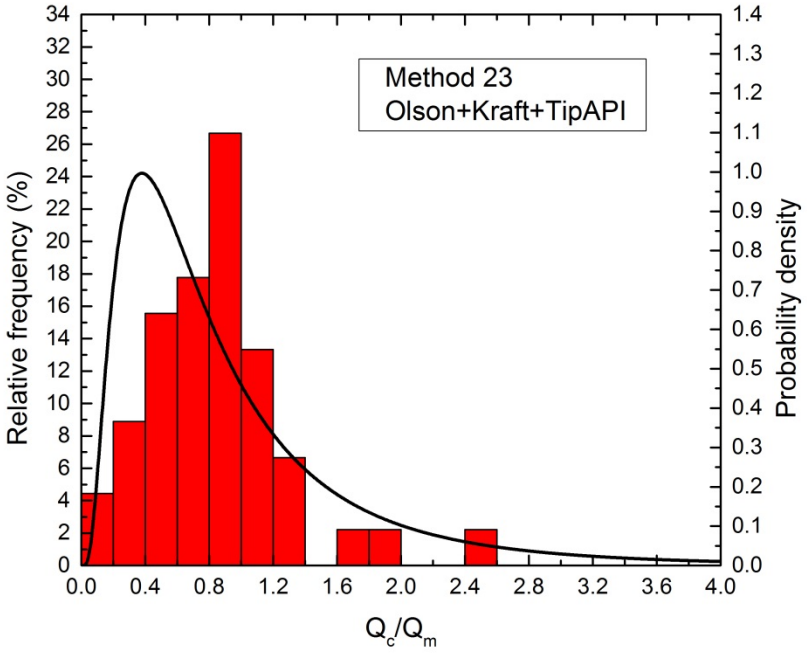

Figure 4-58 Histogram and PDF curve of Q_c/Q_m for method 23

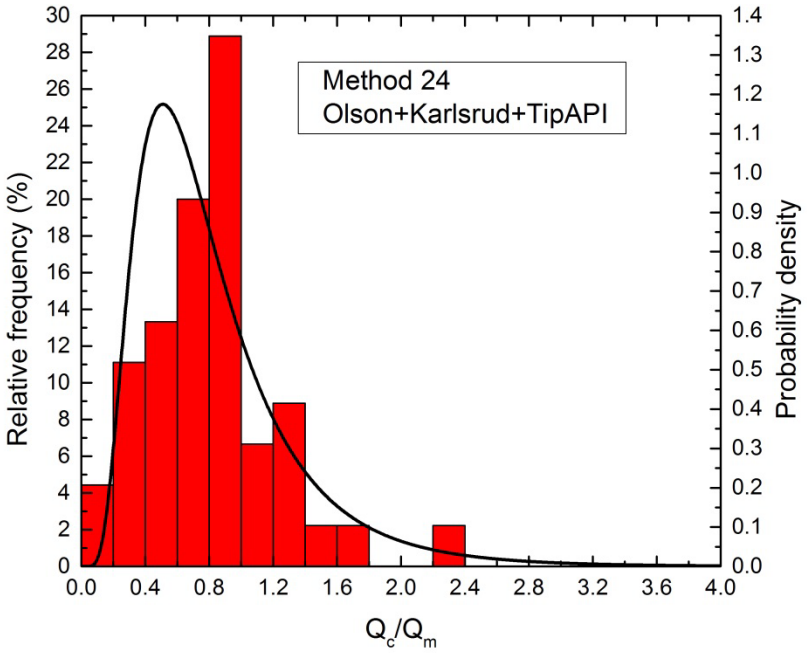

Figure 4-59 Histogram and PDF curve of Q_c/Q_m for method 24

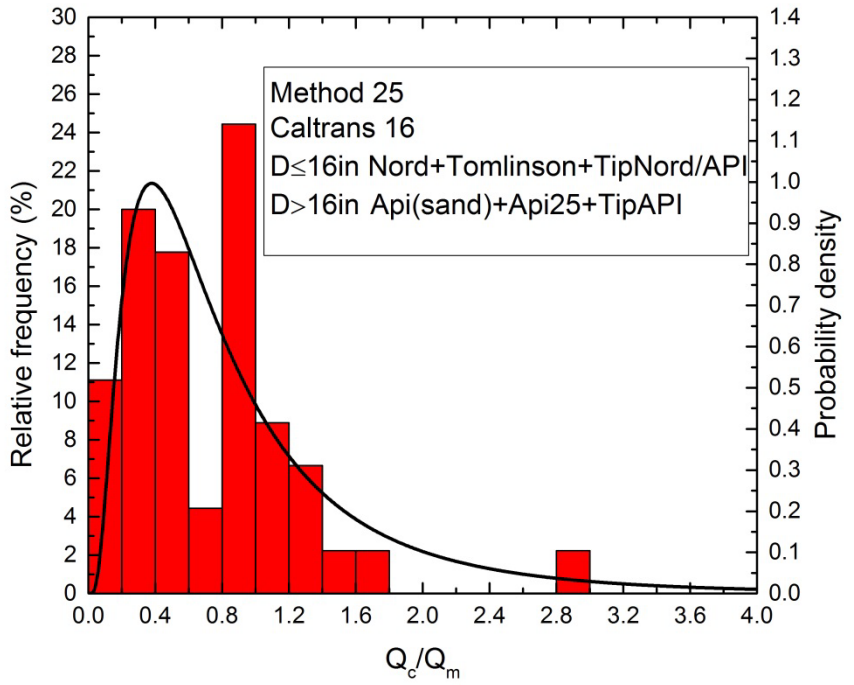

Figure 4-60 Histogram and PDF curve of Q_c/Q_m for CALTRANS 16 (Method 25)

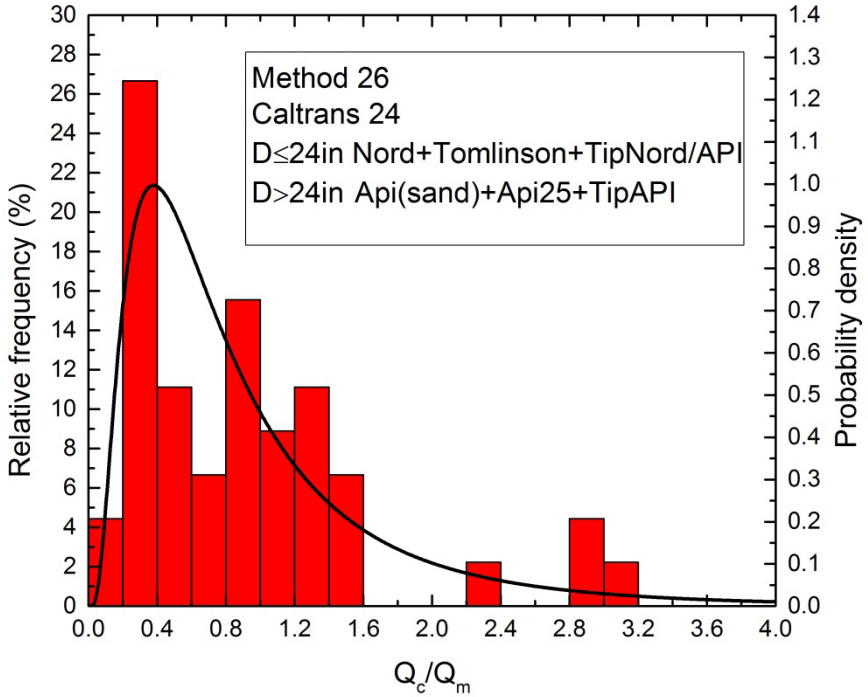

Figure 4-61 Histogram and PDF curve of Q_c/Q_m for CALTRANS 24 (Method 26)

The histogram and log-normal probability density function curves showing previously were used to calculate the probability of predicting the ultimate load capacity within 20% accuracy. At this 20% specified accuracy level, the probability of predicting ultimate pile capacity was determined by calculating the total area underneath the PDF curve within the accuracy limits. Under this criterion, in order to get the predicting probability within 20% accuracy level, the accuracy limits here corresponding to 20% accuracy are $0.8Q_m$ and $1.2Q_m$, showing estimated pile capacity within $0.8Q_m \leq Q_c \leq 1.2Q_m$ is the situation under the consideration. The more the area covered under the curve within this certain 20% accuracy limit, the better the performance of the predicting method. Figure 4-62 depicts the comparison of log-normal distributions for 26 different methods in this study, the shaded area below each PDF curve presents the 20% accuracy probability, total area underneath each PDF curve equals to 1. This probability was also determined on histograms by summating relative frequency of Q_c/Q_m values falling into the range from 0.8 to 1.2.

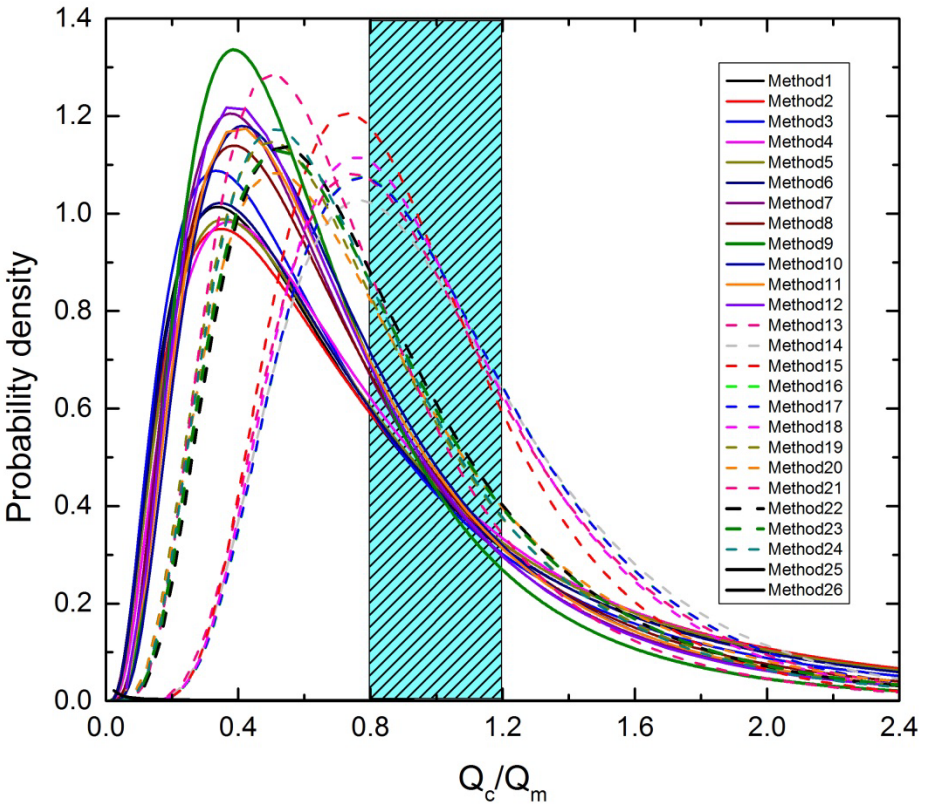

Figure 4-62 Log-normal distribution curves and the area according to 20% accuracy limit

The integral operation is used to get the shaded area, also known as probability, since the total area covered by each PDF curve is 1 underneath each log-normal probability density curve. The equation is defined as:

$$\int_{0.8}^{1.2} f(x) = \int_{0.8}^{1.2} \frac{1}{\sqrt{2\pi}\sigma_{ln} x} exp\left[-\frac{1}{2}\left(\frac{\ln(x) - \mu_{ln}}{\sigma_{ln}}\right)^2\right] \quad (4\text{-}3)$$

The varied levels of prediction accuracy obtained from log-normal distribution for the 26 different methods are plotted in Figure 4-63.

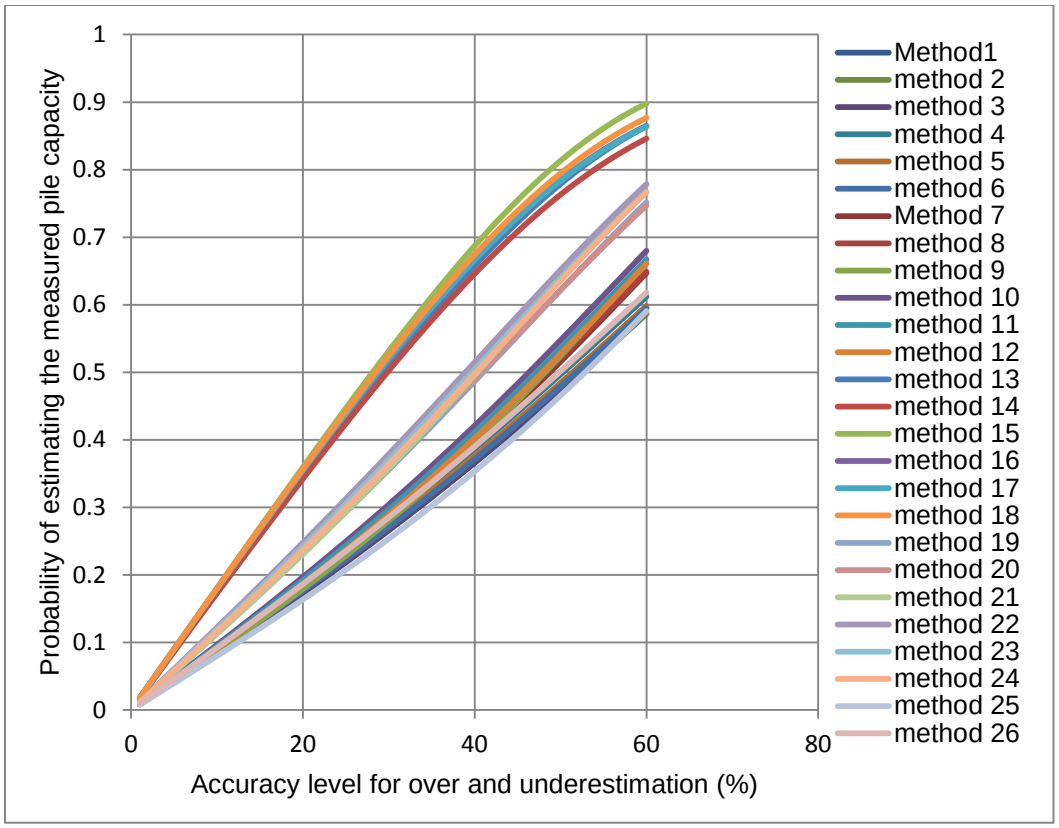

Figure 4-63 Relationship between varied accuracy level and corresponding probability

The probability of predicting the ultimate load capacity with 20% accuracy, lnμ, lnσ, are calculated and are presented in Table 4-4.

Table 4-4 Evaluation of performance of 26 methods according to criterion 4

Criterion 4 ± 20% Accuracy (%)					
Method	LN MEAN	LN STD	Area within 0.8 to 1.2 below the PDF	Probability within 0.8 to 1.2 from the histogram	R4
1	-0.4	0.83	0.17	0.27	22
2	-0.36	0.84	0.18	0.24	24
3	-0.46	0.80	0.17	0.22	26

Table 4-4—*Continued*

4	-0.36	0.79	0.19	0.27	20
5	-0.37	0.81	0.18	0.27	21
6	-0.40	0.81	0.18	0.24	25
7	-0.50	0.69	0.18	0.36	15
8	-0.45	0.71	0.19	0.33	16
9	-0.55	0.63	0.18	0.31	18
10	-0.45	0.66	0.20	0.38	12
11	-0.46	0.67	0.19	0.36	14
12	-0.50	0.67	0.19	0.33	17
13	-0.09	0.45	0.35	0.42	3
14	-0.06	0.46	0.34	0.38	6
15	-0.14	0.42	0.36	0.38	5
16	-0.07	0.44	0.36	0.40	4
17	-0.07	0.44	0.35	0.42	2
18	-0.10	0.43	0.36	0.42	1
19	-0.35	0.59	0.23	0.38	10
20	-0.31	0.60	0.24	0.38	9
21	-0.40	0.54	0.23	0.33	13
22	-0.31	0.56	0.25	0.42	7
23	-0.32	0.57	0.24	0.40	8
24	-0.35	0.57	0.24	0.36	11
25	-0.56	0.76	0.16	0.31	19
26	-0.36	0.78	0.19	0.24	23

Based on the 20% accuracy, method 18, which shows highest probability values 35.7% under PDF and 42.2% under histogram, respectively, is the best prediction method (R4=1). Then followed by method 17, which ranks No.2(R4=2), covering 35.4% probability under PDF and 42.2% from histogram.

4.2 Final Rank

The overall performance of the capacity prediction methods is based on all four criteria via RI. For each method, $RI = R1 + R2 + R3 + R4$. The RI values for all 26 methods are presented in Table 4-5, then the final rank for each method can be calculated based on RI, the lower the RI value, the better the prediction method.

Table 4-5 Evaluation of performance of 26 predicting methods

Method	R1	R2	R3	R4	Total RI	Final Rank
1	15	22	21	21	79	23
2	13	19	20	22	74	21
3	23	24	23	24	94	26
4	9	20	19	19	67	17
5	16	21	24	20	81	24
6	17	23	22	23	85	25
7	22	17	12	15	66	18
8	19	14	17	16	66	18
9	24	18	1	18	61	16
10	18	13	15	12	58	13
11	20	16	8	14	58	14
12	21	15	10	17	63	15
13	5	2	13	3	23	5
14	2	6	18	6	32	8
15	6	3	9	5	23	4
16	1	5	5	4	15	1
17	4	4	11	2	21	2
18	3	1	16	1	21	2
19	12	11	4	10	37	10
20	8	8	14	9	39	10
21	14	12	2	13	41	12
22	7	7	7	7	28	6
23	10	10	3	8	31	7
24	11	9	6	11	37	9
25	26	22	17	19	84	22
26	13	21	19	23	76	20

Based on the results of all the analysis, method 16, which is Decourt (sand) +Tomlinson (clay) +TipAPI ranks number one, showing the best performance according to these 4 evaluation criteria. Then followed by method 17 and 18, they both rank as number two. The method 3, which is Nordlund (sand) + Dennis (clay) + TipNord/API,

shows the lowest accurate performance among all methods. It can be seen that method 25 and 26 recommended by CALTRANS have high rank index, showing they are not good predicting methods based on our database.

This chapter presented an evaluation of 26 methods to estimate bearing capacity of pipe piles driven in California. Analysis was conducted on 45 pipe piles coming from CALTRANS database, in which over half of piles were driven in mixed soil. The measured ultimate resistance for each pile was determined from the load-settlement curve and defined as Q_m corresponding to 1 inch settlement. The predicted ultimate resistance of each pile Q_c was determined from 26 static prediction methods.

The evaluation was conducted to estimate the performance of those 26 methods by comparing the predicted and measured ultimate pile capacities. The evaluation system was based on 4 criteria: best fitting line for Q_c vs. Q_m, the arithmetic mean and standard deviation of Q_c/Q_m, the cumulative probability P_{50} and P_{90} of Q_c/Q_m, histogram and log-normal distribution of Q_c/Q_m. Those 26 methods were ranked based on each individual criterion, then a final rank of all methods was conducted considering all 4 criteria by using Rank Index (RI). Based on above, method 16, which is Decourt (sand) +Tomlinson (clay) +TipAPI ranks NO.1, is the best predicting method for pipe piles in California.

Chapter 5

RESISTANCE FACTOR CALIBRATION USING MONTE CARLO SIMULATION

This chapter presents the calibration process of resistance factors for using Load and Resistance Factor Design (LRFD) method of steel pipe piles driven into California soil based on reliability theory.

The allowable stress design (ASD) method is usually applied by researchers to account for uncertainties by applying a factor of safety (FS). The magnitude of FS, which has been empirically developed over time depending on the importance of the structure, the confidence levels of material properties, and the design methodology, is defined as ultimate pile capacity over allowable design load. However, for this method, uncertainties of load and resistance are combined together and may lead to a design with a different level of safety for similar structures(Abu-Farsakh et al. 2009). In order to separate uncertainties of load effect from uncertainties of resistance, also provide a consistent margin of safety for the design of structure, LRFD method has been introduced to incorporate with uncertainties in the foundation design based on reliability theory.

The use of Load and Resistance Factor Design (LRFD) for highway bridges has been approved by the Subcommittee for Bridges and Structures of the American Association of State Highway and Transportation Officials (AASHTO). It has been mandated that all bridge design were based on this approach since October 2007. Statistical analysis and development of resistance factor in this study were using Monte Carlo simulation and following Transportation Research Circular E-C079 (Allen et al. 2005). Since the resistance factor from the current AASHTO design specification is based on the soil sites that may not necessarily reflect local soil in California, using reliability theory analysis to produce resistance factor consistent with local soil becomes practicable.

5.1 Reliability Theory

There are two limit states that are usually checked in foundation design. One of them is ultimate limit state (ULS), which requires factored resistance should be at least as large as factored load, the other one is serviceability limit state (SLS), which requires deformation should be less than tolerable deformation. Since deep foundation is primarily controlled by the ultimate state, therefore, only ultimate limit stated is considered in the following analysis. The ultimate limit state equation can be present as:

$$\sum \gamma_i Q_{ni} \leq \phi R_n \qquad (5\text{-}1)$$

Where

γ_i = load factor applicable to a specific load component;

Q_{ni} = a specific nominal load component;

$\sum \gamma_i Q_{ni}$ = the total factored load for the load group applicable to the limit state being considered;

ϕ = the resistance factor; and

R_n = the nominal resistance.

Load and resistance factors in Equation 5-2 are used to account for material variability, uncertain in magnitude of applied loads, design model prediction uncertainty and other sources of uncertainty (Transportation Research Circular E-C079).

If there is only one load component, equation can be shown as:

$$\phi_R R_n - \gamma_Q Q_n \geq 0 \qquad (5\text{-}2)$$

Where

R_n = the nominal resistance value;

Q_n = the nominal load value;

ϕ_R = a resistance factor; and

γ_Q = a load factor.

The limit state equation corresponds to above is:

$$g = R - Q \geq 0 \qquad (5\text{-}3)$$

Where

g = a random variable representing safety margin

R = a random variable representing resistance; and

Q = a random variable representing load.

The probability density functions for the load and resistance can be presented by Figure 5-1. Failure can be defined as when applied loading exceeds resistance. For example, as it is shown in Figure 5-1, the magnitude of red spot on the Load Probability density curve is larger than that of black spot on the resistance probability density curves.

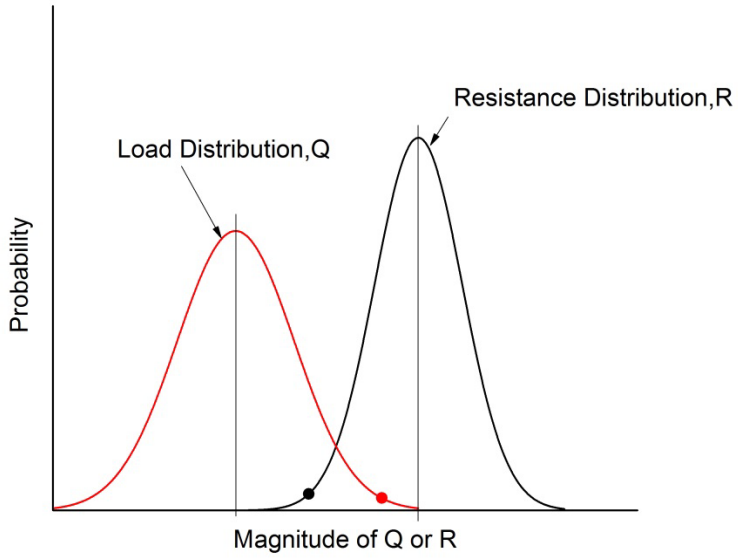

Figure 5-1 Probability density functions for load and resistance

If combined two curves into one, then the Figure 5-2 can be obtained. Failure is defined as shaded area when curve $g = R - Q < 0$ happens. Parameter β is equal to 1/COV for the limit state function, $g = R - Q$, and is related to the probability of failure.

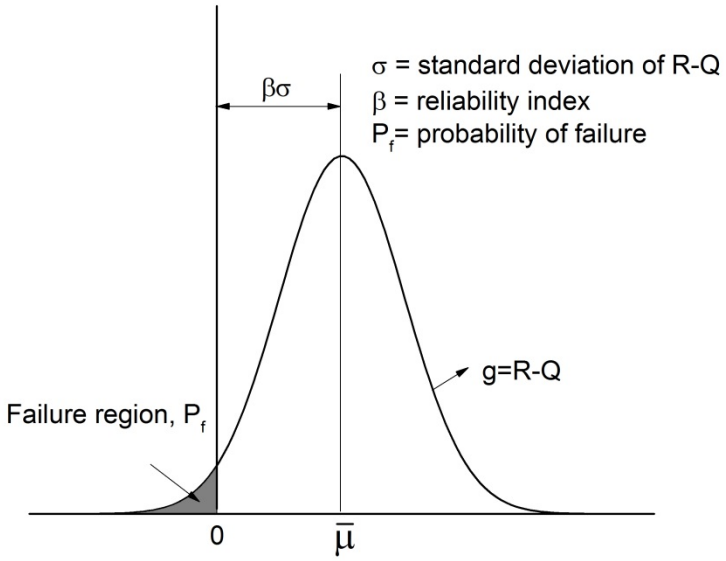

Figure 5-2 Distribution of limit state equation

For the normally distributed function g showing above, failure probability will decrease when reliability index β value increases, this relationship can be shown using excel function:

$$\beta = NORMSINV(P_f) \qquad (5\text{-}4)$$

Also reliability index β and probability of failureP_f can be illustrated as follows:

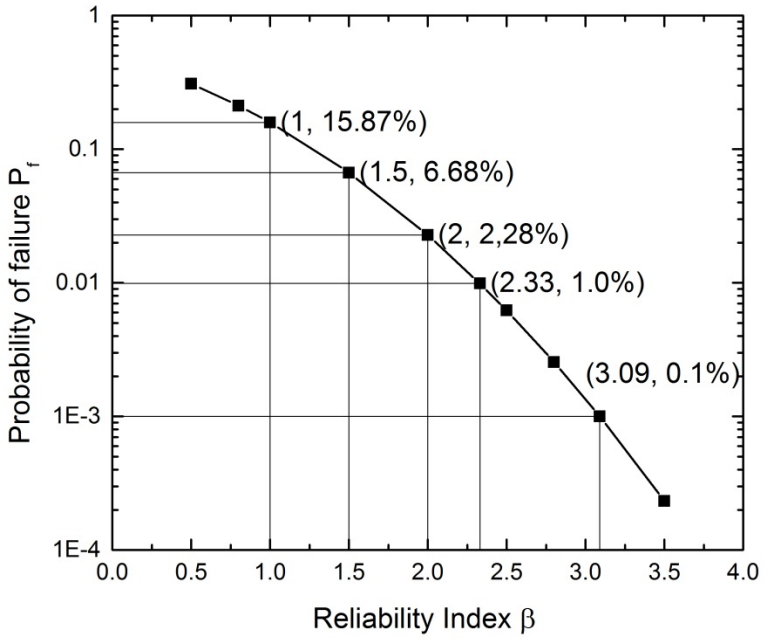

Figure 5-3 Probability of Failure corresponding to varies β values

The relationship showing in Figure 5-3 applied on normal distribution g, the more limit state equation g departs from normal distribution, the more approximation the relationship is.

The limit state equation in this thesis considers both dead load and live load affect, which can be expressed as:

$$\phi R_n = \gamma_{DL} Q_D + \gamma_{LL} Q_L \qquad (5\text{-}5)$$

Where

γ_{DL} = load factor resulting from dead load;

γ_{LL} = load factor resulting from live load;

Q_D = the dead load contribution to total load at specified location;

Q_L = the live load contribution to total load at specified location.

Load statistics and load factor are selected (AASHTO 2012) as follows:

Table 5-1 Statistical characteristics and load factor

	Bias	COV	Load factor
Live load	$\lambda_{LL} = 1.15$	$COV_{LL} = 0.2$	$\gamma_{LL} = 1.75$
Dead load	$\lambda_{DL} = 1.05$	$COV_{DL} = 0.1$	$\gamma_{DL} = 1.25$

Where

λ_{LL} = Mean value of measured live load over predicted live load;

λ_{DL} = Mean value of measured dead load over predicted dead load:

COV_{LL} = Coefficient of variation for live load;

COV_{DL} = Coefficient of variation for dead load;

The ratio of dead load over live load (DL/LL) is a function of a bridge's span length (Allen et al. 2005). Large span length results in larger dead load. In this case, a ratio of DL/LL equals to 3 is selected for calibration, which corresponding to 50m span length.

In order to perform calibration of resistance factor based on reliability theory, mean value, standard deviation, coefficient of variation and type of distribution best fits of the data must be obtained for random variables in the limit state equation. The bias values, defined as the ratio of measured resistance or load over corresponding predicted resistance or load, are used to generate those needed data. Since resistance factor calibration is the priority goal and that load component factors have been selected, bias that still needed to be analyzed in this case can be represented/calculated as the ratios of individual measured resistance over predicted resistance for those 45 steel pipe piles.

5.2 Calibration Using Monte Carlo Simulation

Monte Carlo method is more rigorous when compared to other calibration methods. It is a technique utilized as a random number generator that has two main

advantages: 1) to extrapolate the CDF values for random variable in the limit state equation; 2) to randomly generate many more measured load and resistance values than that were available by original data from local soil based on statistical characters. Once load and resistance values have been generated, the limit state function g can be estimated from each paired resistance and load values. The failure probability P_f can therefore be directly obtained by counting case number which is less than 0 divided by the total generated case number. This method for CDF curve extrapolation makes estimation reliability index β become possible by increasing quantity of measured data, by which statistical analysis could be applied on to reliably predict β.

To generate available measured load and resistance values and obtain resistance factors according to varied reliability index value β using Monte Carlo method, the following steps can be taken:

1. Establish the limit state equation. For this case, since both dead load and live load have been considered, it can be defined as:

$$g = R - Q$$

$$g = \lambda_R \left(\frac{\gamma_{DL} Q_{DL} + \gamma_{LL} Q_{LL}}{\phi} \right) - \left(Q_{DL} \lambda_{DL} + Q_{DL} \frac{LL}{DL} \lambda_{LL} \right) \quad (5\text{-}6)$$

   Assume a nominal value of $Q_{DL} = 1$ for convenience, since positive or negative of g value is the only factor needed to be focused.

2. Select a target value $\beta = \beta_T$. In this case, a target value of 2.33 is chosen, which corresponds to 1% failure probability.

3. If load is following log-normal distribution, the generated dead measured load can be defined

$$Q_{DLi} = EXP(\mu_{ln} + \sigma_{ln} z_i) \quad (5\text{-}7)$$

Where

μ_{ln} = $LN(\overline{Q_{DL}}) - 0.5{\sigma_{ln}}^2$

σ_{ln} = $\{LN[(COV_{DL})^2] + 1\}^{0.5}$

Q_{DDi} = a randomly generated load value of load using specified set of statistical parameters

$\overline{Q_{DL}}$ = normal mean of load and equal to $\lambda_{DL}Q_D$, λ_{DL} defined previously as mean of bias for dead load;

COV_{DL} = the coefficient of variation of bias for Q_{DL};

z_i =NORMSINV(RAND()), is the random standard normal variable generated using the EXCEL function.

Equation for generating log-normal live load can be followed as:

$$Q_{LLi} = EXP(\mu_{ln} + \sigma_{ln}z_i) \quad (5\text{-}8)$$

Where

μ_{ln} = $LN(\overline{Q_{LL}}) - 0.5{\sigma_{ln}}^2$

σ_{ln} = $\{LN[(COV_{LL})^2] + 1\}^{0.5}$

Q_{LLi} = a randomly generated load value of load using specified set of statistical parameters

$\overline{Q_{LL}}$ = normal mean of live load and equal to $\lambda_{LL}Q_L$, λ_{LL} defined previously as mean of bias for live load; (Since DL/LL =3 has been chosen, $\overline{Q_{LL}}$=$\lambda_{LL}Q_L = \lambda_{LL} * \frac{1}{3} * Q_D$)

COV_{LL} = the coefficient of variation of bias for Q_{LL};

z_i is same as previous.

Similarly, if resistance values are log-normally distributed, generated resistance values can be generated by a log-normal mean and log-normal standard deviation as:

$$R_i = EXP(\mu_{ln} + \sigma_{ln}z_i) \quad (5\text{-}9)$$

Where

μ_{ln} = $LN(\bar{R}) - 0.5{\sigma_{ln}}^2$

σ_{ln} = $\{LN[(COV_R)^2] + 1\}^{0.5}$

R_i = a randomly generated load value of load using specified set of statistical parameters

$\bar{R}$ = normal mean of resistance and equal to$\lambda_R R$, λ_R defined as mean of bias for resistance; (R can be calculated as a function of resistance factor and load), then

$$R = \left(\frac{\gamma_D Q_D + \gamma_L Q_L}{\phi}\right) = \left(\frac{\gamma_D * 1 + \gamma_L * \frac{LL}{DL}}{\phi}\right) \quad (5\text{-}10)$$

COV_R = the coefficient of variation of bias forQ_R;

z_i is same as previous defined.

4. Calculate random values of g using the limit state equation,

$$g_i = R_i - Q_{DD} - Q_{LL} \quad (5\text{-}11)$$

10000 values of g will be generated.

5. Calculate the probability of failure, P_f, by taking the number of values of g calculated that are less than 0 and dividing them by the total 10000 number of g. Probability index β is related to P_f, defined as previously.

$$P_f = \frac{count(g \leq 0)}{N(10000\ cases)} \quad (5\text{-}12)$$

Then the corresponding probability index is calculated as:

$$\beta = NORMSINV(P_f) \quad (5\text{-}13)$$

6. Since statistical characters for load has been specified, (i.e. dead and live load factor, mean of bias, coefficient of variation, and ratio of dead load to live load), and that the mean of bias and coefficient of variation for resistance can be obtained from local sample data, the only uncertain parameter here is resistance

factor. If a trial resistance factor does not result in the desired β values in step 2, change this resistance factor, regenerate random measured load values, count the cases with g values less than 0 again, until designed β value has achieved.

The load and resistance factors used to get target β value are the ones that can be utilized for the design in the local area to keep this designed failure probability.

5.3 LRFD Calibration Results

As mentioned previously, bias, defined as the ratio of measured resistance to predicted resistance, can be used to obtain needed statistics data for calibration. In this study, measured resistance were coming from pile load test (45 steel pipes data from California), predicted resistance were calculated following various design methods. To characterize the resistance data, a cumulative distribution function (CDF) can be developed, which represents probability that a bias value less than or equal to a given value occur, and this can be transformed to the standard normal variable, z, against the bias value of each individual data. This can be processed in following steps:

1. Sort the bias values for pile resistance from lowest to highest, probability associated with each bias value in the cumulative distribution as i/(n+1), in this case the total cases n equals to 45.

2. The probability value calculated in step 1 associated with each ranked bias can be convert to standard normal variable z, this process can be finished by using Excel function:

$$z = NORMSINV(\frac{i}{n+1}) \qquad (5\text{-}14)$$

Where I is the sorted rank of each bias, n is total number of bias. Once z values have been generated, the relationship between standard normal variable z and bias can be found.

The theoretical normal distribution is represented as straight dash line, calculated using equation below:

$$Bias = X = \lambda + \sigma z \quad (5\text{-}15)$$

Where

X = bias, which is measured over predicted value

λ = normal mean of bias;

σ = standard deviation of bias;

The theoretical log-normal distribution curve which is showing solid curve can be obtained as follows:

$$Bias = X = EXP(\mu_{ln} + \sigma_{ln} z) \quad (5\text{-}16)$$

Where

μ_{ln} = $LN(\mu_s) - 0.5{\sigma_{ln}}^2$

σ_{ln} = $\{LN[(\sigma/\mu_s)^2] + 1\}^{0.5}$

From the shape of plot, log-normal distribution fits bias data much better than normal distribution curve. The distribution of resistance bias can be assumed to follow log-normal distribution, therefore log-normal statistic characters will be used to evaluate those 26 predicting methods, and also resistance factor calibration process will be based on it.

For resistance factor calibration, there is another approach used to fit lower tail data, where the ratio of measured over predicted is relative low, representing the dangerous cases with predicted resistance close to or even larger than measured resistance. Some judgments had been used to select tail region, as there are significant gaps and jumps in dataset. It will be more conservative to fit the lower tail slightly to the left of actual data. The best fit to tail regions (using only lower tail black data to fit) in

comparison to the theoretical log-normal distribution based on the entire data, illustrating z of each associate bias are showing Figure 5-4 to Figure 5-29.

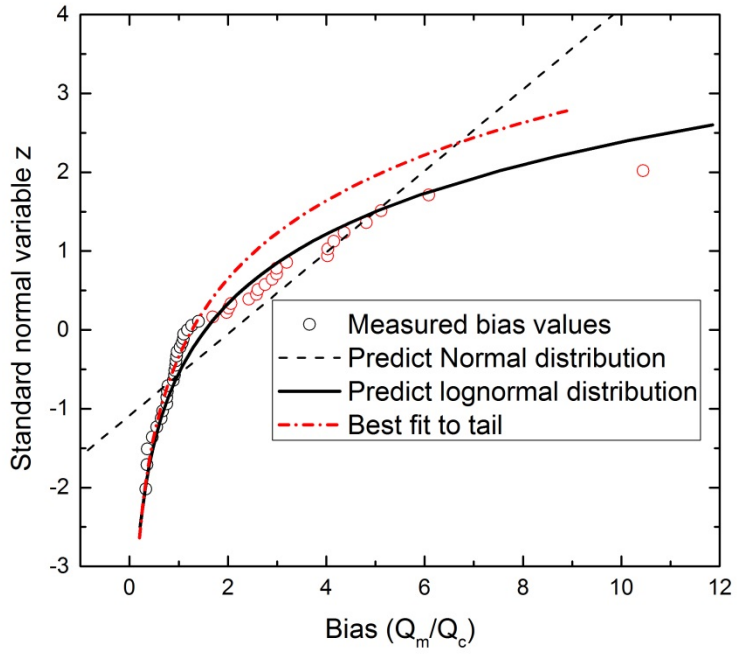

Figure 5-4 Standard normal variable, z, as a function of resistance bias for 45 steel pipe piles (Predicting Method 1)

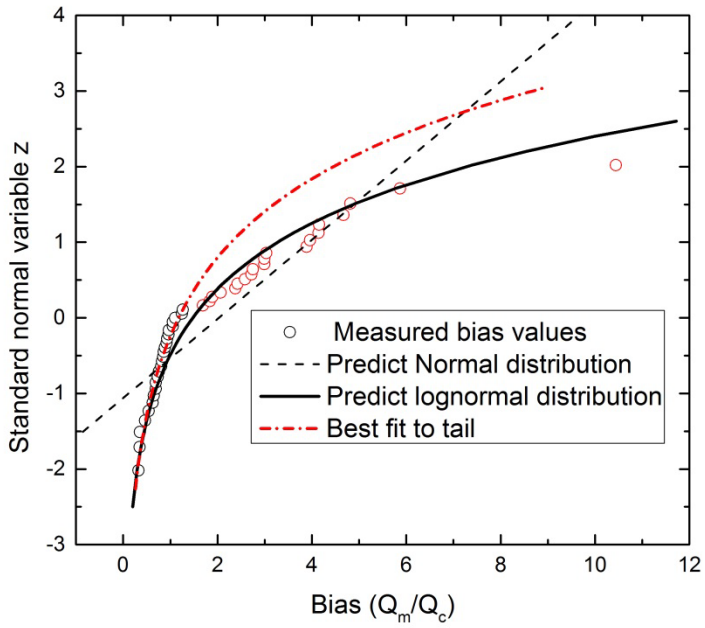

Figure 5-5 Standard normal variable, z, as a function of resistance bias for 45 steel pipe piles (Predicting Method 2)

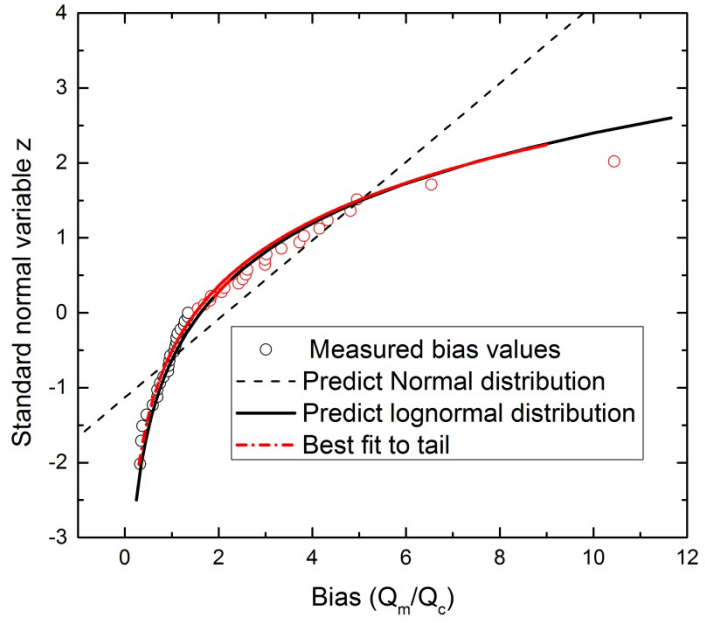

Figure 5-6 Standard normal variable, z, as a function of resistance bias for 45 steel pipe piles (Predicting Method 3)

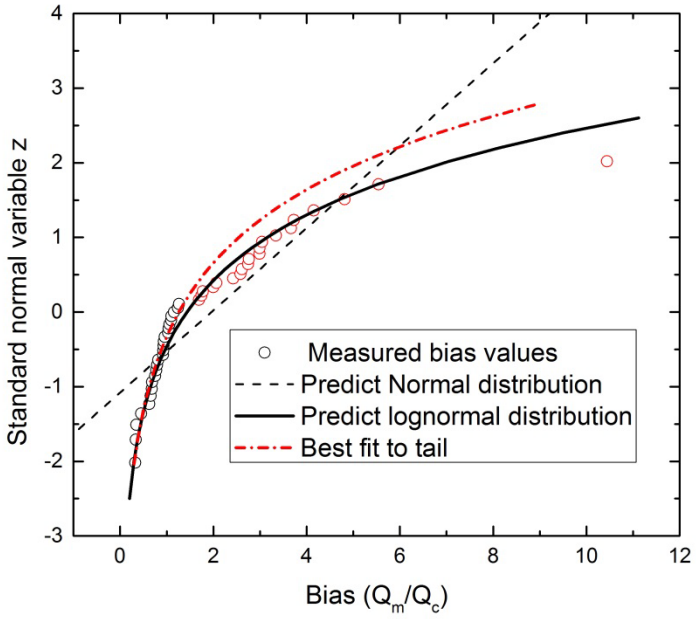

Figure 5-7 Standard normal variable, z, as a function of resistance bias for 45 steel pipe piles (Predicting Method 4)

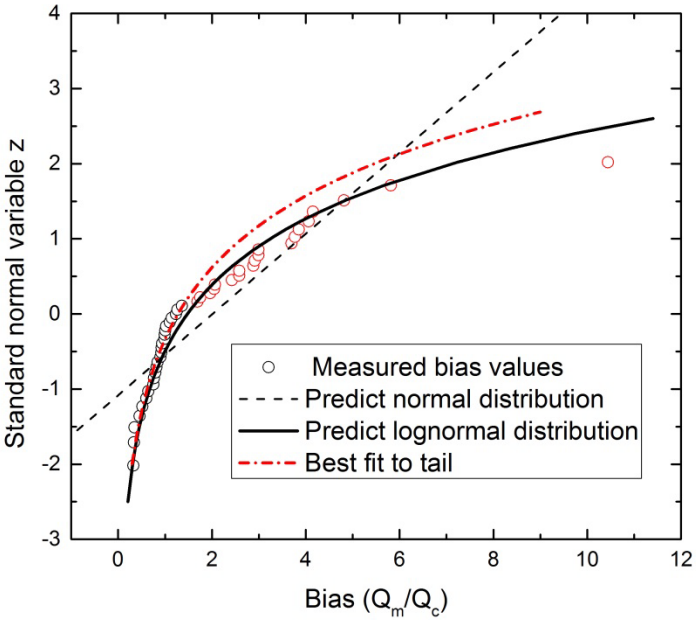

Figure 5-8 Standard normal variable, z, as a function of resistance bias for 45 steel pipe piles (Predicting Method 5)

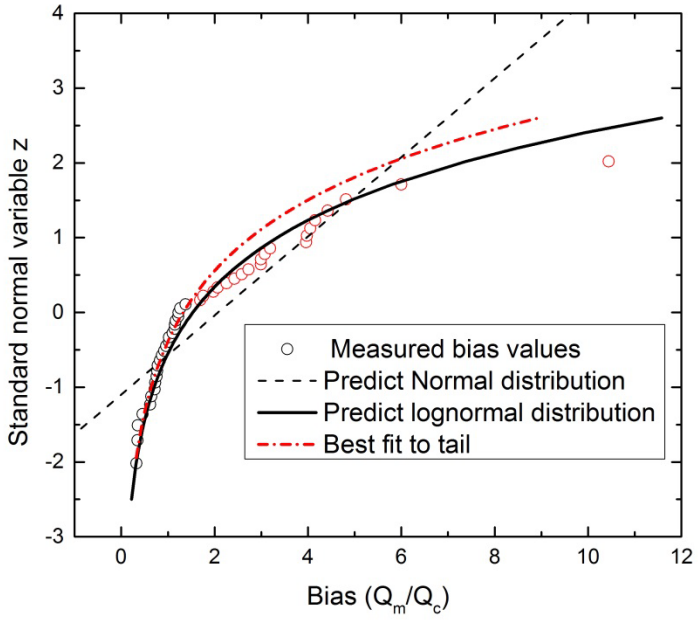

Figure 5-9 Standard normal variable, z, as a function of resistance bias for 45 steel pipe piles (Predicting Method 6)

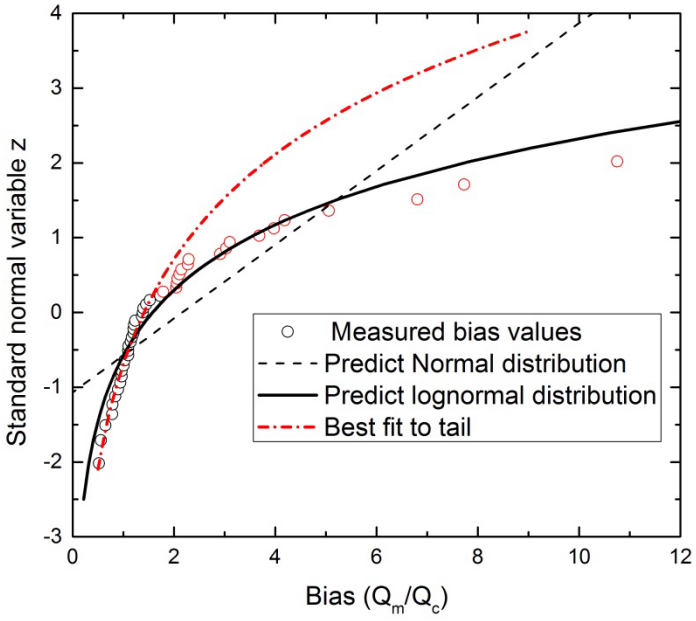

Figure 5-10 Standard normal variable, z, as a function of resistance bias for 45 steel pipe piles (Predicting Method 7)

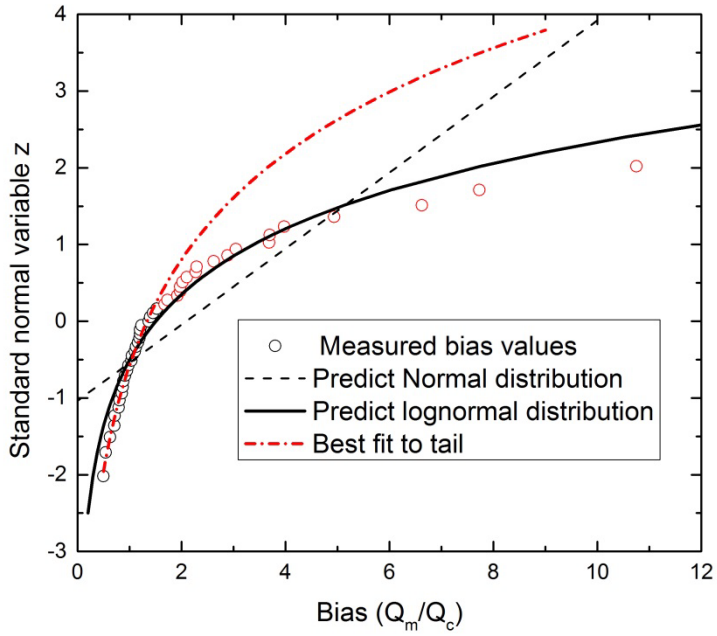

Figure 5-11 Standard normal variable, z, as a function of resistance bias for 45 steel pipe piles (Predicting Method 8)

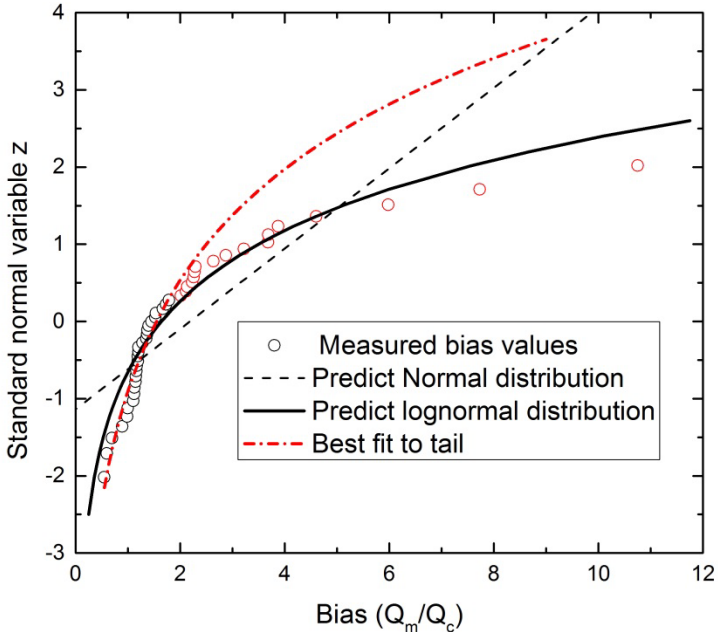

Figure 5-12 Standard normal variable, z, as a function of resistance bias for 45 steel pipe piles (Predicting Method 9)

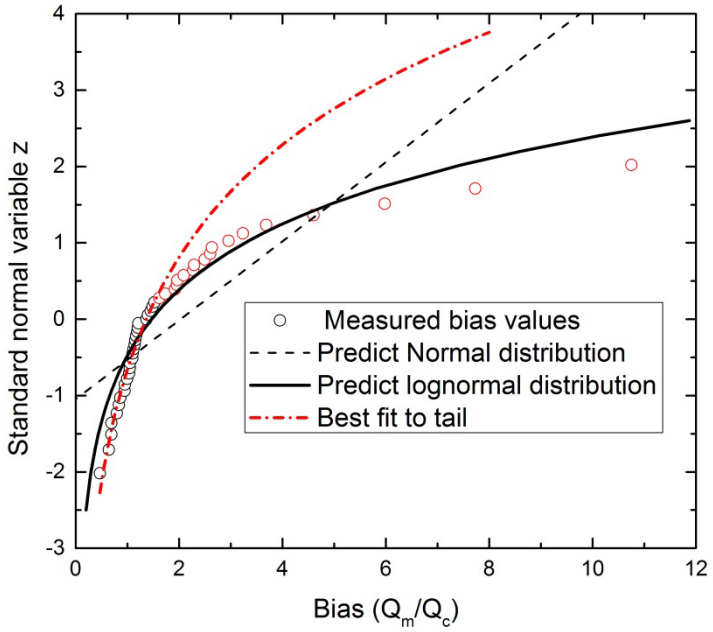

Figure 5-13 Standard normal variable, z, as a function of resistance bias for 45 steel pipe piles (Predicting Method 10)

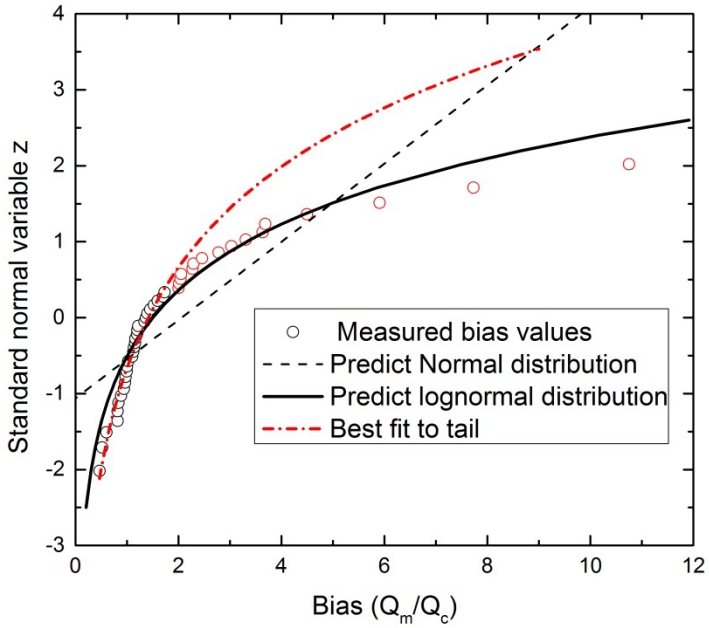

Figure 5-14 Standard normal variable, z, as a function of resistance bias for 45 steel pipe piles (Predicting Method 11)

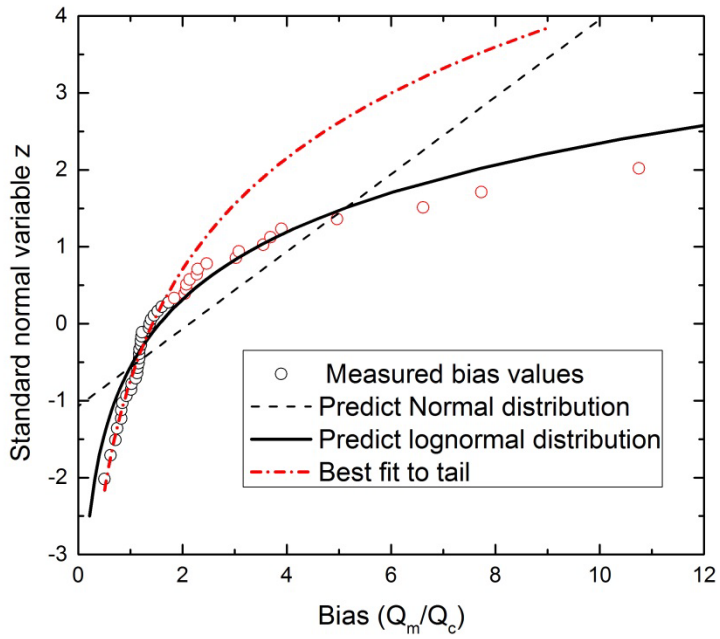

Figure 5-15 Standard normal variable, z, as a function of resistance bias for 45 steel pipe piles (Predicting Method 12)

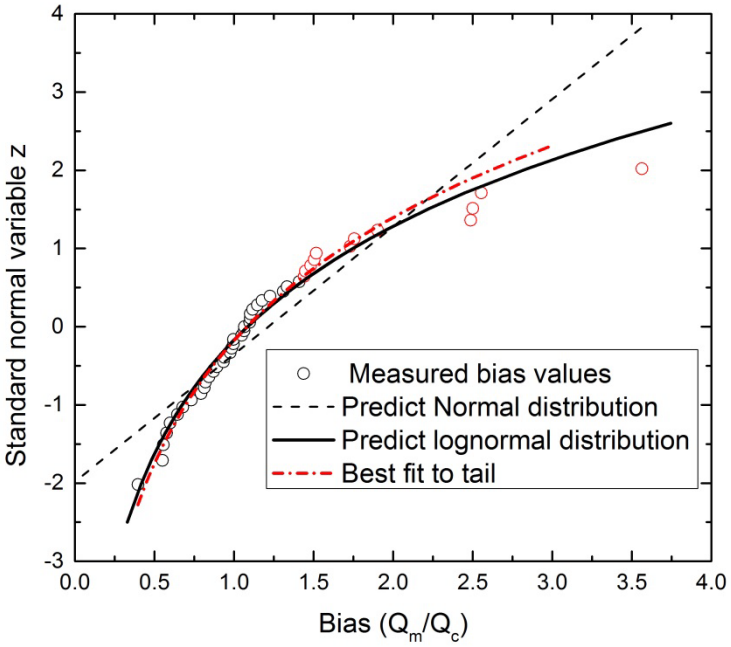

Figure 5-16 Standard normal variable, z, as a function of resistance bias for 45 steel pipe piles (Predicting Method 13)

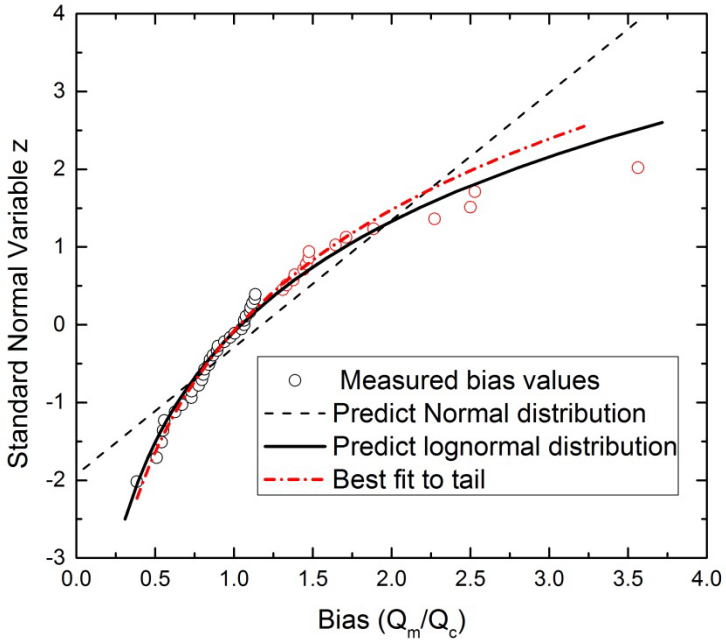

Figure 5-17 Standard normal variable, z, as a function of resistance bias for 45 steel pipe piles (Predicting Method 14)

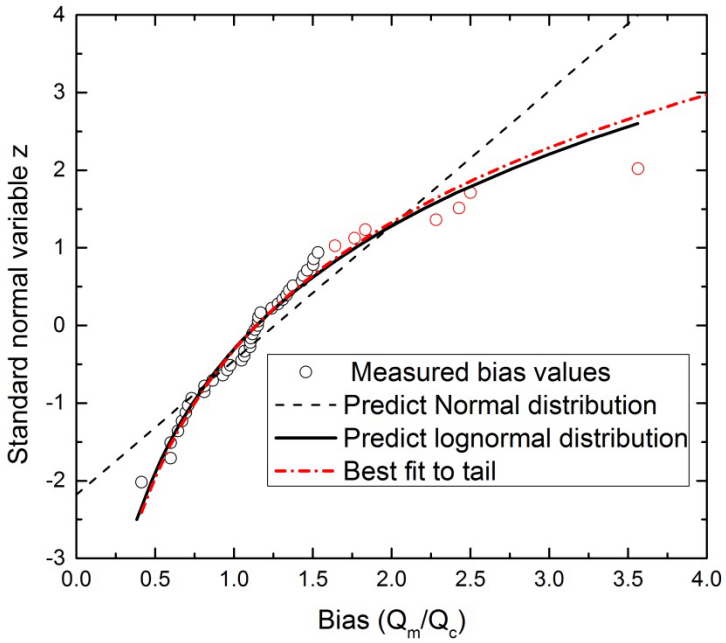

Figure 5-18 Standard normal variable, z, as a function of resistance bias for 45 steel pipe piles (Predicting Method 15)

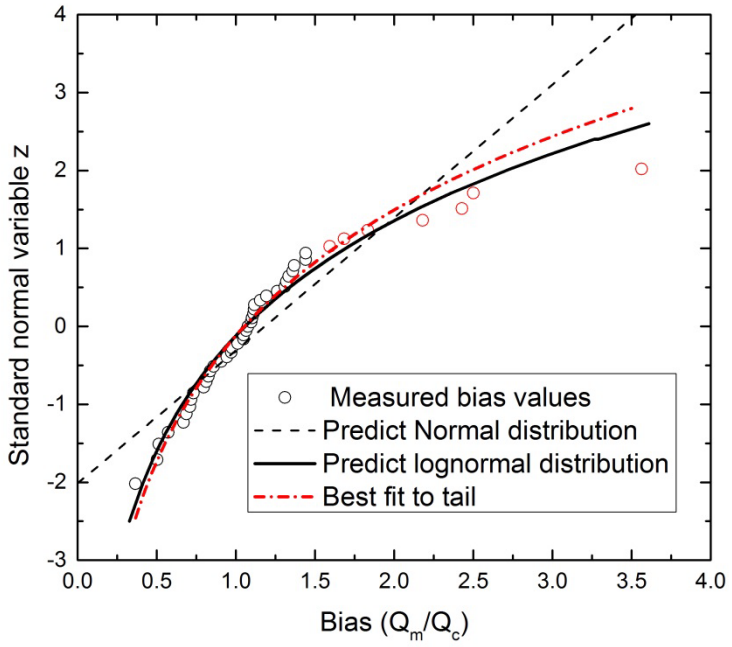

Figure 5-19 Standard normal variable, z, as a function of resistance bias for 45 steel pipe piles (Predicting Method 16)

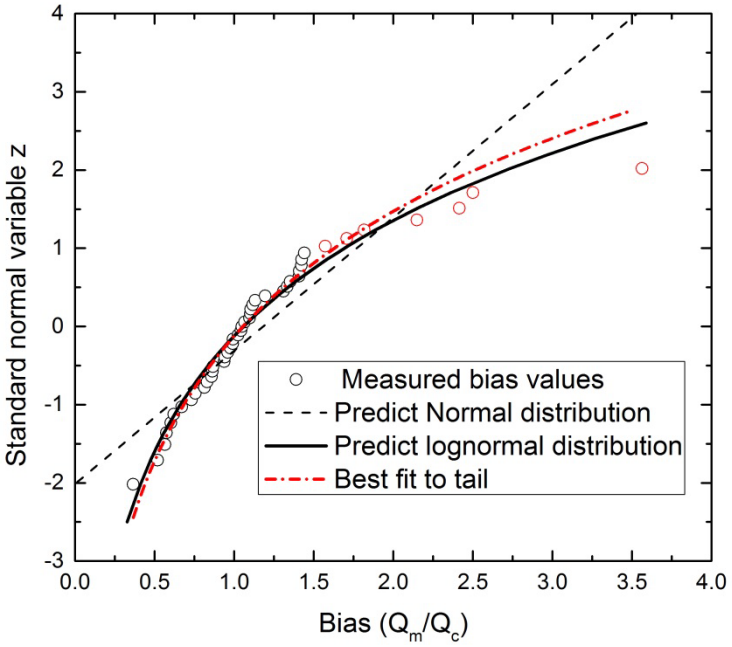

Figure 5-20 Standard normal variable, z, as a function of resistance bias for 45 steel pipe piles (Predicting Method 17)

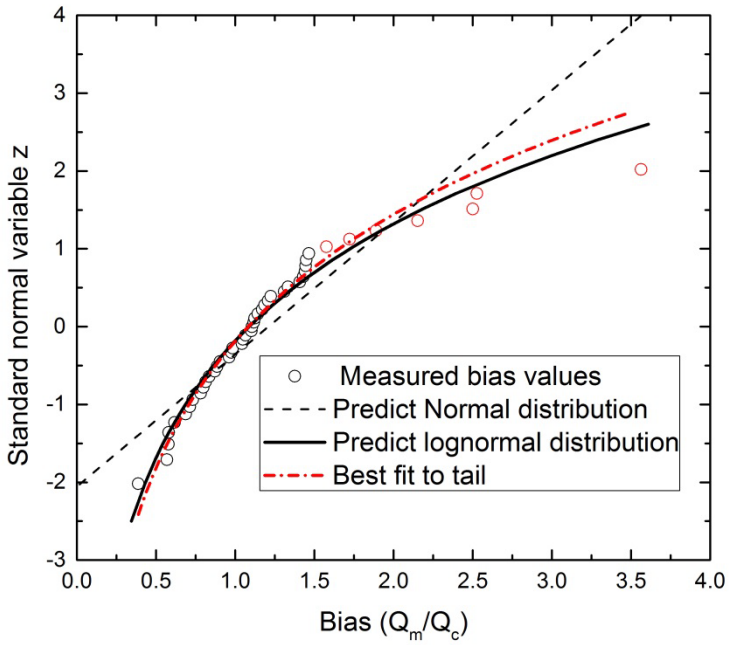

Figure 5-21 Standard normal variable, z, as a function of resistance bias for 45 steel pipe piles (Predicting Method 18)

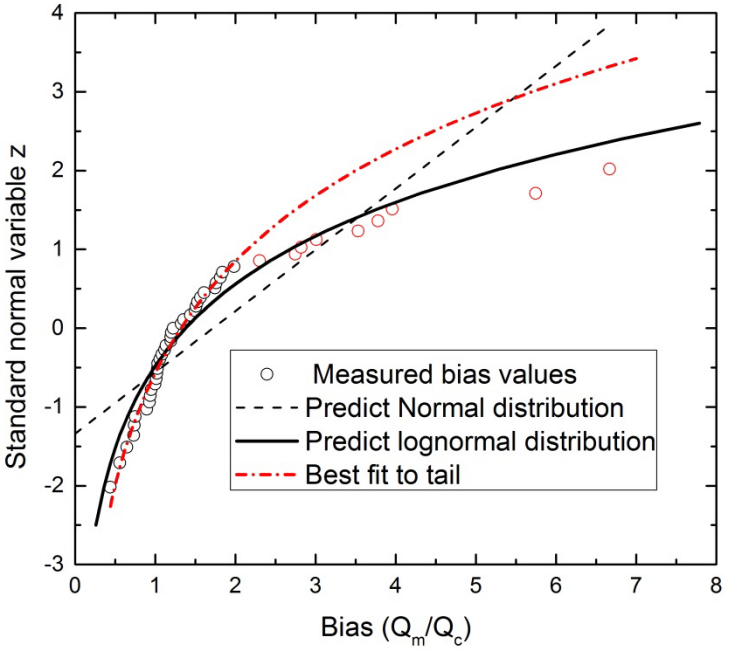

Figure 5-22 Standard normal variable, z, as a function of resistance bias for 45 steel pipe piles (Predicting Method 19)

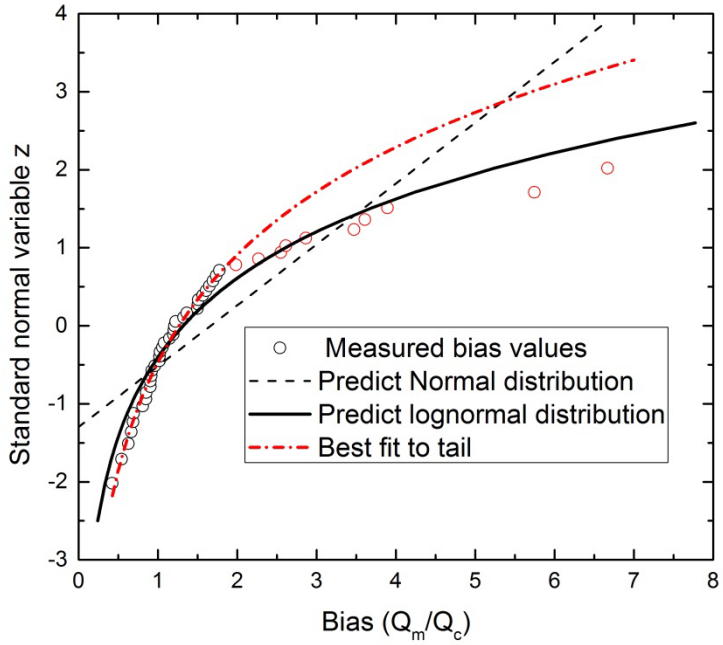

Figure 5-23 Standard normal variable, z, as a function of resistance bias for 45 steel pipe piles (Predicting Method 20)

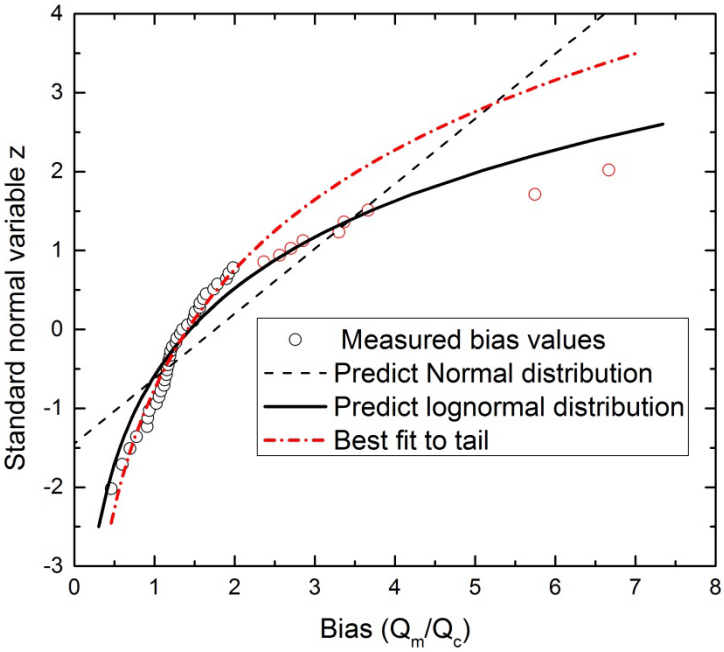

Figure 5-24 Standard normal variable, z, as a function of resistance bias for 45 steel pipe piles (Predicting Method 21)

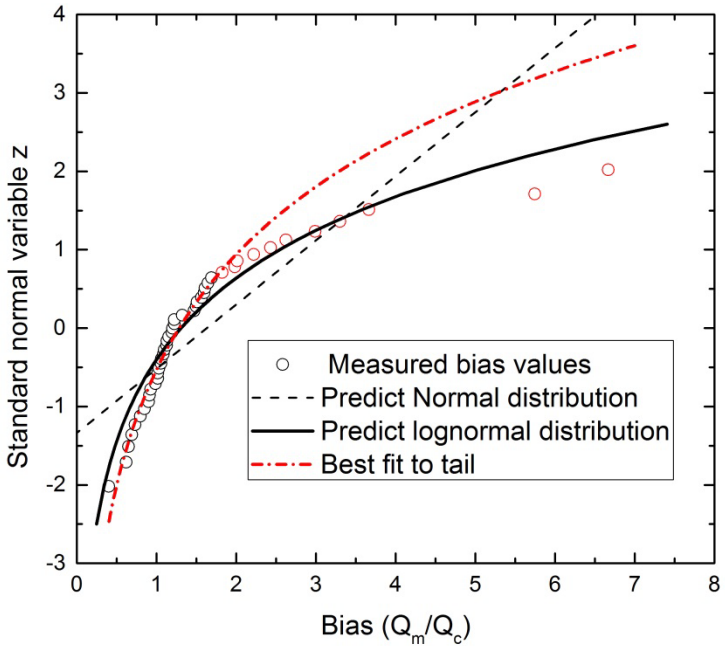

Figure 5-25 Standard normal variable, z, as a function of resistance bias for 45 steel pipe piles (Predicting Method 22)

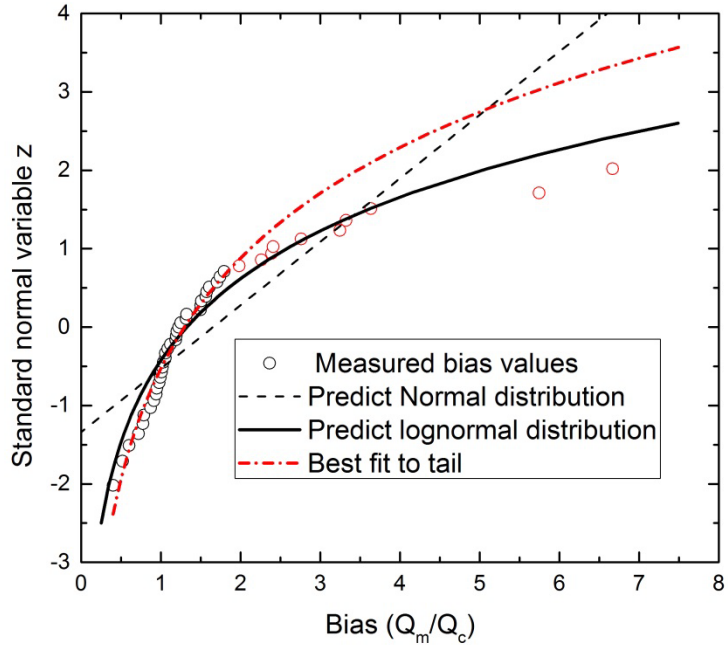

Figure 5-26 Standard normal variable, z, as a function of resistance bias for 45 steel pipe piles (Predicting Method 23)

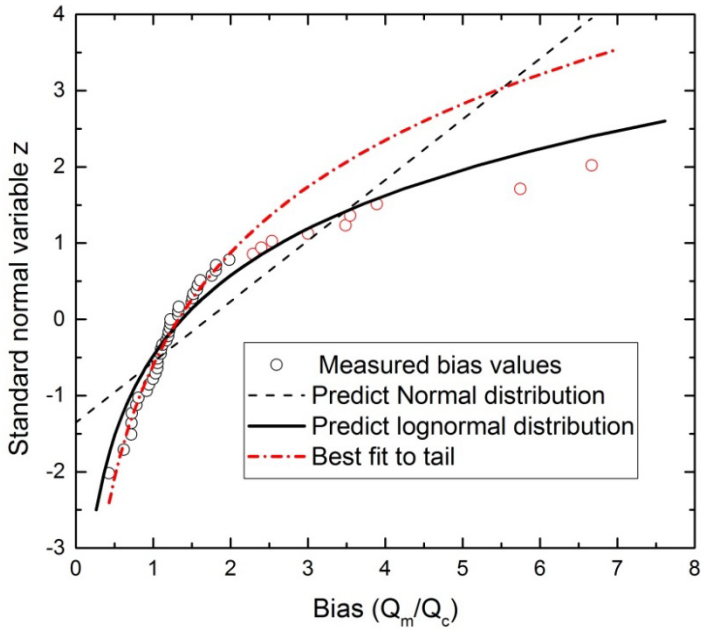

Figure 5-27 Standard normal variable, z, as a function of resistance bias for 45steel pipe piles (Predicting Method 24)

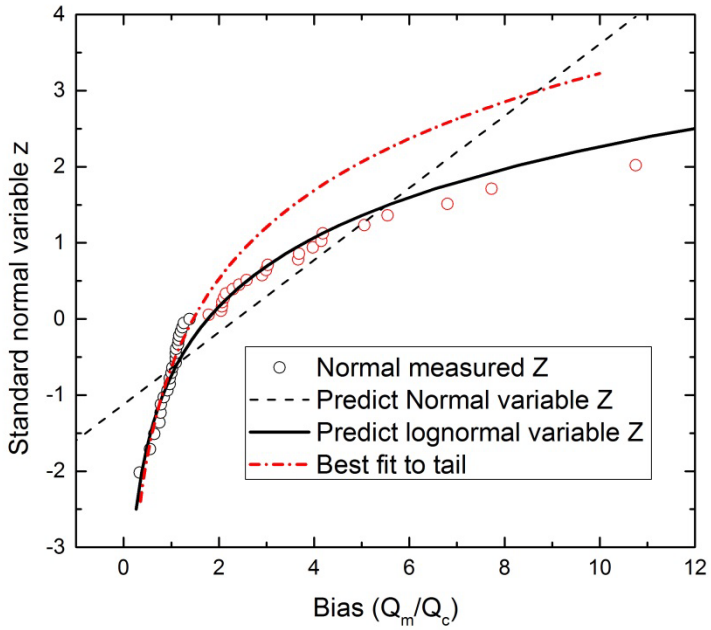

Figure 5-28 Standard normal variable, z, as a function of resistance bias for 45 steel pipe piles (CALTRANS 16)

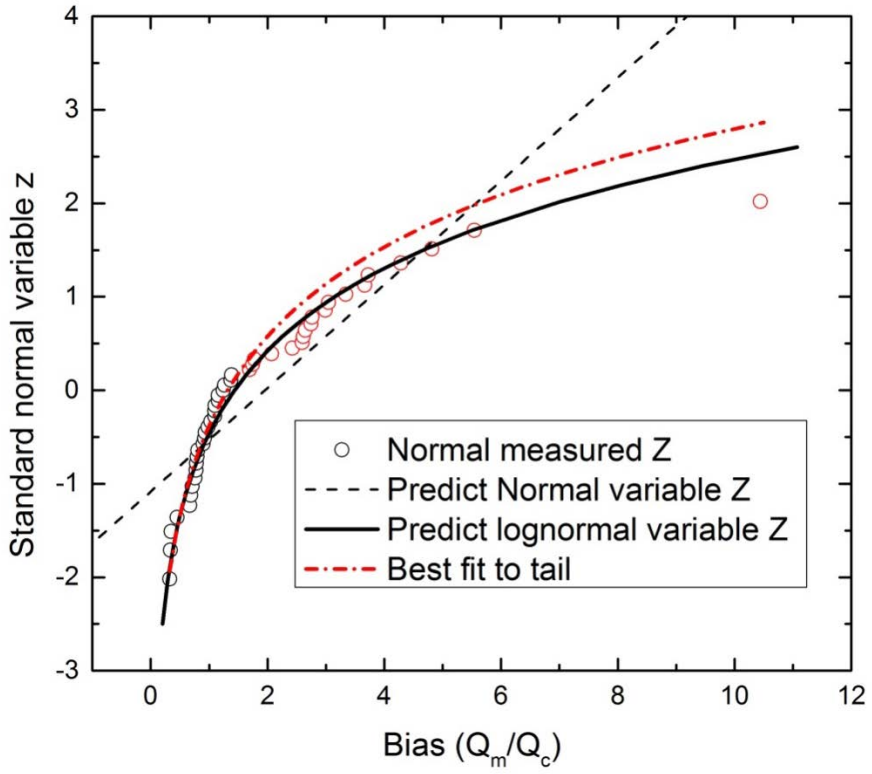

Figure 5-29 Standard normal variable, z, as a function of resistance bias for 45 steel pipe piles (CALTRANS 24)

Resistance factors were determined based on Statistical characteristics, following the process of Monte Carlo simulation for measured data and best fit to tail method. Summarized in Table 5-2 is mean of bias μ for each design method and associated standard deviation σ, coefficient of variation COV. As mentioned in chapter 2, The values of the resistance factors alone do not provide a measure for evaluating the efficiency of the design methods, efficiency can be evaluated through the ratio of the resistance factor to the bias factor (ϕ/μ), according to values of this ratio, method 15 is most economical (ϕ/μ=0.41) based on entire data, and method 16 preferred as most economical (ϕ/μ=0.43) based on best fit to tail data. They are more than twice as cost

effective as using Nordlund method in first 6 methods. In addition, it can be seen from table, lower COV value leads to higher value of ϕ/μ, which means more economical.

Table 5-2 Calibrated resistance factors for different design methods at reliability index β=2.33

Method.	Entire measured data				Best fit to tail			
	ϕ (β=2.33)	u	Sigma	COV	ϕ (β=2.33)	u	Sigma	COV
1	0.32	2.10	1.93	0.92	0.32	1.62	1.29	0.80
2	0.30	2.03	1.91	0.94	0.32	1.47	1.10	0.75
3	0.36	2.16	1.91	0.88	0.31	2.07	1.95	0.94
4	0.30	1.96	1.81	0.93	0.32	1.61	1.29	0.80
5	0.31	2.01	1.86	0.92	0.30	1.66	1.39	0.83
6	0.33	2.07	1.89	0.91	0.31	1.74	1.47	0.84
7	0.32	2.16	2.03	0.94	0.56	1.59	0.84	0.53
8	0.30	2.09	2.02	0.96	0.52	1.51	0.81	0.54
9	0.36	2.18	1.92	0.88	0.63	1.74	0.89	0.51
10	0.29	2.03	1.93	0.95	0.57	1.52	0.76	0.50
11	0.31	2.06	1.94	0.94	0.53	1.62	0.91	0.56
12	0.32	2.13	1.99	0.93	0.59	1.60	0.81	0.51
13	0.45	1.22	0.61	0.50	0.49	1.18	0.53	0.45
14	0.42	1.18	0.61	0.52	0.46	1.14	0.53	0.47
15	0.52	1.26	0.58	0.46	0.53	1.25	0.55	0.44
16	0.45	1.18	0.59	0.50	0.49	1.15	0.52	0.45
17	0.45	1.18	0.59	0.50	0.48	1.16	0.53	0.46
18	0.47	1.21	0.59	0.49	0.50	1.19	0.53	0.45
19	0.37	1.72	1.29	0.75	0.53	1.49	0.77	0.52
20	0.35	1.66	1.28	0.77	0.50	1.44	0.77	0.54
21	0.43	1.76	1.21	0.69	0.61	1.57	0.76	0.48
22	0.35	1.63	1.22	0.75	0.54	1.43	0.71	0.50
23	0.36	1.65	1.24	0.75	0.52	1.46	0.77	0.52
24	0.38	1.70	1.26	0.74	0.56	1.48	0.74	0.50
25	0.38	2.37	2.11	0.89	0.46	1.75	1.14	0.65
26	0.29	1.96	1.81	0.92	0.31	1.71	1.42	0.83

Figure 5-30 shows resistance factor calibrated for various design methods under same reliability index β=2.33 (which corresponding to approximate 1.0% failure).

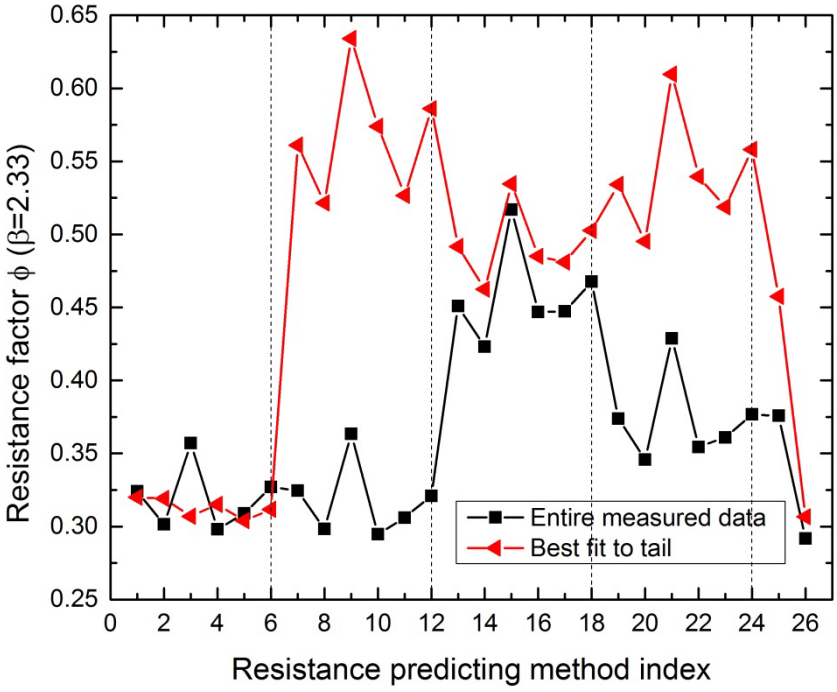

Figure 5-30 Resistance factor for 26 design methods when β_T=2.33

These design methods can be divided into 4 groups based on different predicting way for skin friction in sandy soil (Nordlund for group 1, API for group 2, Decourt for group 3 and Olson for group 4). Within each group of 6 predicting methods, skin friction prediction in sandy soil is constant, skin friction estimating in clay are following various methods. Method 25 and 26 are currently recommended by CALTRANS.

It can be noted based on entire bias that design method 13 through 18 (3rd group using Decourt method for skin friction in sand) show higher resistance factor than other methods, in addition, calibrated resistance factors in first two groups show much lower than it in 3rd and 4th group, which are consistent with the general tendency in final ranking previous chapter, design method with resistance factor closer to 1 may perform as better resistance prediction. The figure also shows Dennis method (3rd point in each group) in

clay skin friction predicting associates with higher resistance factor comparing other estimating ways for clay soil.

As mentioned previously, it is more conservative to fit the lower tail slightly to the left of actual bias, in $2^{nd}$and 4^{th} group, lower tail curve fitting shifted from right (actual data) to left when altered from “best fit to tail” to entire bias fitting, which implies that the entire bias fitting gives out results more conservative than those come from “best fit to tail”, causing higher calibrated resistance factor from “best fit to tail” instead of from entire bias data. In group 3, since “best fit to tail” curve are very similar to entire bias fitting curve, lower tail only shift slightly to right, which leads to a slightly increase of resistance factor value when compared to entire bias fitting. Note that since most design methods have already been relatively conservative, also from data fitting, lower tail fitting moves slightly to right with “best fit to tail” in most of cases (less conservative), it might be better to use resistance factor calibrated from “best fit to tail”.

It is recommended in AASHTO LRFD Specification that resistance factor is ranging from 0.35 to 0.45 when using α method and Nordlund method, which is higher than real calibrated resistance value (shown as method 4, ϕ=0.3 and 0.32, using entire bias and best fit to tail, respectively) based on 45 steel pipe piles in California soil. Consequently the recommended resistance factor value doesn’t really reflect local steel pipe pile resistance estimation, which is the reason why AASHTO suggests calibrating resistance factor which is consistent with local practice. Therefor all the calibrated resistance factors summarized in table associated with different design methods are only valid for soil profile similar to California soil where those pipe pile data collected from.

Resistance factor for method 16, performs best in resistance predicting based on evaluation criteria previous, shows a value of 0.447 (based on entire bias), which is lower than 0.517 given by method 15. This is probably because Monte Carlo simulation is

more sensitive to COV values instead of each individual mean μ and standard deviation σ, less COV value of bias will lead to higher resistance factor. Another reason is that Q_c/Q_m (predict capacity over measured capacity) has been used for evaluation system to determine best predicting method, while preforming Monte Carlo simulation to get resistance factors is based on bias value which is Q_m/Q_c, defined as measured capacity over predict capacity.

CALTRANS recommended using Tomlinson plus Nordlund method for small diameter piles, API method for large diameter piles with pile diameter threshold of 16 inch and 24 inch. Figure 5-31 and Figure 5-32 show relationship between resistance factor ϕ and reliability index β for CALTRANS 16 and CALTRANS 24 method. Summary table for calibrated resistance factors is shown in Table 5-3.

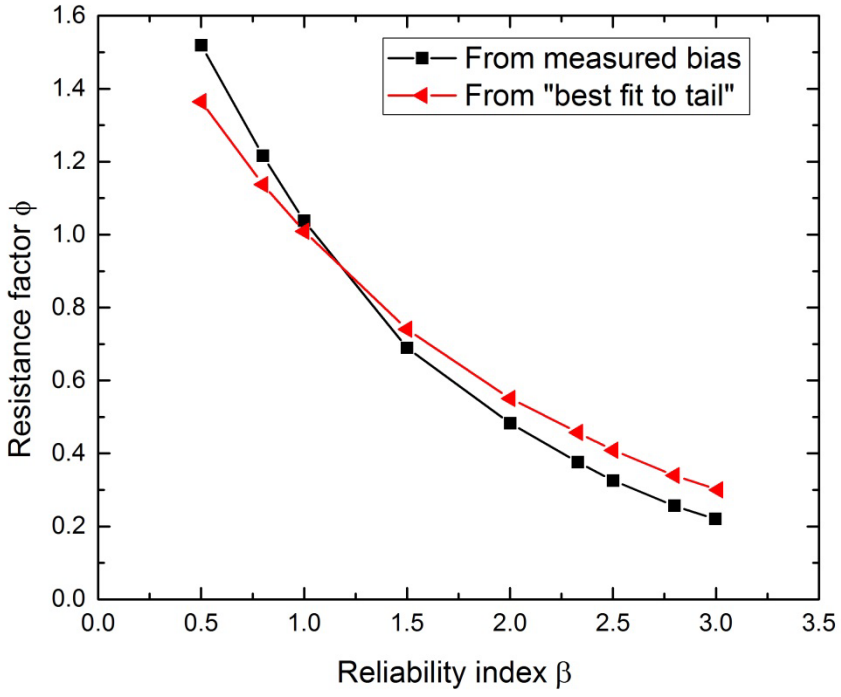

Figure 5-31 Resistance factors with various β for Caltrans 16 method

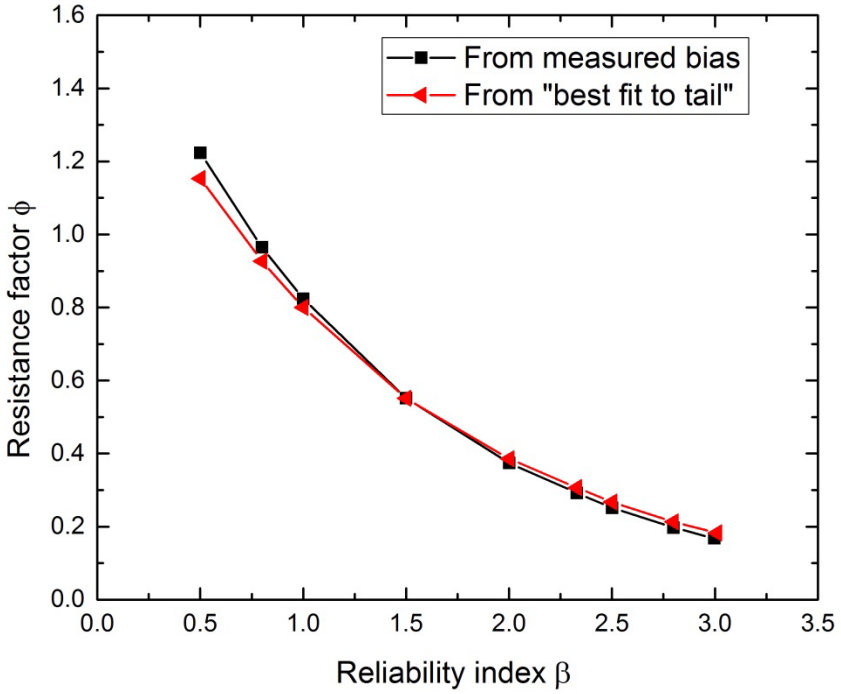

Figure 5-32 Resistance factors with various β for Caltrans 24 method

Table 5-3 Calibrated resistance factor for various target β (CALTRANS 16 and 24)

CALTRANS 16				CALTRANS 24			
Measured		Best fit to tail		Measured		Best fit to tail	
β	ϕ	β	ϕ	β	ϕ	β	ϕ
3.00	0.22	3.01	0.30	3.00	0.17	3.01	0.18
2.80	0.26	2.80	0.34	2.80	0.20	2.80	0.21
2.50	0.33	2.50	0.41	2.50	0.25	2.50	0.27
2.33	0.38	2.33	0.46	2.33	0.29	2.33	0.31
2.00	0.48	2.00	0.55	2.00	0.37	2.00	0.39
1.50	0.69	1.50	0.74	1.50	0.55	1.50	0.55
1.00	1.04	1.00	1.01	1.00	0.82	1.00	0.80
0.80	1.22	0.80	1.14	0.80	0.96	0.80	0.93
0.50	1.52	0.50	1.36	0.50	1.22	0.50	1.15

Since Decourt plus Tomlinson (method 16) is best resistance predicting way based on the previous evaluation criteria, the resistance factors have been determined

for various reliability index β for both fitting methods (entire bias and best fit to tail), and this relationship has shown below:

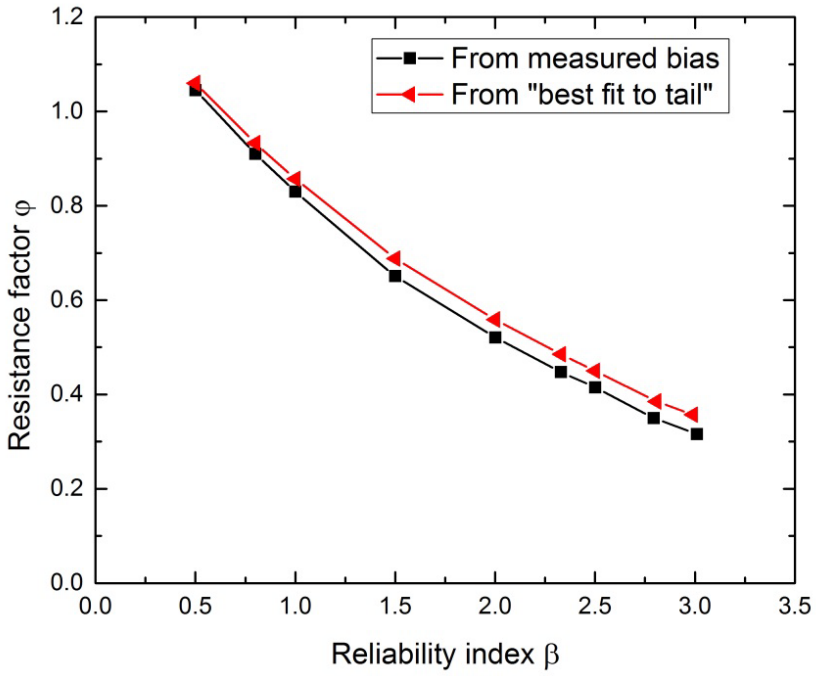

Figure 5-33 Resistance factor for various β for method 16

Table 5-4 Calibrated resistance factor for various target β (Method 16)

Measured		Best fit to tail	
β	ϕ	β	ϕ
3.01	0.32	2.99	0.36
2.79	0.35	2.81	0.39
2.50	0.42	2.50	0.45
2.33	0.45	2.33	0.49
2.00	0.52	2.00	0.56
1.50	0.65	1.50	0.69
1.00	0.83	1.00	0.86
0.80	0.91	0.80	0.93
0.50	1.05	0.50	1.06

Therefore, resistance factor for design method 16, which is a combination of Decourt (sand) +Tomlinson (clay) +TipAPI, according to β =2.33 is 0.45 (0.447 rounded to nearest 0.05) using entire bias data and 0.5 using best fit to tail. When using Method 16 to predict steel pipe pile resistance in California soil, a resistance factor can be selected based on a certain safety level requirement (P_f is related with β), then attached to predict resistance. The total factored resistance ($R\phi$) is the real design capacity.

Chapter 6 SUMMARY, CONCLUSIONS AND RECOMMENDATIONS

6.1 Summary

In this thesis study, 45 high-quality steel pipe piles driven in various soil conditions in California were collected from CALTRANS' load test data to evaluate available design methods and calibrated resistance factors of selected design methods. A total of 26 combined static methods for shaft and tip resistance were selected to predict total static pile capacity. The performance and accuracy of the 26 design methods were systematically evaluated by comparing the estimated (Q_c) and measured ultimate pile capacities (Q_m). The evaluation was based on 45 Q_c to Q_m values by using criteria of best fit line and coefficient of determination R^2, mean and standard deviation, cumulative probability, and the histogram and log-normal distribution. All the prediction methods were first ranked according to each single criterion and then ranked according to an overall rank index (RI) which considered the combination of all four single criterion.

Load and Resistance Factor Design (LRFD) calibration was performed on each prediction method by using Monte Carlo Simulation (MCS) method. Bias statistics were obtained by using the mean and standard deviation of all measured bias and best fit to tail of the measured bias. Monte Carlo Simulation of 10,000 iterations was performed to calibrate resistance factors ϕ at a target reliability index β of 2.33 for investigated methods. In addition, the relationship of resistance factors ϕ with various reliability index β has also been determined for best prediction method, resulting from above mentioned assessment system.

6.2 Conclusions

The main conclusion in this thesis study can be summarized as follows:

1. Based on analysis of 45 pipe piles from CALTRANS, the Decourt method performs best for predicting skin friction in sand, followed by the Olson method, then the API method and the Nordlund method.
2. The Tomlinson method is preferred as the best prediction method for predicting skin friction in clay for pipe piles in California.
3. Considering the performance of prediction methods from 4 evaluation criteria, Method 16, which is a combination of Decourt (sand) +Tomlinson (clay) +TipAPI, is preferred as the best static prediction method for pipe piles driven in California soil.
4. Resistance factors according to different design methods have been calibrated based on the data of 45 pipe piles by using Monte Carlo simulation when reliability index β=2.33 (related to 1% failure).
5. Resistance factors for the 26 prediction methods have been obtained from the best-fit of lower tail curve when β=2.33.
6. Based on the entire 45 pipe piles data, calibrated resistance factors from using the Decourt method for skin friction in sand are higher than resistance factors calibrated from using Olson, API and Norlund, which is in accordance with the trend concluded in the final rank of prediction methods.
7. When performing resistance calibration based on entire 45 pipe data, Method 15, which is combination of Decourt (sand) + Dennis (clay) +TipAPI, gives the highest resistance factor of ϕ=0.52, and is considered the most economical since ϕ/μ=0.41.
8. When using lower tail data to calibrate resistance factors, Method 9 (API(sand) +Dennis (clay)+ Tip (API)) has the highest resistance factor of ϕ=0.63; however, this is not the most economical method. Method 16 (Decourt (sand) +Tomlinson

(clay) +TipAPI) with calibrated resistance factor of ϕ=0.49 is considered most economical method since it has the highest efficiency factor, ϕ/μ=0.43.

6.3 Recommendations

The recommendations for future study are listed below:

1. The soil plug effect is not considered for open-ended pipe piles when using static methods for calculating axial bearing capacity, and this may tend to underestimate pile capacity. Hence the soil plug effect probably need to be incorporated to improve the prediction accuracy in future applications.
2. All the calibrated resistance factors associated with different design methods are for pipe piles, are only valid for soil profiles similar to soil in California, and may not necessarily reflect other pile types in other locations.
3. It is recommended to continue collecting pile load test data from new projects in California soil, especially for those cases in which the end bearing and side frictional capacities can be separated for possible future re-calibration of resistance factors of different pile design methods.
4. It is recommended to select a few projects to demonstrate the cost benefit study and comparison between the LRFD design and the traditional ASD design.

References

AASHTO (2012). "AASHTO LRFD Bridge Design Specifications: Sixth Edition. Parts I and II." American Association of State Highway and Transportation Officials, Washington, DC.

Abu-Farsakh, M. Y., and Titi, H. H. (2004). "Assessment of direct cone penetration test methods for predicting the ultimate capacity of friction driven piles." *Journal of Geotechnical and Geoenvironmental Engineering*, 130(9), 935-944.

Abu-Farsakh, M. Y., Yoon, S., and Tsai, C. (2009). "Calibration of Resistance Factors Needed in the LRFD Design of Driven Piles." 120.

Allen, T. M., Nowak, A. S., and Bathurst, R. J. (2005). *Calibration to Determine Load and Resistance Factors for Geotechnical and Structural Design*, Transportation Research Board.

American Petroleum Institute (API) (2005). *Recommended Practice for Planning, Designing and Constructing Fixed Offshore Platforms: Working Stress Design*, American Petroleum Institute.

API (1993). *Recommended practice for planning, designing and constructing fixed offshore platforms—Working stress design*, American Petroleum Institute, Washington, DC.

Briaud, J.-L., and Tucker, L. M. (1988). "Measured and predicted axial response of 98 piles." *Journal of Geotechnical Engineering*, 114(9), 984-1001.

Decourt, L. "Prediction of the Bearing Capacity of Piles Based Exclusively on N Values of the SPT." *Proc., 2nd European Symposium on Penetration Testing*.

Dennis, N. D., and Olson, R. E. (1983a). "Axial Capacity of Steel Pipe Piles in Clay." *Geotechnical Practice in Offshore Engineering, ASCE*Austin, Texas, 370-388.

DiMillio, A. (1999). "A Quarter Century of Geotechnical Research."Federal Highway Administration.

Gudavalli, S. R., and Safaqah, O. (2013). "Effect of Soil Plugging on Axial Capacity of Open-Ended Pipe PIles in Sands." *Proceedings of the 18th International Conference on Soil Mechanics and Geotechnical Engineering*.

Hannigan, P. J., Institute, N. H., Berg, R. R., and Associates, I. (2006). *Design and Construction of Driven Pile Foundations: Reference Manual*, U.S. Department of Transportation, Federal Highway Administration, National Highway Institute.

Jardine, R. J., and Chow, F. C. (1996). "New design methods for offshore piles."

Karlsrud, K. "Lesson Learned from Instrumented Axial Pile Load Tests in Clay." *Proc., OTRC Conference on Analysis*, Construction and Testing of Deep Foundations.

Kraft, L. M., Focht, J. A., and Amerasinghe, S. F. (1981). "Friction Capacity of Piles Driven into Clay." *Journal of the Geotechnical Engineering Division*, 107, 1521-1541.

Lethane, B. M., and Xu, X. (2005). "The UWA-05 method for prediction of axial capacity of driven piles in sand." *Proceedings of the International Symposium on Frontiers in Offshore Geotechnics (IS-FOG 2005)*, 683-689.

McVay, M. C., Birgisson, B., Zhang, L., Perez, A., and Putcha, S. (2000). "Load and Resistance Factor Design (LRFD) for Driven Piles Using Dynamic Methods—A Florida Perspective." *Geotechnical Testing Journal*, 23(1), 55.

Nordlund, R. L. (1963). "Bearing Capacity of Piles in Cohesionless Soils. ." *Journal of the Soil Mechanics and Foundations Division*, 89(1-35).

Olson, R. E. "Axial Load Capacity of Steel Pipe Pile in Sand." *Proc., Proceedings, Offshore Technology Conference*, 17-24.

Paik, K., and Salgado, R. (2004). "Determination of bearing capacity of open-ended pile in sand."

Paikowsky, S., and LaBelle, V. (1994). "Examination of the Energy Approach for Capacity Evaluation of Driven Piles. ." *Proceedings*

of the International Conference on Design and Construction of Deep Foundations, II, 1133-1149.

Paikowsky, S. G. (2004). "Load and resistance factor design (LRFD) for deep foundations - NCHRP Report 507." Transportation Research Board.

Paikowsky, S. G., Marchionda, C. M., O'Hearn, C. M., Canniff, M. C., and Budge, A. S. (2009). "Developing a Resistance Factor for Mn/DOT's Pile Driving Formula." 294.

Tomlinson, M., J. (1980). "Foundation Design and Construction." (Fourth Edition).

Xu, X., Schneider, J. A., and Lehane, B. M. (2008). "Cone penetration test (CPT) methods for end-bearing assessment of open-and closed-ended driven piles in siliceous sand."

Yu, F., and Yang, J. (2011). "Base capacity of open-ended steel pipe piles in sand." *Journal of Geotechnical and Geoenvironmental Engineering*, 138(9), 1116-1128.

Biographical Information

Yujie Hu graduated with a Bachelor's degree in Building and Environment Engineering (also known as HVAC) from Beijing University of Technology, Beijing, China, in 2013. Later, she started her graduate studies at the University of Texas at Arlington (UTA) in January 2014, majoring in Civil Engineering under the supervision of Dr. Xinbao Yu. She has mainly been working on Load and Resistance Factor Design (LRFD) for deep foundations. She successfully completed the course and thesis work, and received her master degree in Civil Engineering with emphasis on Geotechnical Engineering in May, 2016.